Author: Woldhuis, Erik
Title: Foam rheology near the jamming transition
Issue Date: 2013-12-11

Foam Rheology near the jamming transition

Proefschrift

ter verkrijging van
de graad van Doctor aan de Universiteit Leiden,
op gezag van Rector Magnificus prof. mr. C. J. J. M. Stolker,
volgens besluit van het College voor Promoties
te verdedigen op woensdag 11 december 2013
klokke 8:45 uur

door

Erik Woldhuis
geboren te Alkmaar
in 1984

Promotiecommissie:

Promotor:	Prof. dr. M. L. van Hecke (Leiden)
Copromotor:	Dr. B. P. Tighe (Technische Universiteit Delft)
Leden:	Dr. P. Schall (UvA)
	Prof dr. E.R. Eliel (Leiden)
	Dr. V. Vitelli (Leiden)
	Prof dr. H. Schiessel (Leiden)
	Prof dr .T. Schmidt (Leiden)

Casimir PhD series, Delft-Leiden 2013-3
ISBN: 9789085931737

Dit werk maakt deel uit van het onderzoeksprogramma van de Stichting voor Fundamenteel Onderzoek der Materie (FOM), die financieel wordt gesteund door de Nederlandse Organisatie voor Wetenschappelijk Onderzoek (NWO)

Contents

Chapter 1

Introduction

Soft disordered materials, like foams, emulsions, suspensions, granular media or gels, display mechanical properties that are neither those of a crystalline solid nor those of a molecular liquid. Instead, these materials often combine solid- and liquid like behavior. Such disordered matter is extremely interesting, not in the least because many disordered materials are incredibly important in applications. The flow and dripping behavior of paint, the way forces distribute in a ton of wheat grains contained in a silo or the tear-resistance of cell walls are all problems whose practical interest is obvious. But these materials are also inherently interesting on a theoretical level because of their disorder.

Initially, there was hope that the disorder in these systems could be treated as a perturbation to crystalline solids or molecular liquids, for example by simple effective medium theories [1–3]. But after intense interest in these materials in recent years [4–7], it is now clear that the disorder in these systems makes them intrinsically different from either crystalline solids or simple random systems. In addition, many of these materials are out of equilibrium, either because their constituent particles are too large to be affected by thermal fluctuations, as in sand [8] or foams [9], or because relaxation times exceed experimental timescales, like in glasses [10].

In this thesis, we bring together two different approaches that are used to study soft disordered materials: jamming and rheology. *Jamming* takes its cue from hard condensed matter and aims to describe the elastic response of soft materials [4]. This approach makes heavy use of simulations and bases much of its framework on critical scaling theory, which is used as a model to describe a transition from liquid-like to solid-like behavior. The jamming approach has been successful in describing the elastic properties of disordered media with phenomenological scaling functions. The second approach, *rheology*, is more experimental in nature. It describes the flow-behavior of materials, often resulting in phenomenological relations between the stress and the strain rate called flow curves (see section 1.2 for a precise definition of stress and strain rate).

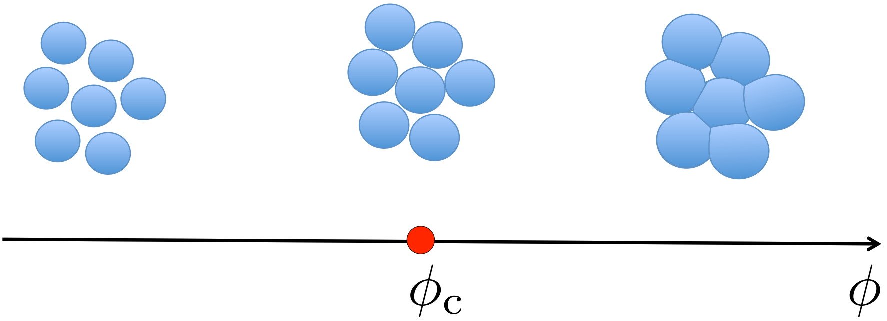

Figure 1.1: Schematic representation of soft repulsive particles as a function of their packing fraction ϕ in relation to the critical packing fraction ϕ_c. Below ϕ_c, particles are not touching, the pressure is zero, and there is no resistance to deformations of the system as a whole. Above ϕ_c particles are jammed: they deform each other, there is finite pressure and, in general, finite resistance to further compression and deformations.

Here we aim to combine the scaling approach from jamming with the focus on flowing behavior from rheology. We are not the first to do so: the 2007 paper of Olsson and Teitel [11] is an important milestone and combined studies of jamming and rheology are much older than that [12]. Our aim is not only to characterise the scaling of the rheology of soft particles near jamming, but also to come to predictive (scaling) models for the rheology.

1.1 Jamming

When compressing a collection of loosely packed, purely repulsive, soft, athermal particles in the absence of gravity, no resistance to compression is felt at first, but at some critical compression the particle system can no longer be freely compressed further: it is said to be jammed [4–7, 13, 14]. All materials that consist of soft, mesoscopic particles show a similar transition: foams, emulsions, colloidal suspensions and granular materials.

In describing this phenomenon, the packing fraction of the mesoscopic particles (bubbles, emulsion droplets, colloids or grains) in the material is a crucial parameter. The packing fraction, ϕ, is given by the fraction of the total volume or area that is taken up by the mesoscopic particles. If ϕ is low, none of the particles are in contact, see the left of fig 1.1. At this point, compressing the system does not cost any energy as there are no forces to overcome: the particles will be brought closer together, but as long as they don't overlap there is nothing that resists the compression.

Then, at some critical packing fraction, ϕ_c, also called the jamming density, all particles suddenly come in contact with their closest neighbours, see the middle of figure 1.1. The density at which this happens is around 0.64 in three dimensions and around 0.84 in two dimensions [5]; these values coincide with the respective random close packing densities in two and three dimensions[1]. When the particles come in contact they can suddenly resist compression because they need to deform, which costs energy, see the right panel of figure 1.1. Therefore the system now resists compression. The exact definition of when something can be said to be jammed is more complicated than this simple picture and we will discuss this in more detail below.

If the system is compressed further beyond the critical density ϕ_c, as shown on the right of figure 1.1, the material starts to behave more and more like a regular elastic solid, but at or near the jamming density, the system exhibits anomalous behavior. As an example of this anomalous behavior we discuss here the response of jammed systems to small deformations. Specifically we compare the bulk modulus K and the shear modulus G, defined by

$$\begin{aligned} \sigma_{xx} &= K\gamma_{xx} && (1.1)\\ \sigma_{xy} &= G\gamma_{xy}, && (1.2) \end{aligned}$$

where γ is the strain or deformation of the material, σ_{xx} is the pressure and σ_{xy} is the shear stress[2]. O'Hern *et al.* have found [5] that the shear modulus scales with the difference between the density and the critical density, $\Delta\phi = \phi - \phi_\mathrm{c}$. For harmonic particles they found that

$$G \sim \Delta\phi^{\frac{1}{2}} \tag{1.3}$$

In other words: $G = 0$ at the jamming density. The bulk modulus, in contrast, as O'Hern *et al.* have also found, has a finite value at the jamming transition [5]. As a consequence $\frac{G}{K}$ becomes arbitrarily small upon approaching the jamming density ϕ_c. This means that as we approach the jamming transition from above it will become infinitely easier to shear the system than to compress it. K and G are not the only quantities that show scaling with $\Delta\phi$. The jamming transition can be described as critical transition with $\Delta\phi$ as the control parameter [5]. One of the features of a critical transition that is present is a diverging length scale, although it is not an obvious one [14, 15].

One way, to define a jammed solid is to demand that there must be a finite critical stress below which the system behaves elastically for at least some finite time [5].The time scale in this definition is important because reducing the density is not the only way to go from the solid-like jammed state to the unjammed state. Increasing the temperature, T, and increasing the driving, σ also drive a system away from the jammed state. This idea can be represented in a so-called jamming diagram shown in figure 1.2. In both cases, the extra excitations fluidize the system by introducing plasticity. This interplay of three

---

[1] In two dimensions it is necessary to use polydisperse particles to prevent crystalization

[2] see section 1.2 for an exact definition of the shear stress

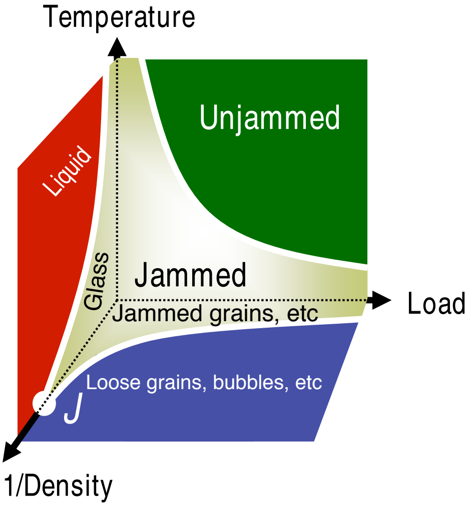

Figure 1.2: There are three ways to take a system from a jammed state to an unjammed state: decreasing the packing fraction ϕ, increasing the temperature T or increasing the driving σ. Figure from [6]

different variables is complicated, however, and the simplest case of $\sigma = T = 0$ is therefore studied extensively. Here we expect a sharp transition, called point J, and that is indeed what is found [5].

For foams, the system that inspires the numerical and theoretical work in this thesis, shear driving is crucial a crucial parameter in addition to the packing fraction, or wetness of the foam. When exposed to stresses below some critical threshold called the yield stress, foams show solid-like behavior, but when exposed to stresses above this threshold, foams exhibit plastic flow [16]. In other words: large stresses unjam foams, just as the jamming diagram describes. Evidently this means that the other perspective on soft matter, the rheological perspective that studies flow, is also relevant for foams.

1.2 Rheology of Complex Fluids

Rheology is the study of the flow of materials. The most basic ways in which one can classify the flow behavior of a material is by its rheological curve. The rheological curve of a material gives the relation between the flow rate and the amount of driving, where driving is measured by the *shear stress*, σ_{xy}. In two dimensions this is the force in the direction of the flow per unit length, see figure 1.3. The amount of flow is measured by the *strain rate*, $\dot{\gamma}$, which is the

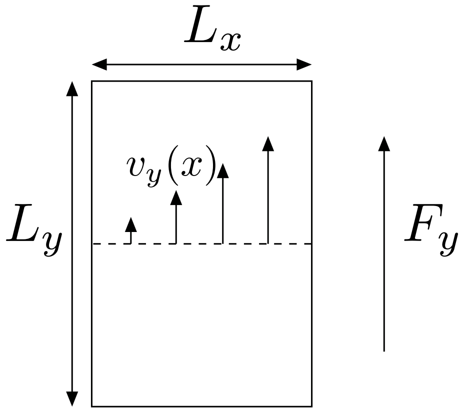

Figure 1.3: A force F_y is applied on one side of a lump of material with length L_y and width L_x, resulting in a position dependent shear flow with velocity profile $v_y(x)$. The shear stress σ_{xy} is defined as F_y/L_y. The strain rate $\dot{\gamma}$ is defined as $\left(v_y(L_x) - v_y(0)\right)/L_x$.

difference in flow speed per unit of length perpendicular to the flow direction, see figure 1.3. Both quantities are assumed to be distributed homogeneously throughout the system, at least on average.

Simple fluids, such as molecular materials in the liquid state, like water or oil, exhibit the simplest form of rheological behavior. They are called Newtonian fluids and the shear stress needed to induce flow is directly proportional to the desired strain rate:

$$\sigma_{xy} = \eta\dot{\gamma}, \tag{1.4}$$

in which the constant of proportionality η is called the viscosity [17]. Besides simple fluids, there is also a large variety of complex fluids: foams, granular media or gels, for example. The rheological curves of such complex fluids are usually different from that of a Newtonian fluid and they are therefore called non-Newtonian fluids. Their rheological curves typically include a number of common ingredients that we will discuss here.

The first such ingredient is the yield stress, σ_{y}. A yield stress is the minimal stress that needs to be applied for persistent flow in the system. In some materials, the stress needed to start persistent flow, which is called the static yield stress, is higher than the stress needed to sustain flow, which is called the dynamic yield stress. In our simulations, though, they are equal and we will no longer distinguish between the two. If a stress smaller than the yield stress is applied, the system will usually display elastic or plastic behavior but no steady flow. A fluid that only differs from a Newtonian fluid in the fact that it has a non-zero yield stress is called a Bingham (plastic) fluid [18]. A rheological curve for a Bingham fluid is shown and compared to the curve of a Newtonian fluid in figure 1.4 a and c.

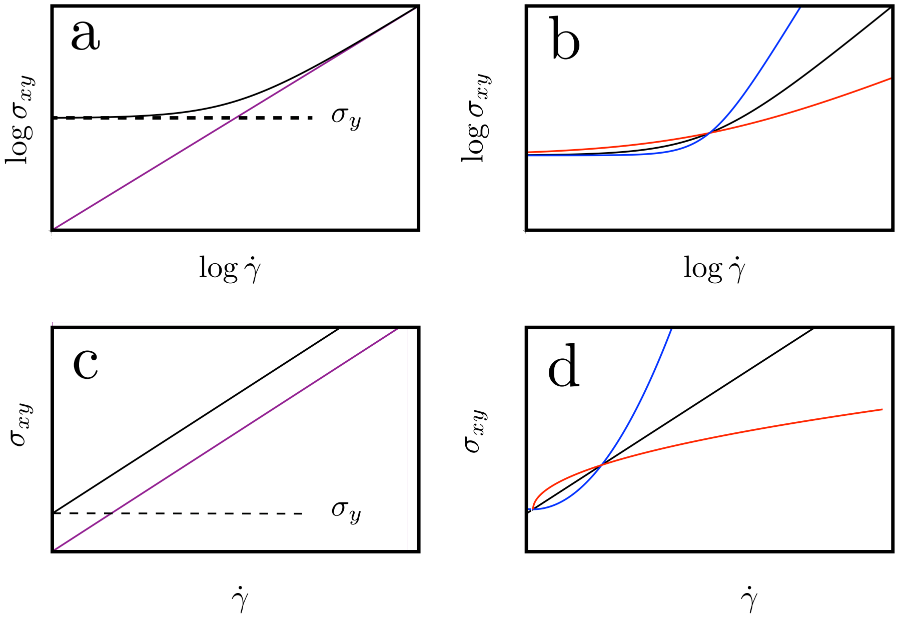

Figure 1.4: Examples of rheological curves on double logarithmic axes (a and b) and linear axes (c and d). The purple line represents a Newtonian fluid, the black lines represent Bingham (plastic) fluids, the red line represents a shear-thinning fluid and the blue line a shear-thickening one. The yield stress is indicated by σ_y in panels a and c.

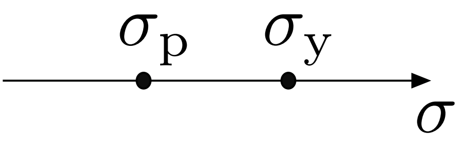

Figure 1.5: Different levels of stress on a material elicit different responses. A stress below the plastic stress σ_p results in purely elastic behavior. A stress between σ_p and the yield stress σ_y yields plastic behavior and creep. Only if a stress above σ_y is applied can a system sustain steady flow.

How does the yield stress compare to the critical stresses discussed in section 1.1? In the rheological approach, σ_{y} is the minimal stress needed to get a material to sustain steady flow. In the jamming description, one is interested in the maximum stress before a material stops displaying a purely elastic response. We call this the plastic stress, σ_{p}. There can be a whole range of stress between these two limits where a system no longer exhibits elastic behavior, but no steady flow either, see figure 1.5.

In addition to the presence of a yield stress, the second way in which the rheology of non-Newtonian fluids can differ from that of Newtonian fluids is that the variation of the shear stress with the strain rate is no longer linear, but, for example, a power law (once the stress exceeds the yield stress). This may be considered a shear stress dependent viscosity: if $\sigma_{xy} = \sigma_y + \eta_0 \dot{\gamma}^\beta$, this can also be written as $\sigma_{xy} - \sigma_y = \eta_{\mathrm{eff}} \dot{\gamma}$ with $\eta_{\mathrm{eff}} = \eta_0 \dot{\gamma}^{\beta-1}$. If $\beta < 1$, the fluid is called shear thinning as the effective viscosity decreases when the flow rate is increased. If $\beta > 1$, the material is called shear thickening. Many materials that have a yield stress are also shear thinning and the two can be hard to distinguish in everyday life (as in both cases flow becomes easier when more shear stress is applied). Shear thickening materials are rarer, but examples include silly putty and corn starch in water. A fluid that has both a non-zero yield stress and a power law relationship between shear stress and strain rate is called a Herschel-Bulkley fluid [19].

Other deviations from Newtonian behavior make it impossible to describe the flow behavior of a system with a single rheological curve at all. Two of these are shear banding and thixotropy. In the case of shear banding the flow is not homogeneous in the system. While this is often caused by an inhomogeneous distribution of the shear stress[3], it can also be caused by instabilities in the fluid itself, [21]. If the strain rate becomes location dependent, as is the case for shear banding, it is no longer clear that it is meaningful to look at the global strain rate.

In thixotropic fluids the viscosity decreases over time when the system is sheared. This can be seen in many dairy desserts that are packaged in cups: when just opened they appear fairly solid, but stirring them briefly makes them much more fluid. This process is called shear rejuvenation. If a thixotropic fluid is allowed to rest, its viscosity will increase again; this is called ageing [21]. The reverse of thixotropy, in which the viscosity increases while sheared, also exists and is called rheopecty. It is much less common than thixotropy. Since a rheological curve assumes time-independence it cannot represent such effects.

In the foam systems that we will describe, and that we will introduce in depth below, neither shear banding nor thixotropy plays a significant role [22], and we can describe our system using rheological curves.

---

[3] The Taylor-Couette cell, an apparatus often used in rheology, has inhomogeneous distribution of shear stress due to its cylindrical shape, for example [20].

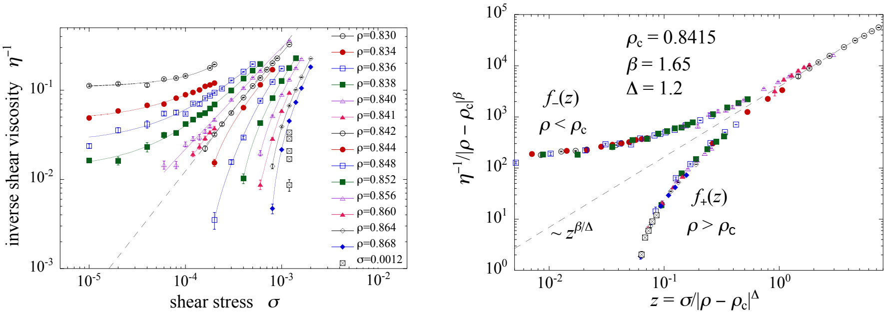

Figure 1.6: Rheological curves from the simulations of Olsson & Teitel. Left panel: raw data that depends on the density. Right panel: data collapsed onto master curve by rescaling with appropriate powers of $\Delta\phi$. Figure from [11]

1.3 Jamming & Rheology

Most of what has been described in the previous section is phenomenological. It is often unknown how the meso-/microscopic properties of complex liquids determine their rheology and whether there are universal mechanism that lead to the appearance of, for example, shear-thinning. Conversely, in jamming we have seen that many - static - quantities show critical scaling. An obvious question is, then, whether the rheology near the jamming point will also be governed by critical scaling functions.

This question was first asked by Olsson & Teitel in 2007 [11], using simulations of soft and repulsive model particles. They found that the rheological curve of a jammed system depends on the packing fraction, although they represent this through the inverse shear viscosity $\eta^{-1} = \frac{\dot{\gamma}}{\sigma}$, see the left panel of figure 1.6. When both axes, and therefore the stress and the strain rate, are rescaled by appropriate powers of the packing fraction, $\Delta\phi$, all data collapses onto two master curves, one below jamming and one above jamming, see the right panel of figure 1.6. Just as in the case of static jamming, this is reminiscent of critical scaling theory, with $\Delta\phi$ as the scaling parameter.

Specifically, Olsson & Teitel found a critical regime for high strain rate and small $|\Delta\phi|$ where the original rheological curve is independent of the density. Rheologically, this regime corresponds to the power law portion of a Herschell-Bulkley description. Therefore, the exponent of this critical regime or power law regime, which we will call β, is interesting both from a scaling and therefore jamming perspective, where it can be used to identify universality classes, and from a rheological perspective, where it differentiates between shear-thinning and shear-thickening behavior.

Therefore, it is somewhat disheartening that there is a complete lack of agreement over the value of this exponent. Olsson & Teitel themselves have shifted down their value for β from 0.42 [11] to 0.3 [23]. Other people find higher values: 0.54 [24], 0.64 [25], 0.72 [26] and even 1 [27]. Luckily, all these different exponents are at least found in slightly different systems. For example, some results are obtained using particles without mass [11,23,27], whereas other results were obtained using particles with mass [25, 28, 29], though in some cases the mass was explicitly assumed to be so small as to be negligible [24]. Another area of big differences between approaches is how the energy that is put into the system by driving is dissipated. Possible dissipation mechanisms include viscous friction between particles moving past each other [24], viscous friction with a background flow [11, 23, 27], inelastic collisions [29, 30] or even thermostats [25, 28].

In the traditional critical scaling paradigm, such details of the microscopic interactions might not be important for the critical exponents. However, in static jamming we know that scaling relations often *do* depend microscopic details. For example, the scaling relation for G of Eq. 1.3 is changed to $G \sim \Delta\phi$ if the particles under consideration are not harmonic but hertzian, meaning that their repulsive forces scale with overlap to the power $\frac{3}{2}$ [5].

All this suggests that the details of the interactions are crucial to understand the rheology. Inspired by jamming studies, in this thesis we study bubble models where the interactions between the bubbles are strictly repulsive. Moreover, we use local dissipative (viscous-like) interactions and do not resort to mean field or other dissipation mechanism: we know that non-affine deformations are crucial for capturing scaling behavior in static jamming [14] and expect that the same is true in flow. Finally, in most of our work inertia will be absent, which technically means that elastic and viscous forces have to balance at all times. Although this leads to numerical complications, it is simpler conceptually. After introducing our numerical model, we will perform extensive simulations capturing both the global rheology and the microscopic bubble motion. We will then develop a scaling model that predicts the rheological curve by explicitly linking microscopic fluctuations and the anomalous shear elasticity near jamming.

1.4 Our Approach

In light of what was discussed above, we will start chapter 2 with introducing the minimal jamming model that we use in our simulations. We will discuss the microscopic interactions between our particles as well as our simulation system and the way we implemented the dynamics in our simulation code. We finish chapter 2 by showing some of the phenomenology of our microscopic model such as rheological curves and probability distributions of velocities.

In chapter 3 we introduce the second pillar of our approach: the scaling model that we will base our predictions on. Our model is based on three relatively simple assumptions and will be called the 3E model - for Energy, Effective strain and Elasticity, the three ingredients. We continue by solving the 3E model and note that it predicts different behavior in three different regimes, depending on whether the system is densely packed and flowing slowly, loosely packed and flowing fast, or somewhere in between. In the end, we compare the predictions of the 3E model with our simulation results and find that the model is consistent with our data. To go beyond 'consistent' and test its predictive power, we need a more complete, quantitative model.

Therefore we go beyond the simple scaling formulation of the model in chapter 4 to develop a quantitative model. We will call this model the Q3E model to distinguish it from the scaling model. The quantitative Q3E model allows us to make more precise predictions. These predictions are consistent with our numerical data, further strengthening our model. The quantitative formulation of Q3E also allows us to test the three assumptions of the model. We find that they, too, are correct. In chapter 5 we then expand the model to the normal components of the stress. If we formulate a natural extension of our model to the normal stress we need to introduce a new elastic equation to make the model work.

In chapter 6 we delve further into the remarkable behavior of the particles in jammed systems. In particular the distribution function of the relative velocities, the source of energy dissipation, shows rich behavior that is surprisingly amenable to a phenomenological description. We also delve into the relationship between the global stress and the microscopic forces to answer the question how elastic and viscous forces can balance on the bubble scale while elastic stresses are so much bigger than viscous stresses.

Finally, we extend our microscopic model to include systems with nonlinear microscopic interactions in chapter 7. We hypothesise an extension of our scaling models and compare their predictions to two different experimental studies to good effect. In chapter 8 we introduce a new computer implementation of our nonlinear microscopic model to test our nonlinear scaling model. To extend our microscopic model we also need to include mass. While the results of those studies are still very preliminary we can certainly say that changing the microscopic interactions changes the global rheology. However, we have also found evidence that the inclusion of mass is a singular perturbation, making comparison to previous results complicated.

Chapter 2

Bubble Model and Simulations

2.1 Microscopic Model

If a computer model is supposed to represent and describe the transition from an unjammed state to a jammed state, it needs at least two properties. First, the particles in the system need to have some concept of being ‘in contact’ or not, where forces between contacting particles are stronger than between particles that are not in contact. Second, it needs some ‘softness’, meaning that particles can still be compressed if they are in contact, so that it makes sense to discuss densities higher than the jamming density.

The simplest of such a system, that has been used extensively in simulations [5,11,27], is a system of discs that exert a hookean (linear) elastic force on each other when they are in contact and that do not interact when not in contact: particles i and j interact via an elastic force $\mathbf{F}^e_{ij}$ given by

$$\begin{aligned} \mathbf{F}^e_{ij} &= k\delta_{ij} \quad d_{ij} < r_{ij} && (2.1) \\ \mathbf{F}^e_{ij} &= 0 \quad d_{ij} > r_{ij}, && (2.2) \end{aligned}$$

in which k is a spring constant, δ_{ij} is the overlap between bubbles i and j, see figure 2.1, d_{ij} is the distance between (the centers of) bubbles i and j and r_{ij} is the sum of their radii. In addition to satisfying the two minimum demands introduced above (contacts and compressibility), these particles have a number of properties that make them very simple, both conceptually and computationally.

First of all, as shown by Eq. 2.2, these particles only interact when they touch: there is no long range attraction or repulsion. Second, the interactions between the particles are pairwise additive, meaning that the force between particle i and j does not depend on whether particle i is also in contact with

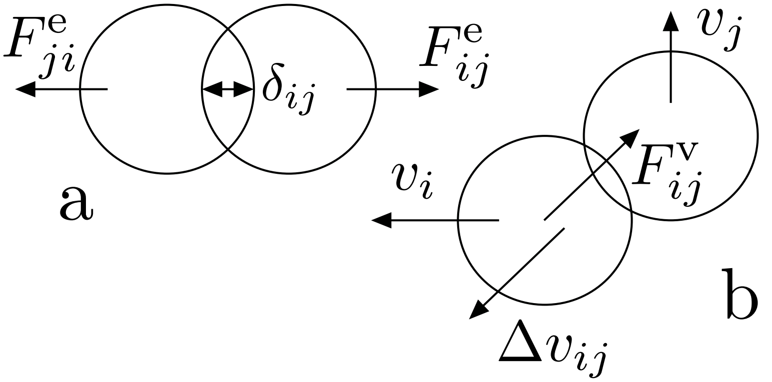

Figure 2.1: **a** two bubbles with a non-zero overlap δ_{ij} exerting forces $F^{\mathrm{e}}_{ij} = k\delta$ on each other. **b** two overlapping bubbles with different velocities v_i and v_j. As a consequence bubble i experiences a velocity difference Δv_{ij} and a force $F^{\mathrm{v}}_{ij} = -b\Delta v_{ij}$. The opposite velocity difference and force working on bubble j are not shown.

other particles. And third, since all forces are central, there are no torques that need to be balanced to attain static equilibrium, only forces. Simulations with these particles are often performed in two dimensions [5, 6, 11] as this allows for a relatively small amount of particles (computationally cheap) with relatively large linear size of the system (to minimise finite size effects) compared to three dimensions. The disadvantage is that monodisperse particles crystallize easily in two dimensions[1]. To counteract this it is customary to use bidisperse discs, with radii with a ratio of 1:1.4, which prevents crystallization [5]. Additionally, previous jamming research suggests that there are no crucial differences between two and three dimensions [5].

The minimum requirements to expand this simple model to flowing or dynamic systems are a means of energy dissipation, to offset the energy put into the system by driving it, and equations of motion, to link forces to velocities. For this, we use Durian's bubble model [27]. In this model, if particles i and j have relative velocity $\Delta\mathbf{v}_{ij}$ they experience a viscous drag $\mathbf{F}^v_{ij}$ given by

$$\mathbf{F}^v_{ij} = -b\Delta\mathbf{v}_{ij} \quad d_{ij} < r_{ij} \tag{2.3}$$

$$\mathbf{F}^v_{ij} = 0 \quad d_{ij} > r_{ij}, \tag{2.4}$$

with b the viscous force constant, see figure 2.1 for a simple illustration. Note that such a force model still only has pairwise additive contact forces, but the viscous force can make discontinuous jumps from zero to a finite value when particles make or break contact, as the viscous force, once in contact, does

---

[1] because the locally optimal packing, the triangle, can tile space; i.e. there is no frustration [31]

not depend on the overlap. The model takes the equations of motion to be overdamped: forces balance at all time. Since the viscous forces depend on the velocities, this allows the velocities to be determined once the positions are given. Note that, even though the viscous force is not central, we still disregard, as is customary [11, 27], torque balance.

As the name implies, Durian's bubble model was developed to describe collections of bubbles, i.e. foams, though it is also thought to describe emulsions well, since emulsions and foam share many of their important properties [6]. This is also the way we think about our minimal jamming model. Although real foams deviate from the model as described above in several ways, we will argue that these deviations are small in the regimes near jamming that we study. First of all, the amount and arrangement of contacts on a bubble influences the contact force that that bubble will exert on other bubbles due to deformation of the bubble. This effect does not become relevant until very high densities, though, which is why we choose to neglect it. Second, gas bubbles have non-zero mass and therefore will not strictly obey overdamped dynamics. Still, since the mass of gas bubbles is small, bubbles accelerate rapidly and any force imbalance will be very short lived. Finally, bubbles will show some reaction to unbalanced torques, which this model does not take into account. However, bubbles will certainly not rotate as rigid bodies under the effect of torques - at best there will be fluid flow in the interface. In addition it has been shown that the presence or absence of torque balance makes no difference in linear response [32]. Therefore it is reasonable to not include torque balance.

2.1.1 Intermezzo: Roads not Traveled

Besides the microscopic model presented above, we have considered a number of other options that were in the end discarded for various reasons. They are briefly discussed here.

Mean Field Dissipation The method of dissipation described above is not the simplest imaginable. A simpler method was introduced as an approximation by Durian in his original model [27] and has since been used often [11]. This simpler method of dissipation is called 'Mean Field dissipation' and has dissipation take place not when contacting bubbles move relative to each other, as in Eq. 2.3, but when bubbles move relative to the time averaged flow field:

$$\mathbf{F}_i^v = -b\left(\mathbf{v}_i - \mathbf{v}\left(x_i, y_i\right)\right), \tag{2.5}$$

where $\mathbf{v}\left(x_i, y_i\right)$ is the value of the time averaged flow field at the position of particle i. While this approximation was introduced mainly for its computational benefits, it has a clear physical interpretation: viscous drag with the background fluid. Still, in actual foam systems dissipation takes place mostly between bubbles and not between bubbles and the fluid [16].

Therefore we must ask ourselves what the effect of this approximation might be. Since we expect that non-affine flow, which is exactly the flow that gets energetically punished by the mean field dissipation model, is prevalent around jamming, we expect that this approximation will have a large effect. We have nevertheless performed some simulations with the mean field model for comparison and have found that the differences between the two dissipative models are often small. For example, there seem to be few differences between the stresses. For some quantities, however, the differences between the Mean Field and the full Durian model are very big, see for example the correlation lengths in section 2.3.3 and [33].

Overlap-Dependent Viscous Force We know from experiments that the viscous force between bubbles depends not only on their relative velocity, but also on their overlap [34]: if particles have a bigger overlap, they will experience more viscous friction. Therefore, inclusion of this effect into our model would make it more realistic, and could also take away the conceptual problem that results from the fact that the viscous force is discontinuous when contacts are made or broken.

Tangential Friction We have investigated a model in which the viscous force was restricted to the direction perpendicular to the contact/parallel to the contact line: bubbles moving strictly towards or away from each other do not feel any viscous forces, only elastic forces.

This microscopic model has consistency problems, especially since we are doing simulations without inertia. Consider the following situation: bubble A and B are overlapping with each other, but not with any other bubbles. A and B will feel, equal and opposite, elastic forces, acting parallel to the vector connecting their centers. Whatever their relative velocities however, the viscous force that they feel will always be perpendicular to the vector connecting their centers; therefore force balance is impossible, independent of their velocities. Because of these problems, that will not occur often but are hard to overcome when they do, we have implemented a full vectorial dissipative force.

2.2 Simulations

Before we discuss our simulations in depth, it is useful to switch to dimensionless units. There are a number of free parameters in our model, shown in table 2.1, that can be used to construct non-dimensional units for length, time and stress; these can then be used to construct units for any other quantity, such as force or strain rate. As unit of length we pick the radius of the smallest bubbles, r_s, as the bubble size seems more relevant than the system size. We fix the other length scales by using the customary 1:1.4 ratio between small and large bubbles discussed above and by taking a square box with $L_x = L_y = 75$

Parameter		SI unit
width of the system	L_x	m
height of the system	L_y	m
small bubble radius	r_s	m
large bubble radius	r_l	m
spring constant	k	N/m
viscous force constant	b	Ns/m

Table 2.1: Free parameters in our system that set dimensions. k and b are defined in the microscopic force laws of Eqs. 2.1 and 2.3.

which leads, depending on density, to a particle number around 1000. We use k as unit of stress since, in two dimensions, the unit of stress is also N/m. Finally we construct a unit of time as b/k. This is the timescale over which a relative displacement and an overlap of 1 (r_s) result in equal forces. While this is a huge overlap, due to the linearity of the forces this is also the timescale over which a relative displacement and an overlap of 0.1 result in equal forces, etc.

In our simulations we impose a fixed packing fraction, ϕ, and a fixed strain rate, $\dot{\gamma}$, and we measure the stresses that are needed to maintain this driving. We change the packing fraction by changing the number of particles in our system. Since the number of particles has to be an integer, this limits the resolution of our packing fraction to $\frac{\pi 1^2}{75^2} \approx 0.0006$. In order to go beyond this resolution we also slightly change the size of our box to fine-tune the packing fraction and achieve a higher resolution.

We apply a constant strain rate using Lees-Edwards boundary conditions. This means that we use normal periodic boundary conditions in the vertical direction, the direction of flow. But along the horizontal direction, periodic copies of the system are given an extra velocity $\dot{\gamma} L_x$, both for updating the positions of bubbles and for calculating the viscous force over the periodic boundary, see figure 2.2.

2.2.1 Nuts and Bolts

We use a 'forward Euler' iteration scheme for our simulations, which works as follows: at time t we know the positions, $r(t)$, and the velocities, $v(t)$, of all bubbles. To move to the next time step, $t + \delta t$, we then move all bubbles forward with their velocity: $r(t + \Delta t) = r(t) + v(t)\Delta t$. This leads to a new contact network in which we can calculate all elastic forces, as these depend only on position[2]. We can then use the condition of force balance

---

[2] and the radii, but these are constant and known.

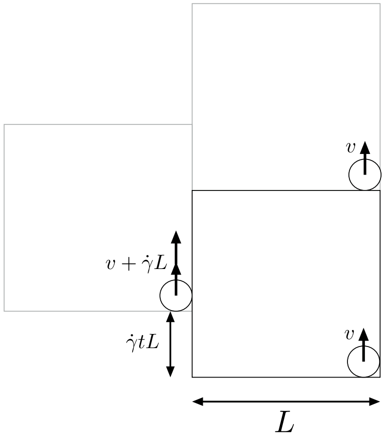

Figure 2.2: Lees-Edwards boundary conditions: particles are simply copied along the vertical, stream wise, direction and are copied with an extra velocity $\dot{\gamma}L$ in the transverse direction.

together with the elastic forces on all bubbles to calculate the velocities of all bubbles, as there is one 2-dimensional unknown velocity and one 2-dimensional force balance constraint per bubble. We use a Newton-Raphson solver for this problem. We now have the positions and velocities of all bubbles at time $t+\Delta t$ and we can repeat the procedure.

We make this mathematically explicit to show why this is computationally more involved than the Mean Field approximation. Let us define the contact matrix $\hat{C}$, this is a Z by N matrix, Z being the total number of contacts between bubbles and N the total number of bubbles in the system. If bubble j is one of the two bubbles in contact i then $\hat{C}_{ij} = 1$ if j has the higher index of the two participating bubbles and -1 if it has the lower[3]. With this definition $\hat{C}\mathbf{V}$, $\mathbf{V}$ being a vector with the velocities of all N bubbles, gives a vector with the relative velocities of all Z contacts. Conversely, applying $\hat{C}^T$ to any vector of contact quantities returns a vector of the sums over all contacts per bubble, i.e. if $\mathbf{F}^e$ is the Z-dimensional vector of elastic forces in each contact, then $\hat{C}^T\mathbf{F}^e$ is the N-dimensional vector of total elastic forces on each bubble. This means that once we have the positions, and therefore the contacts and elastic forces, at time t we need to solve the following equation of force balance for $\mathbf{V}$:

$$\hat{C}^T \left(\mathbf{F}^e - b\hat{C}\mathbf{V}\right) = \mathbf{0} \tag{2.6}$$

This inverse problem is computationally expensive to solve.

In contrast, in the Mean Field approximation the viscous force that a bubble experiences depends only on its own position and velocity, not those

---

[3] this is an arbitrary sign convention, corresponding with the definition of bond vectors pointing from the lower to the higher index.

of its neighbours. This makes it possible to solve the velocity of each bubble explicitly. If a bubble has a two dimensional velocity[4] $\mathbf{v}$, then the viscous force on that bubble is $-b\left(\mathbf{v}-\dot{\gamma}\hat{\mathbf{x}}r_y\right)$, where $\hat{\mathbf{x}}$ is the unit vector in the x- or flow direction and r_y is the y- or transverse component of the bubble position. If the elastic force on a bubble is $\mathbf{f}^e$, force balance then requires that

$$\mathbf{f}^e - b\left(\mathbf{v}-\dot{\gamma}\hat{\mathbf{x}}r_y\right) = \mathbf{0} \tag{2.7}$$

or $\mathbf{v} = b\mathbf{f}^e + \dot{\gamma}\hat{\mathbf{x}}r_y$, which can be calculated directly since $\mathbf{f}^e$ and r_y are known.

2.3 Phenomenology

In this section we will describe the main phenomenology of the bubble flows from our simulations. Unless otherwise specified we use simulations of approximately 20 units of strain for all strain rates to ensure proper averaging; the transient is typically less then 1.5 units of strain and is excluded from the averaging. Data samples are taken every 2/3 of a percent of strain, for a total of 3000 data points in the full 20 units of strain. The set of densities and strain rates used differs, and will be discussed individually for each result presented below.

2.3.1 Elastic and Viscous stress

Because we use overdamped equations of motion and the forces therefore balance at all times, we can calculate the shear stress needed to get a bubble system flowing from all the forces between the bubbles with the Born-Huang formulation [35]:

$$\sigma_{xy} = \frac{1}{2V}\sum_{<ij>} r_{ij,x} f_{ij,y}, \tag{2.8}$$

here V is the volume of the simulation box, the sum is over all contacting bubbles and r is the contact vector between two bubbles. A similar expression can be formulated for the three other components of the stress, σ_{xx}, σ_{yy} and σ_{yx}. There are two types of forces between the bubbles: elastic forces, as from Eq. 2.1, and viscous forces, as from Eq. 2.3. This means that we can decompose the (shear) stress into two components: the elastic shear stress, σ^{e}_{xy}, due to the elastic forces and the viscous shear stress, σ^{v}_{xy}, due to the viscous forces. Of course, since $f^{\mathrm{e}}_{ij} + f^{\mathrm{v}}_{ij} = f_{ij}$, the elastic and viscous shear stresses taken together give the same stress as calculated in Eq 2.8, which we will call the total (shear) stress, $\sigma^{\mathrm{tot}}_{xy}$. Note also that, since there is no torque balance, $\sigma_{xy} \neq \sigma_{yx}$

Figure 2.3 shows the elastic, viscous and total shear stresses a function of both strain rate (**a**) and density (**b**). As can be seen, the viscous stress

---

[4] we will now use lower case letters to distinguish two-dimensional vectors from N- or Z-dimensional vectors for which we have used capital letters.

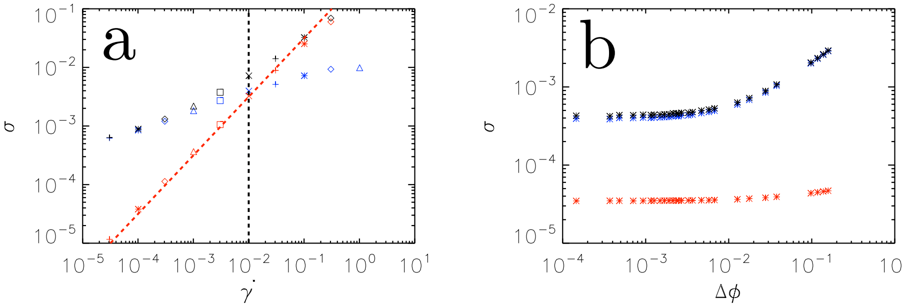

Figure 2.3: The viscous contribution to the stress (red), the elastic contribution to the stress (blue) and the total stress (black). **a**: stresses as function of the strain rate at fixed density ($\phi = 0.87$). The red dotted line indicates linear dependence on strain rate; the black dotted line is our cutoff strain rate. **b**: stresses as a function of density (we have taken $\phi_j = 0.8423$, see section 3.3.2) at a fixed strain rate ($\dot\gamma = 10^{-4}$).

is largely independent of the density and scales linearly with the strain rate; it shows newtonian behavior. The elastic stress depends on both the density and the strain rate and, as we will make abundantly clear below, does so in a complicated fashion. Since we can also see from figure 2.3 that the elastic stress tends to dominate the viscous stress, it is clear that any anomalous behavior of the total stress must be caused by the elastic stress. Therefore, in everything that follows we will study the elastic stress only, unless specified otherwise. In order to minimise the effect of the viscous stress, we limit ourselves to those strain rates where the elastic stress dominates the viscous stress: $\dot\gamma < 10^{-2}$, left of the dotted black line in figure 2.3. This means that to good approximation, $\sigma^{\mathrm{e}} = \sigma^{\mathrm{tot}}$

2.3.2 Rheological Curves

Above, we have seen that the elastic stress has a complicated dependence on both the strain rate and the density. To get a general feel for this dependence, we plot full strain rate sweeps for three different densities in figure 2.4. We have picked a density that is markedly above the jamming density, $\phi = 0.87$, one that is around the jamming density, $\phi = 0.8424$, and one that is below the jamming density, $\phi = 0.8$.

In the rheological curves of figure 2.4 we recognise a number of different aspects of the rheology of complex fluids that we discussed above. The first aspect is that for the density below jamming, there is newtonian behavior in the limit of small strain rates, indicated by the blue dotted line. The asymptotic behavior at $\phi = 0.87$ is very different though, showing a flattening of the curve,

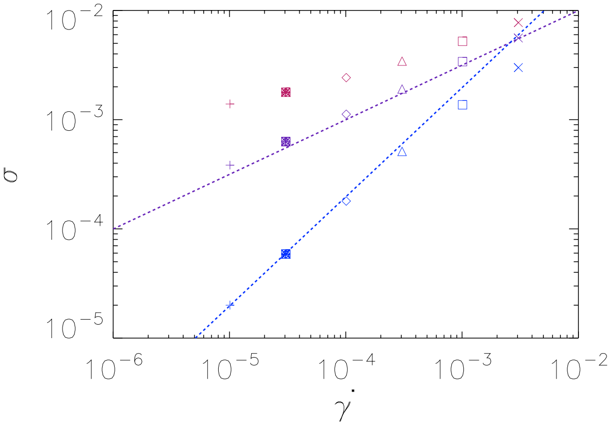

Figure 2.4: The shear stress as a function of strain rate for three different densities: 0.8 (blue), 0.8424 (purple) and 0.87 (pink). All curves approach a similar power law for high strain rate, indicated by the purple dotted line, which has a slope of 1/2. For low strain rates the low density shows steeper behavior and the high density shows flatter behavior. The blue dotted line indicates linear newtonian behavior.

possibly approaching a yield stress plateau[5].

The high strain rate asymptote is also interesting, as here all three densities approach the same behavior, shown by the purple dotted line. In all three cases we see shear-thinning behavior, i.e. a power law with exponent less than one. Moreover this exponent appears to the same for all three densities. At the jamming density this behavior extends all the way to low strain rates; for the densities away from jamming it crosses over into the low strain rate asymptotes discussed before.

All of this is consistent with observations from several other experiments and simulations [11, 24, 27–29]. In fact, Olsson and Teitel have already shown that by rescaling with appropriate powers of $\Delta\phi$ all data can be collapsed onto two branches, one below and one above jamming [11]. In the next chapter we will introduce a scaling model that will predict these exponents, as well as the shear-thinning exponent and a number of other surprising details, from three simple assumptions. We will also find that this way of rescaling the data does not capture the full behavior.

2.3.3 Correlation Length

Another phenomenon that Olsson and Teitel observe is a length scale in the correlation of the non-affine motion. I.e. they calculate the following correla-

---

[5] though that plateau is not reached

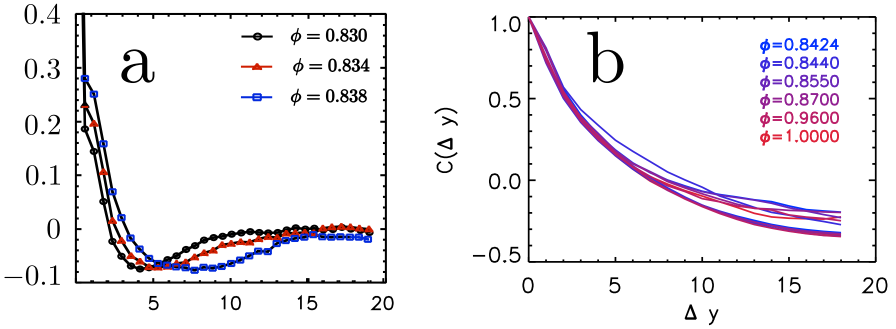

Figure 2.5: Two plots of the non-affine motion correlation length as a function of streamwise displacement. **a**: the original data from Olsson and Teitel [11] from simulations with Mean Field dissipation. **b**: data from our simulations with fully resolved bubble-bubble dissipation; a strain rate of 10^{-5} and $3 \cdot 10^{-3}$ are shown for each density.

tion function:

$$C\left(y\right) = \left\langle v_x(0) v_x(y) \right\rangle, \tag{2.9}$$

where <> denotes averaging over time and over all bubble pairs that are displaced only in the stream wise direction[6], v_x is the x-component, and therefore crosswise component, of the velocity of each bubble. Since there is no movement in the x-direction in the average flow profile, all movement in this direction is non-affine. A length scale, ξ, can be extracted from this correlation length and Olsson and Teitel find that $\xi^{-1} \sim |\Delta\phi|^{0.6} f\left(\sigma/\Delta\phi^{1.2}\right)$, [11]. An example of the correlation functions that they find is shown in figure 2.5 **a**.

When we calculate the same correlation function however, we do not find a length scale that changes with the density, see figure 2.5 **b**. In fact, if we perform simulations for different system sizes, we find that we can collapse the correlation data by simply rescaling with the linear size of the system. Additionally, the shape of our correlation functions looks different from those of Olsson and Teitel [33].

The most striking difference between our simulations and those of Olsson and Teitel is the form of the dissipation. Olsson and Teitel use mean-field dissipation, discussed in section 2.1.1, while we use the bubble-bubble dissipation of the full Durian model. Since this is the biggest difference between the two systems, it is the most likely explanation for the difference. In fact,

---

[6] The simulation box is divided into several stream wise 'lanes' and bubble velocities are correlated only between bubbles in the same lane, therefore their cross wise displacement is not necessarily zero, but will be bounded from above by the lane width

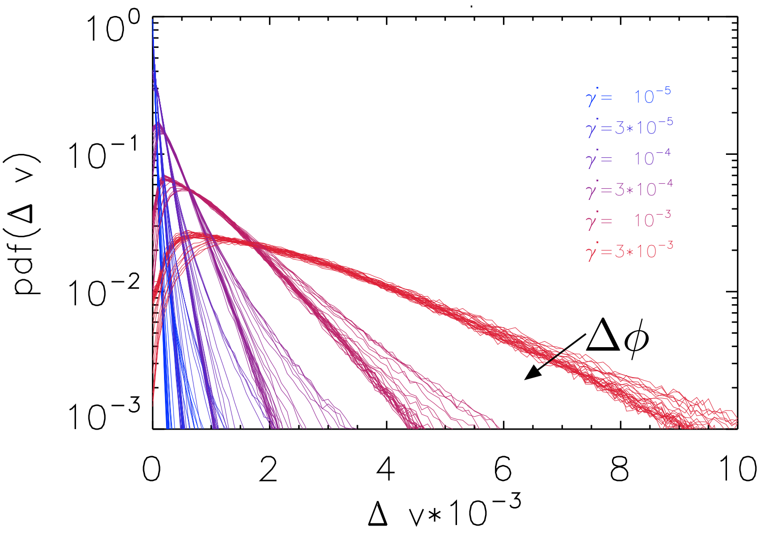

Figure 2.6: The probability distribution function of the relative velocity between particles for different strain rates (color) and different densities ranging from $\phi = 0.8424$ to $\phi = 1$.

if we perform our own simulations with mean field dissipation we recover the Olsson and Teitel correlation functions with their characteristic dip. We cannot fully explain why these two similar systems give such different correlation lengths, especially since most of their other behavior is very similar. However, in a tentative explanation we point to the fact non-affine motion is the source of dissipation in the Mean Field model, but not in the full Durian model. In section 6.1 we show that energy dissipation, which is caused by relative motion between the bubbles[7], sets the (second moment of the) distribution of relative velocities. Therefore it is not unlikely that the non-affine velocity is largely set by considerations of energy dissipation in the Mean Field model, but not in the full Durian model.

We note, however, that the mean field model was introduced as an approximation to the full Durian model under the assumption that it was a harmless computational simplification [27]. As we have shown that there is at least one significant difference between the two models we feel that it is highly preferable to use the full Durian model.

2.3.4 Δv-distributions

The role played by the non-affine velocity in the mean field model, that of source of energy dissipation, is played by the relative velocity in the full Durian

---

[7] in the full Durian model

model. Due to big differences in the energy supplied to systems of different density or strain rate, there are also big differences in the behavior of the relative velocity. As an example of this we show the probability distribution functions of a wide range of data in figure 2.6. Note the incredible difference in the fatness of the tails of the distributions. These differences lead to wildly different behavior in the systems, an aspect that we will explore in section 6.1.

Chapter 3

Scaling Model

In this section we will introduce an analytical scaling model to capture the variation of the shear stress, σ_{xy}, with the fixed packing fraction ϕ and applied strain rate $\dot{\gamma}$; the rheological curve, as we have called it above. This model is based on three coupled scaling relations for σ, $\dot{\gamma}$, and $\Delta\phi$. As we will discuss, these relations involve two additional variables: the average relative velocity between bubbles, Δv, and an effective strain, γ_{eff}, that we will explain in more detail below. The three scaling relations form a closed system and are therefore enough to express the three dependent variables - σ, γ_{eff} and Δv - in the two independent variables: $\dot{\gamma}$ and $\Delta\phi$.

Our scaling model is based on three assumptions:

1. The system is in power balance.
2. A flowing foam can be mapped to a static system that has been sheared through an effective strain γ_{eff}.
3. The stress as a function of γ_{eff} is given by the constitutive relation for sheared disordered spring networks.

Each of these assumptions will lead us to formulate an expression, these three expressions will be introduced below. For ease of reference we introduce the name 3E model for this model to denote expressions relating to Energy, Effective strain and Elasticity.

3.1 Ingredients

3.1.1 Power Balance

The first relation is the most fundamental: power balance. In steady state, all power that is put into the system by driving must also be dissipated by the viscous drag in the bubble contacts. If a system resists a strain rate $\dot{\gamma}$ with a stress σ, energy is supplied to that system at a rate of $P_{in} \sim \sigma\dot{\gamma}$. The rate of energy dissipation in the bubble contacts is given by $\mathbf{F}^v_{ij} \cdot \Delta\mathbf{v}_{ij}$ and since the viscous force itself scales with $\mathbf{\Delta v}$, Eq. 2.3, the dissipated power scales as $P_{out} \sim \Delta v^2$. This results in the following scaling relation:

$$\sigma\dot{\gamma} \sim \Delta v^2 \tag{3.1}$$

Note that this relation is only true when averaged over long timescales; on short timescales energy is temporarily stored in elastic deformations.

3.1.2 Effective Strain

Next, we would like to formulate an elasticity relation, expressing the elastic stress as a function of the strain. Since for our data we have $\sigma^{\mathrm{e}} \approx \sigma^{\mathrm{tot}}$, this will also be an expression for the total stress. In our flowing system, however, the strain is not a steady state quantity: it increases continuously with a constant strain rate $\dot{\gamma}$. Therefore we define an *effective strain*, γ_{eff}, instead. There are two ingredients. The first is to simply consider the compression of the system: a system compressed to a density $\Delta\phi$ beyond the jamming density ϕ_c will have strain that is proportional to $\Delta\phi$:

$$\gamma_{\mathrm{eff}} \sim \Delta\phi, \tag{3.2}$$

The second ingredient is to consider the actual strain that grows linearly in time with the strain rate. This strain effectively gets relaxed with each bubble rearrangement. If we can therefore deduce a timescale on which rearrangements take place, t_{rex}, we can determine the typical peak strain that can be built up between relaxation events: $\dot{\gamma}t_{\mathrm{rex}}$. The rearrangement timescale depends on the relative velocity between bubbles: if bubbles do not move relative to each other, they cannot rearrange and the rearrangement time is infinite. Therefore the rearrangement timescale scales inversely with Δv and we have:

$$\gamma_{\mathrm{eff}} \sim \frac{\dot{\gamma}}{\Delta v}. \tag{3.3}$$

We connect these two ingredients by assuming that both are valid, but each will dominate in different regimes. The static contribution, Eq. 3.2, dominates in the high density and/or low strain rate regime, while the dynamic contribution, Eq. 3.3, dominates in the low density and/or high strain rate regime.

3.1.3 Elasticity Relation

We can now formulate an elasticity relation as the third ingredient: a dependence of the stress on the effective strain. We will assume that we can use the results from static jamming for this. In the linear response regime we have, by definition, $\sigma = G\gamma$, G being the shear modulus. The static jamming result for

G for harmonic particles is $G \sim \Delta\phi^{1/2}$. Therefore, for small γ_{eff} we assume that we have:

$$\sigma \sim \Delta\phi^{1/2}\gamma_{\text{eff}}. \tag{3.4}$$

For larger strains, outside the linear response regime, we use another static jamming result. Matthieu Wyart *et al.* have found that quadratic scaling in γ, and independent of density, takes over for large strains [36]. Adapting that to our model, using γ_{eff} in stead of γ, leads to

$$\sigma \sim \gamma_{\text{eff}}^2. \tag{3.5}$$

For now we will simply assume that Eq. 3.4 holds for small γ_{eff} and Eq. 3.5 for large γ_{eff}, though we will formulate a single expression for the stress as a function of the effective strain later on. The two relations introduced above will then be the asymptotic behavior of that function for small, respectively large, γ_{eff}.

3.2 Regimes

As indicated above, we can combine these scaling relations into a closed system to express σ as a function of $\dot{\gamma}$. However, since a number of the scaling relations, for example Eq. 3.2, are valid only in a certain regime, the same is true for the resulting systems of equations. Since two of the ingredients, effective strain and elasticity relation, consist of two regimes each, there is a total of four systems of equations, each describing the behavior in a certain region of our $\Delta\phi, \dot{\gamma}$-parameter space.

For example: if we look at strain rates that are ‘very high’ and densities that are ’small’[1], we see that the dynamic strain, Eq. 3.3 will be ‘large’, while the static strain, Eq. 3.2, will not. The effective strain will therefore be dominated by the dynamic contribution. Likewise, the stress will be dominated by the quadratic contribution, Eq. 3.5, which scales faster with γ_{eff}, and therefore $\dot{\gamma}$, than the linear contribution, Eq. 3.4. We call this combination of parameters the Critical regime. We therefore have the following system of equations in the Critical regime:

$$\begin{aligned} \sigma\dot{\gamma} &\sim \Delta v^2 && (3.6)\\ \gamma_{\text{eff}} &\sim \frac{\dot{\gamma}}{\Delta v} && (3.7)\\ \sigma_{xy} &\sim \gamma_{\text{eff}}^2 && (3.8) \end{aligned}$$

This system can be solved for either σ, Δv or γ_{eff} by simple substitution. Here we will demonstrate solving for σ; solving for Δv or γ_{eff} is completely analogous and we will only present the results below. To find an expression

---

[1] the definition of ‘very high’ and ‘small’ will turn out to depend on each other: the bigger $\Delta\phi$, the bigger $\dot{\gamma}$ has to be to be considered ‘large’.

	Critical	Transition
elasticity	$\sigma \sim \gamma_{\mathrm{eff}}^2$	$\sigma \sim \Delta\phi^{1/2}\gamma_{\mathrm{eff}}$
effective strain	$\gamma_{\mathrm{eff}} \sim \dot\gamma/\Delta v$	$\gamma_{\mathrm{eff}} \sim \dot\gamma/\Delta v$
rheology	$\sigma \sim \dot\gamma^{1/2}$	$\sigma \sim \Delta\phi^{1/3}\dot\gamma^{1/3}$
range	$\dot\gamma > \Delta\phi^2$	$\dot\gamma > \Delta\phi^{7/2}$
	$\dot\gamma > \Delta\phi^4$	$\dot\gamma < \Delta\phi^2$
	Yield	Dense
elasticity	$\sigma \sim \Delta\phi^{1/2}\gamma_{\mathrm{eff}}$	$\sigma \sim \gamma_{\mathrm{eff}}^2$
effective strain	$\gamma_{\mathrm{eff}} \sim \Delta\phi$	$\gamma_{\mathrm{eff}} \sim \Delta\phi$
rheology	$\sigma \sim \Delta\phi^{3/2}$	$\sigma \sim \Delta\phi^2$
range	$\dot\gamma < \Delta\phi^{7/2}$	$C < \Delta\phi$
	$C > \Delta\phi$	$\dot\gamma < \Delta\phi^4$

Table 3.1: The four rheological regimes with their definitions, results and ranges of validity.

for the stress, we start by taking the dependence of the stress on the effective strain, in which we substitute the expression for the effective strain:

$$\sigma_{xy} \sim \frac{\dot\gamma^2}{\Delta v^2} \tag{3.9}$$

Then we rewrite Eq. 3.6 to an expression for Δv:

$$\Delta v \sim \sqrt{\sigma_{xy}\dot\gamma}, \tag{3.10}$$

which we substitute to yield:

$$\sigma_{xy} \sim \frac{\dot\gamma^2}{\sigma_{xy}\dot\gamma} \tag{3.11}$$

or,

$$\sigma_{xy} \sim \dot\gamma^{1/2}. \tag{3.12}$$

This means that for ‘high enough’ strain rates and ‘low enough’ densities we find density independent shear thinning behavior. We summarise the full results for this regime, giving not only σ, but also Δv and γ_{eff} as a function of $\dot\gamma$ and $\Delta\phi$ below:

$$\begin{cases} \sigma\dot\gamma \sim \Delta v^2 \\ \gamma_{\mathrm{eff}} \sim \frac{\dot\gamma}{\Delta v} \\ \sigma_{xy} \sim \gamma_{\mathrm{eff}}^2 \end{cases} \Rightarrow \begin{cases} \Delta v \sim \dot\gamma^{3/4} \\ \gamma_{\mathrm{eff}} \sim \dot\gamma^{1/4} \\ \sigma_{xy} \sim \dot\gamma^{1/2} \end{cases} \tag{3.13}$$

In a similar way we can define three other regimes, that we call the Transition, Yield and Dense regime respectively, we will explain this terminology below.

Yield Regime The Yield regime is the opposite of the Critical regime: it is the regime we access for high density and low strain rate. This means that the Yield contribution to the effective strain will dominate the dynamic one and the stress will be dominated by the linear behavior:

$$\begin{cases} \sigma\dot{\gamma} \sim \Delta v^2 \\ \gamma_{\text{eff}} \sim \Delta\phi \\ \sigma_{xy} \sim \Delta\phi^{1/2}\gamma_{\text{eff}} \end{cases} \Rightarrow \begin{cases} \Delta v \sim \Delta\phi^{3/4}\dot{\gamma}^{1/2} \\ \gamma_{\text{eff}} \sim \Delta\phi \\ \sigma_{xy} \sim \Delta\phi^{3/2} \end{cases} \tag{3.14}$$

As indicated by its name, the stress in the Yield regime is independent of the strain rate and depends solely on the density.

Transition Regime Surprisingly, a third regime can be found 'in between' the Critical and Yield regimes. If the density is low enough that the effective strain is dominated by the dynamic contribution, but high enough that we can still use the linear expression for the elasticity expression we are in what we call the Transition regime:

$$\begin{cases} \sigma\dot{\gamma} \sim \Delta v^2 \\ \gamma_{\text{eff}} \sim \dot{\gamma}/\Delta v \\ \sigma_{xy} \sim \Delta\phi^{1/2}\gamma_{\text{eff}} \end{cases} \Rightarrow \begin{cases} \Delta v \sim \Delta\phi^{1/6}\dot{\gamma}^{2/3} \\ \gamma_{\text{eff}} \sim \Delta\phi^{-1/6}\dot{\gamma}^{1/3} \\ \sigma_{xy} \sim \Delta\phi^{1/3}\dot{\gamma}^{1/3} \end{cases} \tag{3.15}$$

Just as the ingredients for the Transition regime are shared partially with the Critical and partially with the Yield regime, so does the rheology show both $\dot{\gamma}$-dependence, as in the Critical regime, and $\Delta\phi$-dependence, as in the Yield regime. The existence of this regime is a novel and surprising prediction of our scaling model.

Dense Regime The fourth and last regime is even more curious than the Transition regime. We call this regime the Dense regime because it occurs for densities that are very high. At very high densities, not only does the yield strain dominate the dynamic strain, but the non-linear term in the elasticity relation, which is quadratic in the strain and therefore in the density[2], dominates the linear contribution, which scales only as $\Delta\phi^{3/2}$:

$$\begin{cases} \sigma\dot{\gamma} \sim \Delta v^2 \\ \gamma_{\text{eff}} \sim \Delta\phi \\ \sigma_{xy} \sim \gamma_{\text{eff}}^2 \end{cases} \Rightarrow \begin{cases} \Delta v \sim \Delta\phi\ \dot{\gamma}^{1/2} \\ \gamma_{\text{eff}} \sim \Delta\phi \\ \sigma_{xy} \sim \Delta\phi^2 \end{cases} \tag{3.16}$$

---

[2] because the yield contribution to the strain is proportional to the density

As we will show in section 4.3, the densities for which are actually in the Dense regime are so large that the Dense regime is irrelevant in practice.

3.2.1 Crossovers

We can now also make the definitions of the regimes more precise, defining what 'large strain rate' or 'low enough density' mean precisely. For example, If we compare the Yield and the Transition regime, we see that they agree on the elasticity relation:

$$\sigma_{xy} \sim \Delta\phi^{1/2}\gamma_{\mathrm{eff}}, \tag{3.17}$$

but do not agree on which of the two contributions to the effective strain dominates: if the yield contribution dominates we are in the yield regime but if the dynamic contribution dominates we are in the Transition regime. This means that we crossover from one to the other around the point where these two contributions are equal:

$$\frac{\dot{\gamma}}{\Delta v} \sim \Delta\phi. \tag{3.18}$$

We rewrite this expression by substituting the expression for Δv of Eq. 3.10:

$$\frac{\dot{\gamma}}{\left(\sigma_{xy}\dot{\gamma}\right)^{1/2}} \sim \Delta\phi. \tag{3.19}$$

For σ_{xy} we can now enter either the Yield or the Transition expression as both will be equal exactly at the crossover[3]. Here we pick the simpler expression of the two, the Yield one, Eq. 3.14:

$$\frac{\dot{\gamma}}{\left(\Delta\phi^{3/2}\dot{\gamma}\right)^{1/2}} \sim \Delta\phi, \tag{3.20}$$

or:

$$\dot{\gamma} \sim \Delta\phi^{7/2}. \tag{3.21}$$

So, if $\dot{\gamma} > \Delta\phi^{7/2}$ the dynamic contribution to the effective strain dominates and we are in the Transition regime. Conversely, if $\dot{\gamma} < \Delta\phi^{7/2}$, the yield contribution to the effective strain dominates and we are in the Yield regime.

An equivalent derivation starts at the expressions for the stress in both regimes. Exactly at the crossover these two expressions must be equal:

$$\Delta\phi^{3/2} \sim \Delta\phi^{1/3}\dot{\gamma}^{1/3} \rightarrow \dot{\gamma} \sim \Delta\phi^{7/2}, \tag{3.22}$$

which is the same as above, as it should be. Since the second approach is computationally easier, we will present only that approach below for the other crossovers. The results are presented on the last rows of table 3.1.

---

[3] This is the case because the only difference in their derivation is the expression we use for the effective strain, but these are equal at the crossover by construction. As a consequence, the stresses will be equal at the crossover as well.

Transition to Critical By comparing the predictions for the stress in the Transition and Critical regimes, we immediately obtain that the two regimes have their crossover when:

$$\Delta\phi^{1/3}\dot{\gamma}^{1/3} \sim \dot{\gamma}^{1/2} \Rightarrow \dot{\gamma} \sim \Delta\phi^{2} \tag{3.23}$$

Combining this result with the result for the crossover from the Yield to the Transition regime above we see that for small enough densities, so that $\Delta\phi^{7/2} < \Delta\phi^{2}$, increasing the strain rate will bring one from the Yield first to the Transition and then to the Critical regime.

Yield to Dense From the Yield regime we can also, theoretically at least, crossover to the Dense regime. This happens when the linear and non-linear contributions to the elasticity balance, but the effective strain is dominated by the yield contribution. Again, we find the crossover by equating the stress in the two regimes:

$$\Delta\phi^{3/2} \sim \Delta\phi^{2} \rightarrow \Delta\phi \sim 1. \tag{3.24}$$

Within this scaling model, we cannot derive the value of this density, though we will find below that it is too large to be relevant. This crossover density will be the same density as the one mentioned above, below which the transition from Yield to Transition to Critical was valid.

Dense to Critical If we are at very high density, higher than the crossover density identified above, we start out in the Dense regime for low strain rate. Increasing the strain rate will still bring us to a different regime: the Critical regime. For any fixed $\Delta\phi$, the dynamic contribution to the effective strain will eventually surpass the yield contribution if the strain rate is high enough. To find this crossover strain rate we equate the stresses in the Dense and Critical regimes:

$$\Delta\phi^{2} \sim \dot{\gamma}^{1/2} \rightarrow \dot{\gamma} \sim \Delta\phi^{4} \tag{3.25}$$

A qualitative graphic depicting all four regimes and their crossovers in a phase-diagram-like way is also depicted in figure 3.1 **a**. Since, as discussed, we cannot realistically access the whole phase space - specifically, the Dense regime is out of reach - a qualitative graphic depicting the accessible regimes is also shown in figure 3.1 **b**.

3.3 Rescaling Flow Curves

Now that we have predictions for the behavior of the stress as a function of the strain rate, we can test these predictions by plotting the results of our simulations and seeing whether the data agrees with our predictions or not.

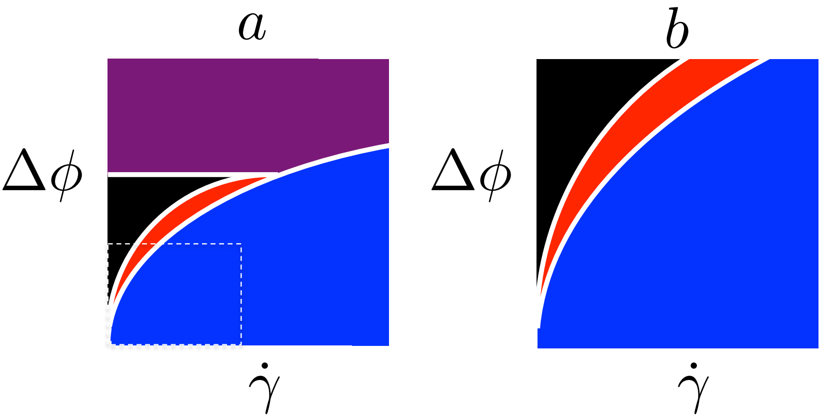

Figure 3.1: **a**: effective phase diagram of the Yield (black), Transition (red), Critical (blue) and Dense (purple) regimes as a function of $\dot\gamma$ and $\Delta\phi$. **b**: the part of this phase diagram that is realistically accessible, demarcated by the dashed line in panel **a**.

3.3.1 Collapse Plots

In principle, one could try to plot all stress vs strain rate data in a single collapsed plot - i.e. with no further $\Delta\phi$ dependence - by plotting not σ vs. $\dot\gamma$ but $\tilde\sigma = \sigma/\Delta\phi^{\Delta}$ vs. $\tilde{\dot\gamma} = \dot\gamma/\Delta\phi^{\Gamma}$ with Δ and Γ well-defined exponents. However, our model suggests that our data can be in more than two regimes, each with their own $\Delta\phi$ dependence in the rheology, and there are only two axes that can be rescaled. Therefore this may not be possible in general. At best it is possible to get collapse in two regimes.

Yield to Transition For example, if we want to attain collapse in the Yield and Transition regimes we start by looking at the stress. Since the stress depends only on the density but not on the strain rate in the Yield regime via $\sigma \sim \Delta\phi^{3/2}$, we can use the expression for the stress in the Yield regime to derive our exponent Δ. If we take $\Delta = 3/2$ then $\tilde\sigma = \sigma/\Delta\phi^{3/2} = 1$, which is independent of $\Delta\phi$. Next, we consider the strain rate. Since the crossover between the Yield and the Transition rate depends only the strain rate via $\dot\gamma \sim \Delta\phi^{7/2}$, we see that by taking $\Gamma = 7/2$ we get $\tilde{\dot\gamma} = \dot\gamma/\Delta\phi^{7/2} = 1$ as location of the crossover, this is again independent of the density.

In the process of deriving Δ and Γ, we made sure that the stress in the Yield regime and the crossover from the Yield to the Transition regime collapse. To get full collapse of the data in the Yield and Transition regimes, we also need to get collapse in the Transition regime itself. And indeed we do get collapse:

In the Transition regime we have:

$$\sigma \sim \Delta\phi^{1/3}\dot\gamma^{1/3} \sim \tilde{\dot\gamma}^{1/3}\Delta\phi^{3/2} \Rightarrow \tilde\sigma \sim \tilde{\dot\gamma}^{1/3} \tag{3.26}$$

Since we can write $\tilde\sigma$ as a function of $\tilde{\dot\gamma}$ without $\Delta\phi$-dependence, we get collapse in the Transition regime as well. Note that this is a mathematical necessity: the crossover between the Yield and Transition is, by construction, the point where the Yield and Transition stresses are equal. If this point is independent of density (due to our choice of Γ) and the Yield stress itself is independent of density (due to our choice of Δ) then the Transition stress must be independent of density as well.

Theoretically, it is possible that this combination of Γ and Δ also results in collapse of the stress in the Critical regime. This is not mathematically required, though, and there are no more free parameters that we can adjust. All we can do is check whether the values of Γ and Δ that we derived for the Yield and Transition regimes also happen to lead to collapse in the Critical regime. In fact, they do not. In the Critical regime we have:

$$\sigma \sim \dot\gamma^{1/2} \sim \tilde{\dot\gamma}^{1/2}\Delta\phi^{7/4} \Rightarrow \tilde\sigma \sim \tilde{\dot\gamma}^{1/2}\Delta\phi^{1/4} \tag{3.27}$$

This expression *does* depend on density and therefore the stress in the Critical regime will not collapse when plotting $\tilde\sigma = \sigma/\Delta\phi^{3/2}$ vs. $\tilde{\dot\gamma} = \dot\gamma/\Delta\phi^{7/2}$.

Transition and Critical If we do want the stress to collapse in the Critical regime, we need to pick different values of Γ and Δ. We can even choose to get collapse in a second regime as well. Since the Transition and Critical regimes are adjacent, it is logical to consider these two regimes first. The crossover between the Transition and Critical regimes occurs when $\dot\gamma \sim \Delta\phi^2$, which implies that $\tilde{\dot\gamma} = \dot\gamma/\Delta\phi^2$. Rewriting our prediction for the scaling of the stress in terms of $\tilde{\dot\gamma}$ we obtain:

$$\sigma \sim \dot\gamma^{1/2} \sim \tilde{\dot\gamma}^{1/2}\Delta\phi \Rightarrow \sigma/\Delta\phi \sim \tilde{\dot\gamma}^{1/2}\ , \tag{3.28}$$

which suggests that $\tilde\sigma = \sigma/\Delta\phi$. Consistently, we reach the same conclusion for the transition regime, where

$$\sigma \sim \Delta\phi^{1/3}\dot\gamma^{1/3} \sim \tilde{\dot\gamma}^{1/3}\Delta\phi \Rightarrow \sigma/\Delta\phi \sim \tilde{\dot\gamma}^{1/3}\ . \tag{3.29}$$

Yield and Critical We can also plot the data to get collapse in the Yield and Critical regimes. At first that may seem strange because these regimes are not adjacent, but in fact there is no problem with having a collapsed Yield and Critical regime, there will just be a non-collapsed Transition regime in between. We again note that the stress in the Yield regime only depends on the density and we can therefore get collapse only if we take $\tilde\sigma_{xy} \sim \sigma_{xy}/\Delta\phi^{3/2}$ as above. We substitute this into the stress in the Critical regime to find:

$$\frac{\tilde\sigma}{\Delta\phi^{3/2}} \sim \dot\gamma^{1/2} \Rightarrow \tilde\sigma \sim \left(\frac{\dot\gamma}{\Delta\phi^{3}}\right)^{1/2} \Rightarrow \tilde{\dot\gamma} \sim \frac{\dot\gamma}{\Delta\phi^{3}}\ . \tag{3.30}$$

Regime Combination	rescaled axes
Critical and Transition	$\sigma/\Delta\phi$ vs. $\dot{\gamma}/\Delta\phi^2$
Yield and Transition	$\sigma/\Delta\phi^{3/2}$ vs. $\dot{\gamma}/\Delta\phi^{7/2}$
Yield and Critical	$\sigma/\Delta\phi^{3/2}$ vs. $\dot{\gamma}/\Delta\phi^3$

Table 3.2: Prescriptions of what to plot for collapse in the indicated regimes.

Strain Rate		Density				
$3 \cdot 10^{-3}$	×	0.8424	0.8436	0.8448	0.849	0.9
10^{-3}	□	0.8426	0.8438	0.845	0.85	0.92
$3 \cdot 10^{-4}$	△	0.8428	0.8440	0.8455	0.855	0.94
10^{-4}	◇	0.8430	0.8442	0.846	0.86	0.96
$3 \cdot 10^{-5}$	∗	0.8432	0.8444	0.847	0.87	0.98
10^{-5}	+	0.8434	0.8446	0.848	0.88	1.0

Table 3.3: In most plots in this thesis, strain rates are labeled with symbols and densities are labeled with colours as indicated in this table.

The results for all three regime combinations are also shown in table 3.2.

3.3.2 Results

Data Range and Legend

Now that we know how to plot our numerical data to get collapse onto master curves according to our scaling model, we can use this to finally test our model by comparing its predictions with the results from the simulations that we discussed in chapter 2. Unless we mention otherwise, all plots use six different strain rates. The highest strain rate that we use is $3 \cdot 10^{-3}$, which is chosen so that $\sigma^{\text{el}} > \sigma^{\text{visc}}$ as discussed in section 2.3.1. The lowest strain rate that we use is 10^{-5}. Unless otherwise specified, these six strain rates are identified with the same symbols as shown in table 3.3.

We have simulated these six strain rates in systems of 30 different densities, ranging from just above the jamming density[4] of 0.8423 to very high densities, $\phi = 1$. Note that a density of one does not mean that the entire system is covered with bubbles as overlaps between two bubbles are counted twice. Unless otherwise specified, these 30 densities are identified with colours ranging from blue for low densities to red for high densities, see table 3.3. The large amount of densities makes the difference in colour between adjacent densities subtle at best. The purpose of this colouring scheme is to identify whether

---

[4] We will discuss how we came to our value of ϕ_c below

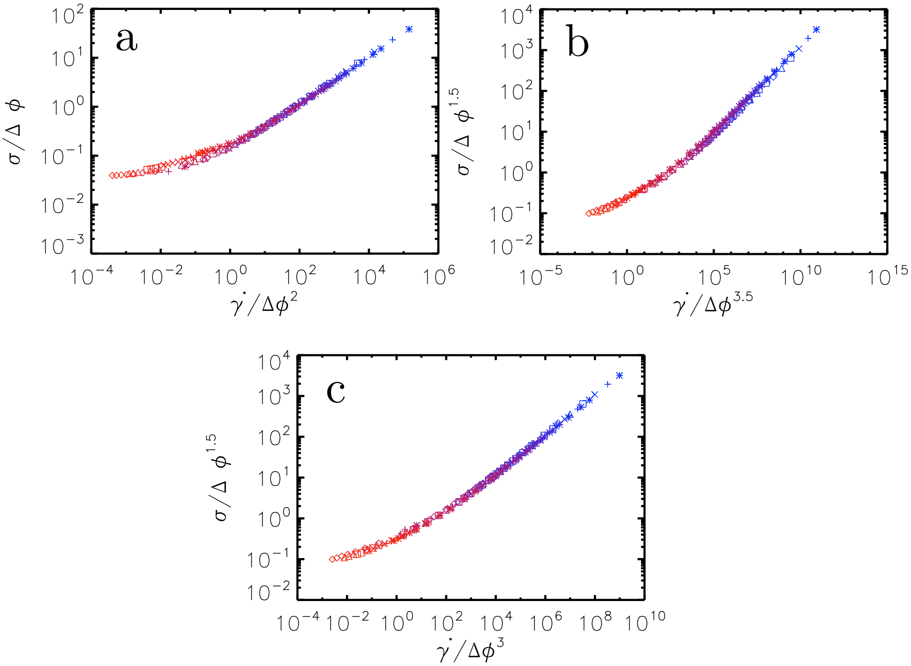

Figure 3.2: Plot of our simulation data. a) Rescaled for collapse in the Transition and Critical regime. b) Rescaled for collapse in the Yield and Transition regime. c) Rescaled for collapse in the Yield and Critical regime on the bottom. A legend is given in table 3.3

certain data points correspond to 'high' or 'low' density. In a few plots it will be necessary to identify the exact value of the density; a different color-and-symbol-scheme will be employed there.

Collapse Plots

Figure 3.2 shows the simulation data plotted for collapse in the three different combinations of regimes: **a** collapse in the Critical and Transition regimes, **b** the Transition and Yield regimes, and **c** the Critical and Yield regimes. All three graphs show decent collapse, and we might conclude from this that our model works as well, but there are two caveats: non-collapsing regimes and logarithmic axes.

First, our model does not just predict that we will get collapse in two regimes by plotting the data in a certain way, as determined above, but also that we will *not* get collapse in the third regime; strong non-collapse is not evident in either of the three graphs of figure 3.2, although deviations are most visible in the regime where no collapse is expected. Secondly, due to our logarithmic axes and many decades of data, it is quite possible for large deviations to be hard to see: being a factor of 1.5 or 2 off is not very visible on 6 decades of logarithmic axes. In this section we will discuss both issues, though thorough treatment of especially the first one will need moving beyond a scaling model, and will therefore have to wait for the next chapter in which we do just that.

The Critical Regime

We start by looking at the Critical regime and note that the power law asymptote on the right of the data in each graph, i.e. the Critical regime, looks decently collapsed in all three panels of figure 3.2. However, it should not collapse in panel **b**: only the Transition and Yield regimes should collapse there. In fact, if we would get collapse in the Critical regime in the Yield and Transition plot of panel **b**, that implies a certain β: if the stress does not depend on $\Delta\phi$ in the Critical regime, which is a basic assumption of critical scaling theory, then the collapse when plotting $\tilde{\sigma}$ vs $\tilde{\dot{\gamma}}$ means that

$$\tilde{\sigma} \sim \tilde{\dot{\gamma}}^{\beta} \Rightarrow \sigma \sim \Delta\phi^{3/2-7\beta/2}\dot{\gamma}^{\beta} \tag{3.31}$$

is independent of $\Delta\phi$ and therefore $\beta = \frac{3}{2}/\frac{7}{2} \approx 0.43$. On the other hand, of course, collapse in panels **a** and **c** implies that $\beta = 1/2$. Obviously, both cannot be true. While 0.43 is clearly not the same as 1/2, they may also not be different enough that plotting data for which $\beta = 1/2$ in the way of panel **b** results in clearly bad collapse. The conclusion is then that judging a straight line on logarithmic axes is not the best way to determine whether data has collapsed onto a power law master curve or not: we need a more discriminating method.

Such a method is easily devised: if we divide out the expected power law - $\sigma \sim \dot{\gamma}^{1/2}$, $\sigma \sim \dot{\gamma}^{0.43}$ or $\sigma \sim \dot{\gamma}^{\beta}$ more generally - the data should asymptote towards a horizontal line. Horizontal lines are easier to identify by eye, but more importantly they allow us to switch to a linear, instead of a logarithmic, vertical axis so that deviations of a factor 1.5 or 2 can be easily detected.

In panels **a** and **b** of figure 3.3, we plot $\sigma/\dot{\gamma}^{\beta}$ as a function of $\dot{\gamma}/\Delta\phi^{\Gamma}$ (in **a** using the values for the Critical and Transition regime: $\beta = 0.50$ and $\Gamma = 2$, in **b** using the values for the Yield and Transition regime: $\beta = 0.43$ and $\Gamma = 3.5$) In neither of these two panels does the data collapse to a flat asymptote on the right and therefore neither $\beta = 0.50$ nor $\beta = 0.43$ is the 'real' β that describes the Critical regime of our simulation data, though we can clearly see that the model prediction of $\beta = 1/2$ leads to better collapse than $\beta = 0.43$. We can now try to find the β for which collapse is optimal. There is the small problem of what Γ to take for the horizontal axis, but since displacing a horizontal line horizontally does not affect the degree of collapse we pick our model value of $\Gamma = 2$ here. From panel **c** of figure 3.3, we see that an exponent of $\beta = 0.47$ gives much better collapse than either $\beta = 0.50$ *or* 0.43.

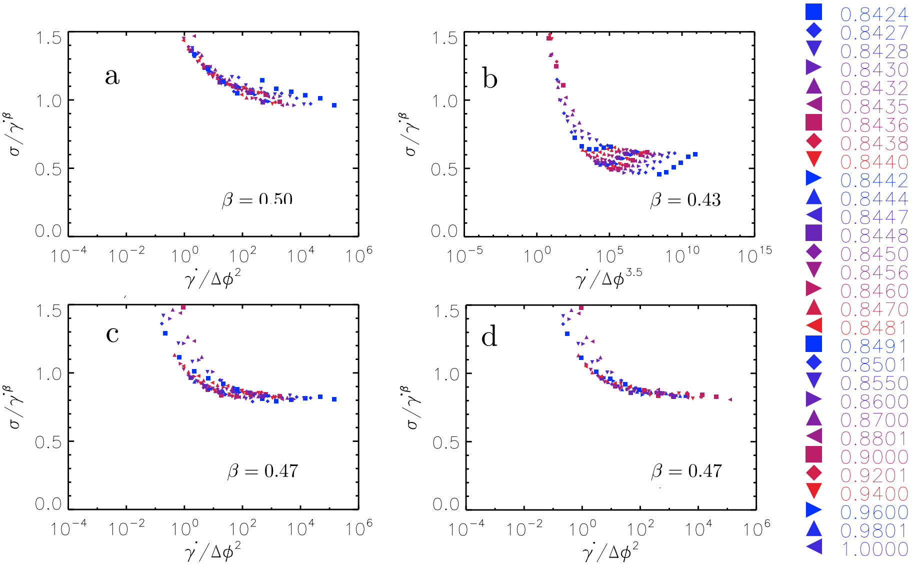

Figure 3.3: The stress in our system with specific power laws of exponent β divided out. The legend indicates which density corresponds to which color-shape combination.

In our opinion, this is a success for our model: with no fit parameters we have predicted the power law exponent of the rheological curve, β, of soft viscous particles to within 10%. The discrepancy may have a number of different causes: higher order terms in the elasticity expression, the presence of non-zero viscous stresses, adjustments to the effective strain or finite size effects. In fact it is quite remarkable that a scaling model with such limited and basic ingredients gets the exponent right to such a high degree of accuracy.

One final caveat is the claim of zero fit parameters above; this is not strictly true: the critical jamming density ϕ_j is not predicted by the model nor is it enforced externally. We have determined that $\phi_j = 0.8423 \pm 0.001$ by determining where our collapse plots look good. However, within this range, β is not sensitive to ϕ_j as we show in figure 3.3 **d**: changing ϕ_j slightly, from 0.8423 to 0.8433 does not change the fact that $\beta = 0.47$ results in a flat residue.

Yield and Transition Regime

Now we turn our attention to the Yield regime. Since we predict that the stress is independent of the strain rate in this regime, the standard collapse plots of figure 3.2 are already have the expected Yield behavior 'divided out': data in the Yield regime should already be horizontal. In none of the three representations, however, do we see a clear horizontal asymptote on the left.

There are two possible explanations for this: the Yield regime does not exist or our data is not dense and/or slow enough to be in the Yield regime.

We have two reasons to think that the second explanation is correct. First of all, the existence of a yield stress in soft viscous systems is fairly well-established and seen in many previous simulations and experiments [11,36,37]. Its existence is not a novel claim of our model, and we actually interpreted the prediction of a yield stress by our model as one of the first positive signs regarding its validity. Secondly, we see a clear flattening out of the data on the left of the curves. While we cannot be sure that this flattening out does not stop before it reaches the horizontal[5] it is certainly consistent with our predictions of a yield stress.

But if there is indeed not much data that is squarely in the Yield regime, why is there a clearly not-fully-collapsing cloud of points on the Critical-and-Transition data plot, figure 3.2 **a**? We claim that this is because the crossover from the Yield to the Transition regime is very soft, meaning that there is a large region of parameter space where the rheological behavior cannot be viewed as either purely Yield or purely Transition but is a mixture between the two. Since only data that is purely in the Transition (or Critical) regime will collapse, this mixed data will not collapse. We will substantiate this claim in the next chapter.

3.3.3 Conclusion

Our 3E scaling model is based on three simple assumptions and includes no fit parameters. Yet, the 3E model is able to predict the scaling of the stress surprisingly well, even though it does not capture the Critical exponent, β, exactly. There are also some questions, for example in which of the three regimes a certain data point is located, that the current 3E model can not answer. Therefore, we will also develop a fully quantitative model, that does not just predict the scaling, but also the value of the stress, in the next chapter.

---

[5] or, in fact, proceeds beyond it and curves up again, although that seems even less likely

Chapter 4

Scaling Model under Scrutiny

In the previous chapter we have seen that our 3E model makes correct predictions for the scaling of the stress with the strain rate and the density. To test the 3E model more thoroughly, we are going to test the individual assumptions that went into the model in detail in this chapter.

4.1 Ingedrients in Full Form

In order to test all three assumptions and their resulting ingredients - power balance, the concept of an effective strain and a constitutive elasticity relation - it is advantageous to formulate these ingredients not in scaling form as we have done above, but in their full form, including all constants and prefactors.

Power Balance The first ingredient of our the 3E model is power balance: the power that is put into the system, P_i, should, when averaged over long times, be the same as the power dissipated by the system, P_d, or $\langle P_i \rangle_t = \langle P_d \rangle_t$. If L_x and L_y are the linear dimensions of our system then the power that is put into the system is given by the force, $\sigma_{xy} L_x$, multiplied by the driving velocity, $\dot{\gamma} L_y$, or $P_i = L_x L_y \sigma_{xy} \dot{\gamma}$. The dissipated power is given by the average power dissipated per contact times the total number of contacts. From our microscopic force law we derive that the power dissipated in the contact between bubble i and j is given by $b \left(\Delta v_{ij}\right)^2$ with b the microscopic viscous force constant and Δv_{ij} the absolute value of the velocity difference between bubble i and j. Since the total number of contacts is given by $NZ/2$, we get for the dissipated power: $P_d = NZ/2 \left\langle b \left(\Delta v\right)^2 \right\rangle_{ij}$, in which $\langle\rangle_{ij}$ denotes averaging over contacts. The full equation for power balance is then given by:

$$L_x L_y \dot{\gamma} \langle \sigma_{xy} \rangle_t = \frac{Nb}{2} \langle Z \rangle_t \langle \Delta v^2 \rangle_{t,ij} \tag{4.1}$$

Effective Strain The next set of ingredients of our scaling model is the definition of three strains: the yield strain γ_{y}, the dynamic strain γ_{dyn} and the effective strain γ_{eff} that is a linear combination of the other two. The yield strain is simply proportional to the compression $\Delta\phi$. If we call the constant of proportionality A, we get $\gamma_{\mathrm{y}} = A\Delta\phi$. The dynamic strain is a measure for the strain that builds up in the system between rearrangements and is proportional to the product of the strain rate and the rearrangement timescale. The rearrangement timescale is proportional to the time that two bubbles that are in contact take to move apart, i.e. move over a distance that is proportional to their average diameter. Since the average speed with which two bubbles move apart is given by $\langle \Delta v \rangle_{t,ij}$, the rearrangement timescale is proportional to $d/\langle \Delta v \rangle_{t,ij}$. Combining this and subsuming all these proportionalities into one constant, B, this yields $\gamma_{\mathrm{dyn}} = B\dot{\gamma}d/\langle \Delta v \rangle_{t,ij}$.

The effective strain, as a linear combination of the yield and dynamic strains, can be written as $\gamma_{\mathrm{eff}} = C\gamma_{\mathrm{y}} + D\gamma_{\mathrm{dyn}}$. In principle, this yields $\gamma_{\mathrm{eff}} = CA\Delta\phi + DB\dot{\gamma}d/\langle \Delta v \rangle_{t,ij}$. However, as long as we cannot measure the yield, dynamic and effective strains *directly* - see section 4.5.2 - we have no information about their exact magnitude. Therefore, the only relevant parameter is one that sets the *relative* magnitude of the two contributions to the effective strain, we will call this parameter B_{eff}:

$$\gamma_{\mathrm{y}} = \Delta\phi \tag{4.2}$$

$$\gamma_{\mathrm{dyn}} = \frac{\dot{\gamma}d}{\langle \Delta v \rangle_{t,ij}} \tag{4.3}$$

$$\gamma_{\mathrm{eff}} = B_{\mathrm{eff}}\gamma_{\mathrm{y}} + \gamma_{\mathrm{dyn}} \tag{4.4}$$

Elasticity Relation The final ingredients of the scaling model are the elasticity equations that link the stress to the effective strain and so close the system of equations. If we assume that, for small effective strain, we can use the static results replacing the strain with our effective strain, we come to the conclusion that $\sigma^{el}_{xy} = G\gamma^{xy}_{\mathrm{eff}} = A_1 k \Delta\phi^{1/2}\gamma^{xy}_{\mathrm{eff}}$, the A_1 being a numerical constant of proportionality. This leads to a problem for the shear stress though: in the jamming limit, $\Delta\phi \downarrow 0$, the stress goes to zero. According to Wyart *et al.* [36], there is a second contribution to the shear stress in spring networks: one that is quadratic in the size of the strain. Therefore we assume that the dependence of the shear stress on the effective strain has two regimes here as well: one for small effective strain and/or large $\Delta\phi$, in which the static contribution is dominant, and one for large effective strain and/or small $\Delta\phi$, in which Wyart's contribution is dominant. If we want to write a single expression that combines these two contributions, a simple addition,

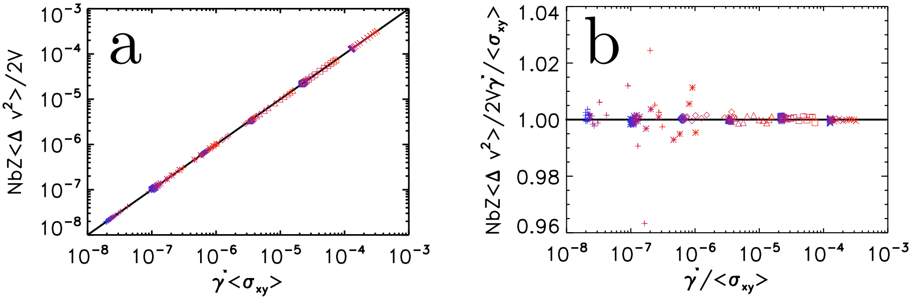

Figure 4.1: **a**: Power input, $L_x L_y \langle \sigma_{xy} \rangle \dot{\gamma}$, vs. dissipated power, $ZNb \langle \Delta v^2 \rangle$. **b**: Ratio of power input and dissipated power vs. dissipated power. The black line represents expected behavior. Colors and symbols indicate density and strain rate as in in table 3.3.

like $\sigma \sim \Delta\phi^{1/2}\gamma_{\text{eff}} + |\gamma_{\text{eff}}|\gamma_{\text{eff}}$, may respect the symmetry, but is not analytic[1]. While we *want* the expression to be non-analytic in the critical jamming point, it needs to be analytic outside of it. We will use the simplest form that is analytic everywhere outside the critical point and respects the symmetries of the system [33]:

$$\sigma_{xy}^{el} = A_1 k \Delta\phi^{1/2} \gamma_{\text{eff}}^{xy} \sqrt{1 + A_2^2 \frac{\gamma_{\text{eff}}^{xy2}}{\Delta\phi}} \tag{4.5}$$

4.2 Testing Power Balance

Power balance is such a fundamental concept that any discrepancy between the simulation results and our formulation of power balance must be interpreted as a problem with the simulations. In this section we will show that the simulations do indeed satisfy power balance. We can test the expression for power balance, Eq. 4.1, directly, because it contains no undetermined coefficients, only known quantities. The values of L_x, L_y, N and b are imposed externally. The situation for Z is slightly more complex. Z is *not* imposed by us, but can be straightforwardly measured form the simulations.

In order to test the expression for power balance we plot the power that is put in to the system, $P_i = L_x L_y \langle \sigma_{xy} \rangle \dot{\gamma}$, versus the total dissipated power, $P_d = ZNb \langle \Delta v^2 \rangle$ in figure 4.1. Power balance predicts that these two are equal: a scatter plot of P_i vs. P_d should result in a straight line with a slope of 1. As figure 4.1 **a** shows, that is indeed the case. Due to the logarithmic scale on the axes of figure 4.1 **a**, small deviations that might exist would be hard to see. Therefore, we also plot the ratio of energy input to energy output, P_i/P_d,

---

[1] another possible formulation, $\sigma \sim \Delta\phi^{1/2}\gamma_{\text{eff}} + \gamma_{\text{eff}}^2$, *is analytic*, but does not respect the reflection symmetry

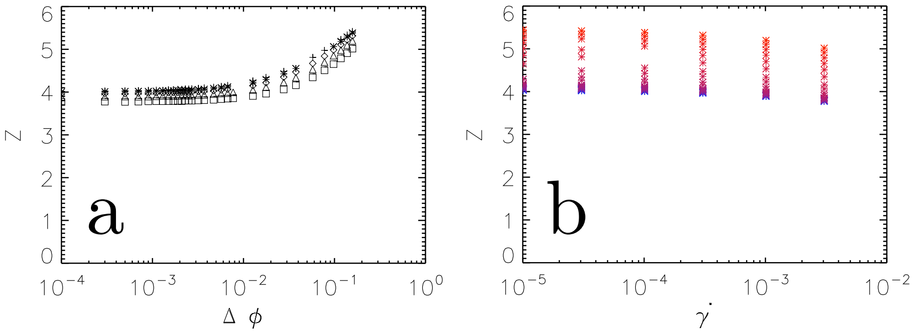

Figure 4.2: The average number of contacts per bubble, Z, **a** as a function of $\Delta\phi$ and **b** as a function of $\dot{\gamma}$. Colors in **a** and symbols in **b** indicate density and strain rate as in table 3.3.

as a function of the dissipated power in figure 4.1 **b**. This ratio should be 1, and this is indeed what we find. Although there are small deviations, these stay within 5%, do not show any trend and are likely due to the fact that the identity only holds for infinite time; we have averaged over a total strain of approximately 17.

In our 3E model we have, however, implicitly made two approximations to power balance. The first approximation concerns Z. As expected from the jamming literature [5] Z in our simulations depends both on $\dot{\gamma}$ and $\Delta\phi$. We have tried to describe the functional form of $Z\left(\dot{\gamma},\Delta\phi\right)$, but have not found a satisfying answer; our attempts are described in detail in appendix 9.1. In our 3E scaling model we have, implicitly, assumed Z to be constant by not including it as a scaling term in the power balance equation 3.1.1, though. Since Z stays between approximately 3.8 and 5.4, see figure 4.2, with lower values being overrepresented, here we have approximate the contact number as $Z = 4$, so that the dissipated power becomes $P_d \approx 2Nb\left\langle \Delta v^2\right\rangle$. The second approximation is that we focus on the regime where the elastic shear stress, σ_{xy}^{el} dominates the viscous stress, σ_{xy}^{visc}, so that $\sigma_{xy} \approx \sigma_{xy}^{el}$ and we can use our expression for the elastic stress, Eq. 4.5. The power input then becomes $P_i \approx L_x L_y \left\langle \sigma_{xy}^{el}\right\rangle \dot{\gamma}$

If we plot our approximated expressions for the power input, P_i, vs. the dissipated power, P_d, as we do in figure 4.3 **a**, we indeed see deviations from the predicted equality. To get a better grasp of the severity of the deviations from equality between power input and dissipated power in our approximation, we again look at the ratio between the two, see figure 4.3 **b**. There are clear deviations from unity. These deviations are strongest for high energy dissipation, the right side of the graph, and low density, blue color. This is exactly as we expected as these are the cases in which the viscous stress is relatively dominant. The worst case scenario sees a deviation of about 40%, which is

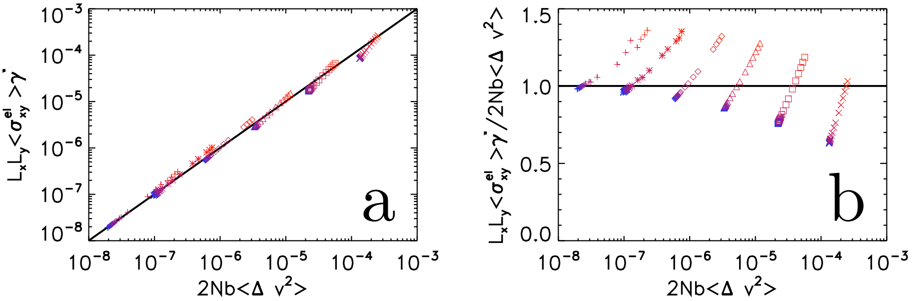

Figure 4.3: **(a)** Approximated power input, $L_xL_y\left\langle\sigma^{el}_{xy}\right\rangle\dot\gamma$, vs. approximated dissipated power, $3Nb\left\langle\Delta v^2\right\rangle$. **(b)** Ratio of approximated power input and approximated dissipated power vs. approximated dissipated power. The black line represents expected behavior. Colors and symbols indicate density and strain rate as in in table 3.3.

Regime	Full Expression
Critical	$\sigma = \sqrt{A_1A_2d^2NZ/2L_xL_y}\ \dot\gamma^{1/2}$
Transition	$\sigma = (A_1d)^{2/3}\,(NZ/2L_xL_y)^{1/3}\,\Delta\phi^{1/3}\dot\gamma^{1/3}$
Yield	$\sigma = A_1B_{\text{eff}}\Delta\phi^{3/2}$
crossover Critical Transition	$\dot\gamma = 2L_xL_yA_1/NZA_2^3d^2\ \Delta\phi^2$
crossover Transition Yield	$\dot\gamma = 2A_1B_{\text{eff}}^3L_xL_y/d^2NZ\Delta\phi^{7/2}$

Table 4.1: Full expressions for the four regimes and their crossovers in dimensionless form.

quite big. When compared to the full range of data that we have available as seen in figure 4.3 **a**, however, these deviations are not very important. In conclusion: the simulations agree with the full expression for energy balance and our approximations, concerning Z and σ^{el}_{xy}, have a clear, but in the end minor.

4.3 Extracting Coefficients

To test either of the other two ingredients, the effective strain of Eq. 4.2 or the elasticity relation of Eq. 4.5, we will need values for A_1, A_2 and B_{eff}. One way to get these values is by extracting them from collapsed rheological plots like those from section 3.3.2. This is possible because, now that we have rewritten all three ingredients in their full form, we can do the same for the resulting expressions of stress as a function of strain rate and density. We can derive these expressions by simply redoing the calculation of section 3.2 with the full

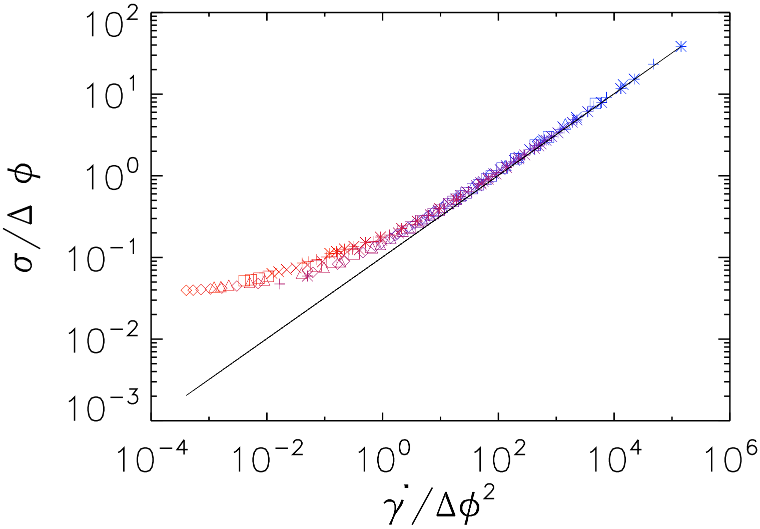

Figure 4.4: Fitted line to the behavior in the Critical regime; the shown line is given by $\tilde{\sigma} = 0.1\ \tilde{\dot{\gamma}}^{1/2}$. Colors and symbols indicate density and strain rate as in in table 3.3.

instead of the scaling ingredients. The resulting expressions are given in table 4.1. The expressions are given in dimensionless form, i.e. all stresses and strain rates in these equations are dimensionless quantities. Note that while these expressions look much less appealing than the scaling expressions above, only numerical constants were added: none of the dependences on $\dot{\gamma}$ and $\Delta\phi$ have changed. We call this model the Q3E model as it is a Quantitative version of our original 3E model.

These expressions allow us to find the values of the three undetermined constants A_1, A_2 and B_{eff} by comparing the simulation data with these expressions. Using automated fitting routines to find the prefactors is problematic because a priori it is unclear which data falls in which regime. Since we do know the shapes of the curves for all regimes, either a simple power law or even a just a flat line in the Yield regime, we can quite easily get a reasonable fit by hand. For example, in figure 4.4 we show the collapse plot of the stress vs. the strain rate that we showed before. It is clear that the data in the Critical regime is well described by $\sigma \approx 0.1\dot{\gamma}^{1/2}$, from which we can deduce, using the expression from table 4.1 that

$$\sqrt{\frac{A_1 A_2 d^2 N Z}{2 L_x L_y}} = 0.1 \pm 0.02 \tag{4.6}$$

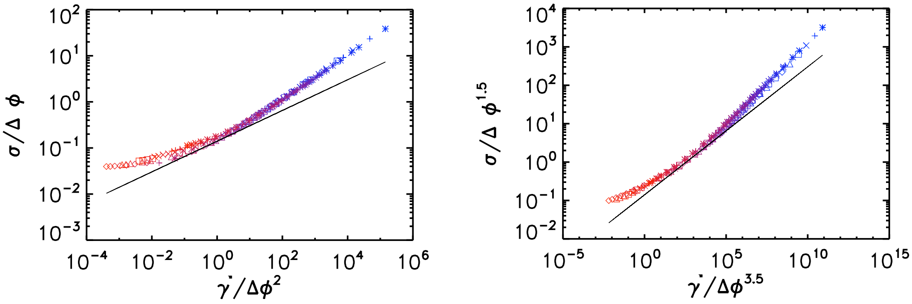

Figure 4.5: Fitted line to the behavior in the Transition regime; the shown line is given by $\tilde{\sigma} = 0.15\ \tilde{\dot{\gamma}}^{1/3}$. Colors and symbols as in figure 3.3

Now we substitute the relevant numerical values:

$$\begin{aligned} d &= 2.4 && (4.7)\\ N &= 1100 \pm 100 && (4.8)\\ Z &= 4 \pm 1 && (4.9)\\ L_x = L_y &= 75 && (4.10) \end{aligned}$$

and we find that

$$A_1 A_2 = 0.0045 \pm 0.001 \tag{4.11}$$

Note that these considerable error bars are due both to the fitting by hand and using single values for the non-constant Z and N. Now we can use the behavior in the other regimes to get extra restraints on other combinations of A_1, A_2 and B_{eff}. The plan is to use the expressions in the other two regimes to get the two additional constraints that we need to get a closed system.

While it was easy to get a good estimate on the prefactor in the Critical regime, because it contains a lot of data and is easily identifiable, it is harder to get a reliable estimate of the prefactor in the Transition regime. Our solution is to test the fit in both in a Critical-Transition collapse plot and in a Transition-Yield collapse plot. Figure 4.5 shows $\tilde{\sigma} = 0.14\tilde{\dot{\gamma}}^{1/3}$ in both collapse plots; it looks convincing in both. Combining this result with our model expression from table 4.1 we find

$$(A_1 d)^{2/3} \left(\frac{NZ}{2L_xL_y}\right)^{1/3} = 0.14 \pm 0.02 \tag{4.12}$$

Using the same numerical values as before, Eqs. 4.7 to 4.10, we find that $A_1 = 0.035 \pm 0.005$. Substituting this into Eq. 4.11 we find $A_2 = 0.13 \pm 0.02$.

This leaves B_{eff} as the only undetermined parameter. B_{eff} appears in the expression for the stress in the Yield regime, but as we have seen before, for example in figure 4.5, we do not have much data that is governed purely by

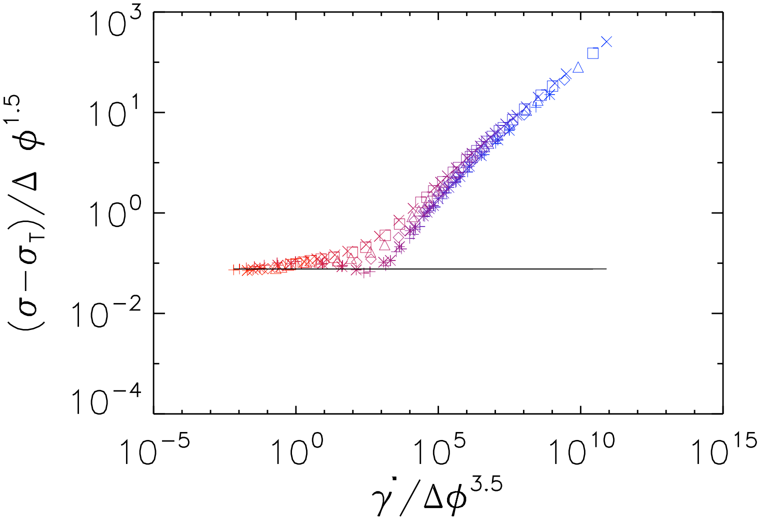

Figure 4.6: Plot $\sigma - \sigma_T/\Delta\phi^{3/2}$. The shown line is the fit to the behavior in the Yield regime: $\tilde{\sigma} = \sigma/\Delta\phi^{3/2} = 0.077$

the flat expression for the stress in the Yield regime. Since we now know, to good approximation, the stress in the Transition regime, we can subtract this contribution, leaving only the Yield contribution. We do this in figure 4.6. Note that a completely flat plateau is not reached. This means that the crossover in the stress is not actually given by $\sigma = \sigma_{\mathrm{Y}} + \sigma_{\mathrm{T}}$, an issue that we will further explore later in this chapter. However, the data is sloping down only very little, and it is reasonable to assign a value of 0.077 to the plateau that the data will reach[2]. Here, the expression for the stress is $\sigma = 0.077\Delta\phi^{3/2}$. Comparing to the result in table 4.1, this means that

$$A_1 B_{\mathrm{eff}} = 0.077 \pm 0.02, \tag{4.13}$$

or $B_{\mathrm{eff}} = 2.2 \pm 0.3$. This we have now determined all three undetermined constants:

$$\begin{aligned} A_1 &= 0.035 \pm 0.005 && (4.14)\\ A_2 &= 0.13 \pm 0.02 && (4.15)\\ B_{\mathrm{eff}} &= 2.2 \pm 0.3, && (4.16) \end{aligned}$$

which means that we can make quantitative predictions, and not just scaling predictions, for all quantities.

For example, we can calculate the density for which we enter the Dense regime from the Yield regime. Above, we have posited that this would be

---

[2] Note that we *assume* here that there will be a plateau, this does not follow strongly form the data.

unrealistically high, now we can substantiate that. Substituting all values into the expression for the crossover from the Yield to the Dense regime from table 4.1 yields:

$$\Delta\phi_{Y\to D} = \left(\frac{1}{2.2\cdot 0.13}\right)^2 = 12 \tag{4.17}$$

Clearly, this density is not attainable in any realistic situation and is certainly far beyond the highest density that we have used in our simulation (which is 1).

4.4 Regimes and Crossovers revisited

Above in section 3.3.2, we claimed that the crossover from the Yield to the Transition regime is very soft. We used this to explain why we had bad collapse in figure 3.2 **a** even though there was little to no data in the Yield regime[3]. Now that we have a full quantitative description off the model, we also have predictions for the size of the regimes and we can test whether the fitted values for our prefactors, the extent of the three regimes and the presence or absence of collapse are mutually consistent.

4.4.1 Regimes

The first thing we can do now is to see which regime is dominant for each individual data point; the Q3E gives a prediction for that without further fitting, making this a consistency test. Figure 4.7 shows a Critical-Transition collapse plot with data points for which the Yield contribution is dominant coloured black, points for which the Transition contribution is dominant coloured red and points dominated by Critical behavior coloured blue. Note that there are very little points in the Yield regime; this is in accordance with our previous observation. It also means that we have to explain why many of the red data points to the left do not collapse even though intuitively our model says that they should, given that we have plotted the data to collapse in the Transition and Critical regime.

Exactly at the crossover $\gamma_{\mathrm{y}} = \gamma_{\mathrm{dyn}}$ by construction and therefore $\gamma_{\mathrm{eff}} = \gamma_{\mathrm{y}} + \gamma_{\mathrm{dyn}} = 2\gamma_{\mathrm{dyn}}$. Furthermore, since $\sigma \sim \gamma$ in both the Yield and Transition regime, if we are just beyond the crossover at the Transition side, the stress is actually twice as big as the Transition contribution alone would have one believe[4]. It may not be strange that data consisting of almost 50% Yield contribution does not show fully Transition-like scaling, resulting in non-collapse when plotted taking only Transition scaling into account. We can now wonder how far beyond the crossover we have to move into the formal Transition

---

[3] As evidenced by the lack of a plateau.

[4] and conversely, on the Yield side of the crossover the the stress is twice as big as the Yield contribution

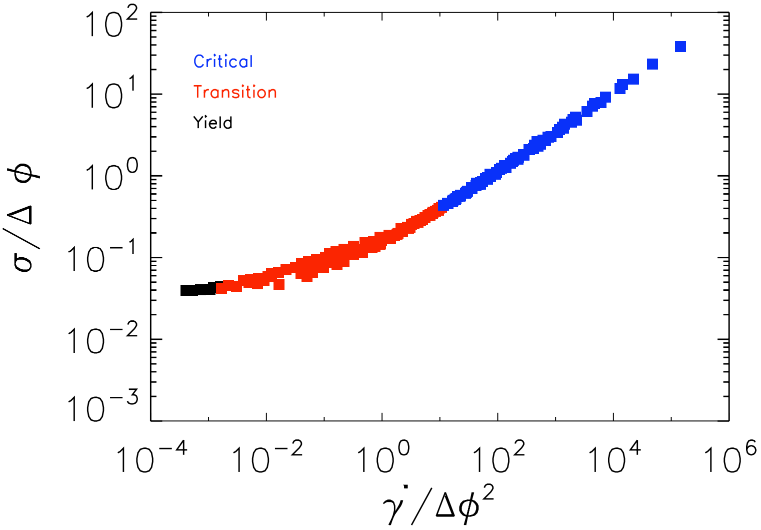

Figure 4.7: Transition-Critical collapse plot with data points coloured according to the regime in which they dominantly are.

regime to reach the ‘real’ Transition regime: where the Transition contribution markedly dominates the Yield contribution.

What we can do is take the actual ratio of the Yield and Transition/dynamic contribution to the effective strain and compare them for all data points, i.e. calculate:

$$R_{YT} = \frac{\gamma_{\mathrm{y}}}{\gamma_{\mathrm{dyn}}} = \frac{B_{\mathrm{eff}}\Delta\phi}{d\dot{\gamma}/\Delta v} = \frac{B_{\mathrm{eff}}\Delta\phi\sqrt{2\sigma V}}{d\sqrt{\dot{\gamma}ZN}}. \tag{4.18}$$

Clearly for data in the Yield regime $R_{YT} \geq 1$ and for data in the Transition (and Critical) regime $R_{YT} \leq 1$. It seems reasonable to demand collapse only from those data points for which the Yield contribution is an order of magnitude smaller than the Transition contribution, $R_{YT} \leq 0.1$. Conversely, we cannot expect pure Yield behavior, i.e. a plateau until the Yield contribution dominates absolutely, $R_{YT} \geq 10$. In figure 4.8 we have coloured those data points for which $0.1 \leq R_{YT} \leq 10$ and neither the Yield nor the Transition contribution dominates. We immediately note that the purple crossover regime is in fact very wide. It completely replaces the actual Yield regime, which was small to begin with, but also a large part of the Transition regime. That part, in fact, that was not collapsing. If we only look at the data that is really in the transition regime, the red data points for which $R_{YT} \leq 0.1$, we find that the data collapses as our Q3E model predicts. Below we will present a second approach to come to the same conclusions.

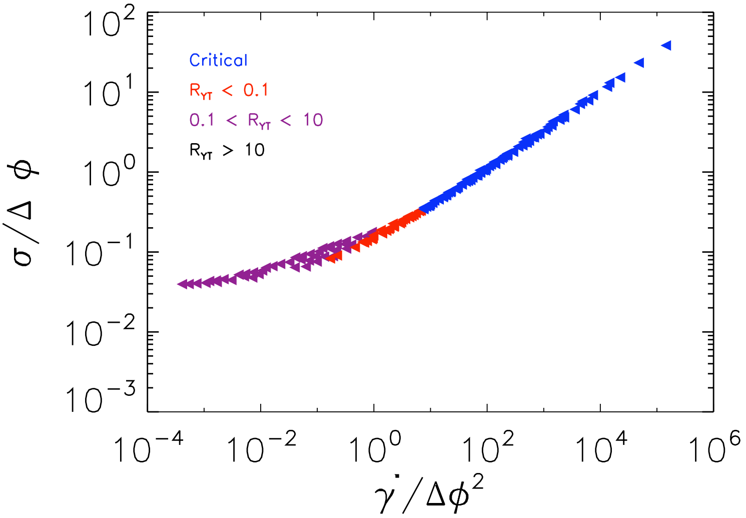

Figure 4.8: Transition-Critical collapse plot with data points coloured according to the regime in which dominantly are. The purple Yield-Transition crossover regime represents this data points for which neither the Yield nor the Transition contribution can be said to be dominant

4.4.2 Synthetic data

A second way in which we can test our claim that the poor collapse in the Transition regime when rescaling for collapse in that regime (and, say, the Critical regime as in figure 3.2 **a**) is to synthesise data which we *know* adheres to our model. If we can then show that this data, too, has weak crossovers and, as a consequence, poor collapse around the crossover, this is strong corroboration of our model.

Since we do not have a full analytical expression for our Q3E model, only piecewise expressions in the three regimes, we will also create the synthetic data in a piecewise fashion. This means that we will need to make a number of approximations. We hope to show two things: first, that the softness from the Yield-Transition crossover explains the bad collapse that we have seen in the Transition regime in figure 3.2. Second, that collapse in the Critical regime does not look bad even when plotting for collapse in the yield and Transition regime[5].

In order to show this we make the following approximations. Data points that are formally in the Critical regime will be considered to be fully in the Critical regime. In other words, we neglect the Transition contribution beyond the Transition crossover, since we only intend to show that the data in the Critical regime looks good despite being plotted for collapse in the Transition

---

[5] and therefore non-collapse in the Critical regime

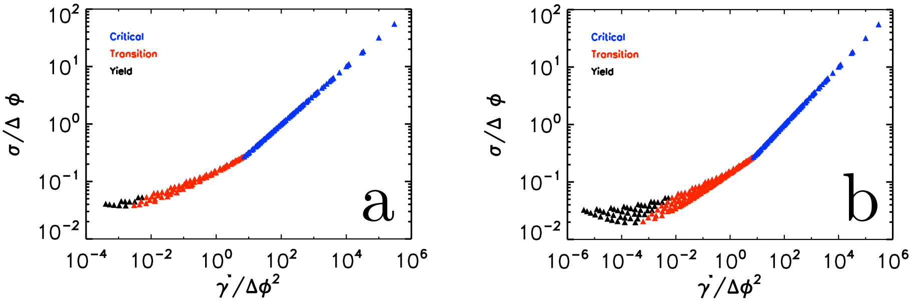

Figure 4.9: Transition and Critical regime collapse plot of synthetic data. The data is coloured according to the regime it is in. **a**: data points corresponding to our simulation data. **b**: data with an extra two slower decades of strain rates.

(and Yield) regime. Disregarding the, collapsing, Transition contribution will not make the data look more collapsed, it will make it look less collapsed.

For data on the dense or slow side of the Transition-Critical crossover we use the following expression for the stress:

$$\sigma = \sigma_{\mathrm{Y}} + \sigma_{\mathrm{T}} = A_1 k \Delta\phi^{1/2}(\gamma_{\mathrm{Y}} + \gamma_{\mathrm{T}}) \tag{4.19}$$

At first this may not seem like an approximation: we use the expression for the elasticity that is valid in both the Yield and Transition regime with the full expression of the effective strain. However, in the Transition regime the effective strain is given by $d\dot{\gamma}/\Delta v$. Δv in turn depends on the stress. In this case, this should be the full stress: the Yield and the Transition contribution. In the derivation of the Transition stress, though we used only the Transition stress. Therefore, the expression of Eq. 4.19 is an approximation, though corrections are of higher order.

In figure 4.9 we show the synthetic data in a Transition-Critical collapse plot. In panel **a** we use exactly the same $\dot{\gamma}$ and $\Delta\phi$ as we use in the simulations. We note that the blue data points in the Critical regime collapse exactly onto a straight line. This is purely a consequence of the way we defined the data. We also note there is clear non-collapse in the red Transition data that borders the, very small, set of black Yield data. This is exactly what we saw in figure 3.2: data in the Transition regime that should collapse is not collapsing. The fact that we see it again here, where we know, by construction, that the data obeys our model, means that the non-collapse in the Transition data of figure 3.2 is perfectly consistent with our model and is likely the consequence of the soft crossover between the Yield and Transition regimes.

If we add two additional slower decades of strain rate, as we do in figure 4.9 **b**, we note two things. First, the amount of data in the Yield regime increases because there is more slow (and dense) data. Second, we note that the

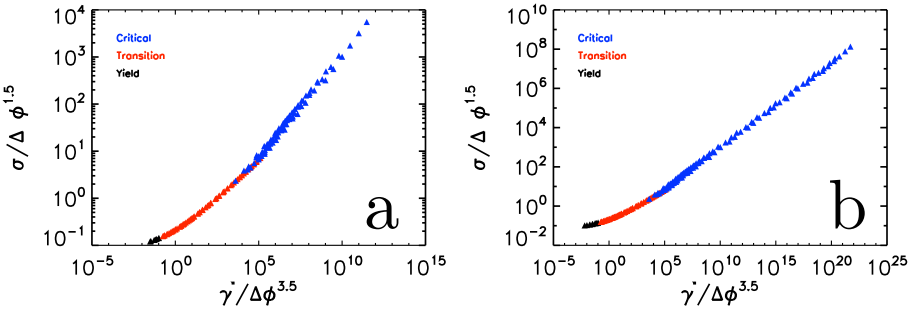

Figure 4.10: Yield and Transition regime collapse plot of synthetic data. The data is coloured according to the regime it is in. **a**: data points corresponding to our simulation data. **b**: data with an extra three decades of density closer to jamming.

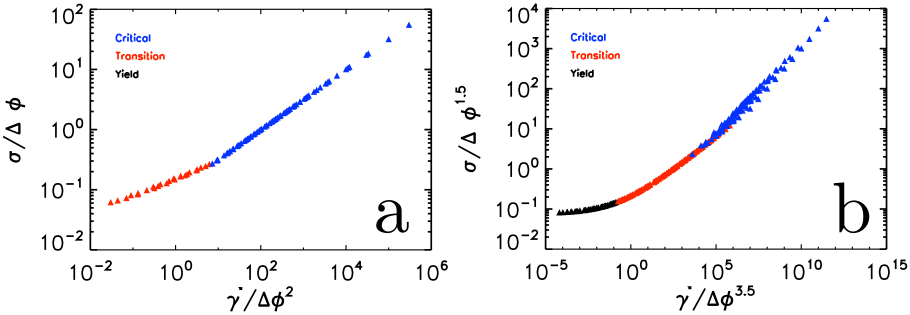

Figure 4.11: Plots of our synthetic data. Panel **a** uses a much smaller data set then our simulation data: $\phi_{\max} = 0.9$ and $\dot\gamma_{min} = 10^{-4}$ rescaled for collapse in the Critical and Transition regime. Panel **b** uses a larger one: $\phi_{\max} = 1$ and $\dot\gamma_{min} = 10^{-7}$ and is rescaled for collapse in the Yield and Transition regime.

cloud of Transition data that does not collapse becomes even more noticeable. Compared to figure 4.9 **b**, panel **a** looks almost nicely collapsed.

In figure 4.10 we show the other side of the coin. We plot our synthetic data, in panel **a** again using the same $\dot\gamma$ and $\Delta\phi$ as our simulations, for collapse in the Yield and Transition regime. We note that these two regimes indeed collapse very well and that we are still quite some distance away from reaching a Yield plateau. We also note that the data in the Critical regime looks reasonably collapsed too, even though, by construction the data does *not* collapse. To see if this is a consequence of not approaching the jamming density close enough, we add three extra decades of density closer to the jamming density in figure 4.10 **b**. Clearly even going down to $\Delta\phi = 10^{-7}$ does not make the collapse look appreciatively bad.

The fact that a collapse plot can *look* good even though it contains data that is not collapsed and the fact that there are three regimes lead to complications when using a fitting algorithm that assumes two regimes, and therefore the possibility of full collapse. You might imagine, for example, that when having data with only moderately slow strain rates, even fewer than in figure 4.9 **a**, a blind fitting algorithm that optimises collapse of all data would return something close to our Transition and Critical collapse, as in figure 4.11 **a**. If this rescaling would be interpreted from a Herschell-Bulkley (and therefore two-regime) perspective, one would assume that the yield plateau would scale as $\Delta\phi^1$, which is inconsistent with our model, and that the high strain rate asymptote would scale as $\dot{\gamma}^{1/2}$, which is consistent.

Improving the data by adding slower and slower strain rates and using the same blind fitting algorithm that assumes two regimes will likely in the end yield our Yield and Transition rescaling like in figure 4.11 **b**. Figure 4.11 **b** is certainly better collapsed than figure 4.9 **b**, which contains the same data points. Interpreting this result from a Herschell-Bulkley perspective yields $\Delta\phi^{3/2}$ scaling in the Yield plateau, which is consistent, and $\dot{\gamma}^{0.42}$ scaling in the high strain rate asymptote, which is inconsistent. This shows that approaching the data with an incorrect theoretical model may lead one to conclusions that may be wrong; in this case finding two shifting exponents where there are three constant ones.

4.4.3 Conclusion

In conclusion, many of the properties of our simulation data that seemed to be in contradiction with our 3E model are perfectly consistent with it. Most importantly, the fact that there is poor collapse well into the Transition regime even when rescaling in such a way that the Critical and Transition regime should collapse, is a consequence of the slow crossover between the Yield and Transition regime. What is more, it is possible to plot the data in ways that look good, but do not actually say much about the data. This latest realisation becomes even more important if one approaches the data with the preconception that there are two regimes and tries to determine the exponents with a blind fitting procedure [11].

4.5 Testing the Other Model Ingredients

Now that we have full, quantitative expressions for all three ingredients, we can test whether the assumptions going into our model were correct. If so, our model describes actual physical behavior. If not, our success in describing the rheology was coincidental.

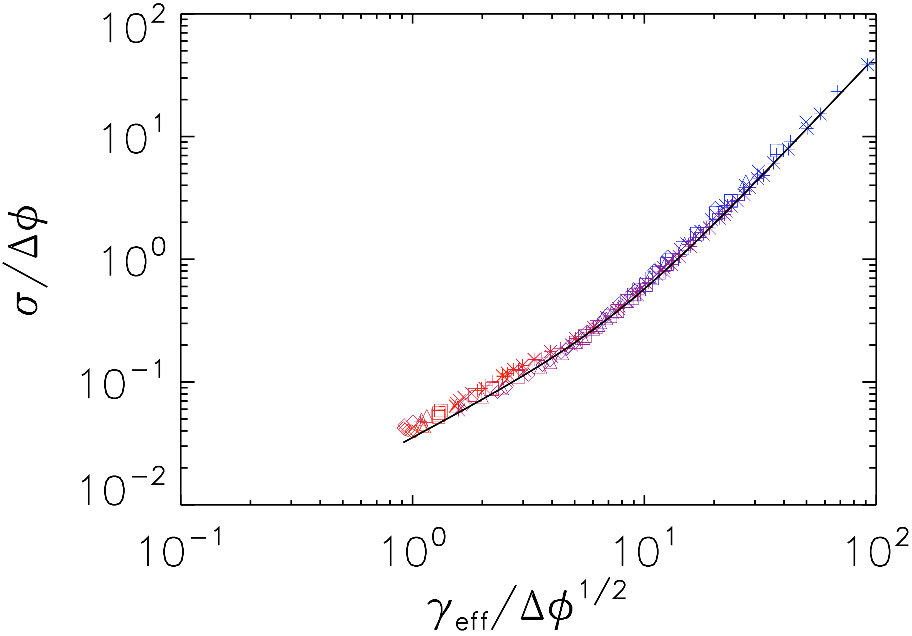

Figure 4.12: The stress plotted vs. the effective strain, rescaled for collapse. The superimposed black line is our model prediction, Eq. 4.5, with the coefficients as determined above.

4.5.1 Testing Elasticity Relations

The second ingredient of the Q3E model that we will test is the elasticity equation 4.5. Since this equation includes the effective strain, we will also indirectly test our expressions for that, but we will look at the effective strain in more depth in the next section.

We predict that the shear stress depends on both the effective strain and the density. This means that, in order to get full collapse if we plot the stress vs. the effective strain, we need to rescale both with an appropriate power of $\Delta\phi$. If we consider $\tilde{\sigma} = \sigma/\Delta\phi$ and $\tilde{\gamma}_{\mathrm{eff}} = \gamma/\Delta\phi^{1/2}$, equation 4.5 becomes

$$\tilde{\sigma}^{xy} = A_1 k \tilde{\gamma}_{\mathrm{eff}} \sqrt{1 + A_2^2 \tilde{\gamma}_{\mathrm{eff}}^2}. \tag{4.20}$$

This means that if we plot $\tilde{\sigma}$ vs. $\tilde{\gamma}_{\mathrm{eff}}$ we predict full collapse of the data, with asymptotic linear behavior for small $\tilde{\gamma}_{\mathrm{eff}}$ and asymptotic quadratic behavior for large $\tilde{\gamma}_{\mathrm{eff}}$. Note that γ_{eff}, and therefore $\tilde{\gamma}_{\mathrm{eff}}$, depends on B_{eff}, which we have just determined above.

As can be seen in figure 4.12, our predictions for the elasticity relation describe the data well. Note that there are no fitting parameters here, all undetermined parameters having been determined from the rheology data above.

One can wonder, of course, whether this test of the model is independent from tests we have performed previously. In principle, it is *not* an independent test since our predictions for the rheology follow purely from power balance on the one hand and the effective strain and elasticity relations on the other. Therefore, if our predictions for the rheology hold, which were tested in figures 3.2 and 3.3 and our expression for power balance holds, which we tested in figure 4.2, then our expressions for elasticity and effective strain *must* also hold. In practice, it is not that clear-cut, however, since the above statement only holds if our predictions were upheld *exactly.* This is not the case, in fact, we have seen that power balance as we use it in our model[6] can lead to acceptable but noticeable errors. Therefore we think it is correct to consider this test of the elasticity relation a useful consistency check.

4.5.2 Testing the Two Strains

The third and final ingredient of the model that we will test is the concept of the two strains: the yield strain, γ_{y}, and the dynamic strain, γ_{dyn}; see equation 4.2. While testing the elasticity relation in the previous paragraph, we have already found indirect evidence that our definition of the effective strain makes sense: the data collapses if plotted as function of this strain. However, we would like to measure actual strains that behave like our effective strain or, even better, the yield or dynamic strain individually.

We have tried a number of different approaches to identify strains in the system. The first approach we have tried was to instantaneously reverse the direction of the strain rate during a simulation. We then planned to determine the strain scale over which the stress achieved its new (reverse direction) steady state. Since the effective strain is in some ways a measure of how deformed the system is due to flow, one would expect the strain scale that we measure this way to reflect the effective strain. However, the stress exhibited much richer behavior than the expected exponential decay towards the new steady state value such as a discontinuous rise or dip directly after reversal. Therefore any strain scale that we might have found in this scenario could hardly be classified as an easily accessible and simple test for the effective strain. We have also looked at the anisotropy in the contact network as a possible measure of the effective strain, another measure of the deformation due to flow, but did not find the proposed scaling with $\Delta\phi$ or $\dot{\gamma}$ in any of the first three Fourier components of the contact density as a function of angle.

Therefore we ended up looking at the strain scale over which the stress signal correlates with itself: in a system with a large effective strain we expect there to be a large strain distance between subsequent ‘hills’ and ‘valleys’ in the stress signal because it takes more strain to deform the system to a new configuration that is just about to rearrange and vice versa. Therefore, we calculated the autocorrelation function of the stress signals, $C_{\sigma\sigma}$, and assigned

---

[6] so based on just the elastic stress and assuming constant Z, see section 4.2

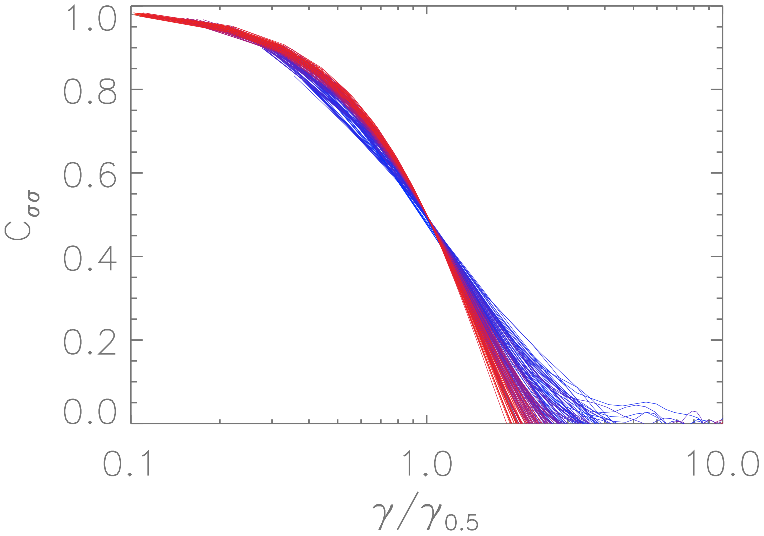

Figure 4.13: Autocorrelation of the stress, rescaled by the strain for which the correlation is 0.5. Data is colored according to density: red curves correspond to high density and blue curves correspond to low density. Colors correspond to table 3.3 but strain rates are not indicated.

a strain scale to the decay of this autocorrelation. This was done by taking the strain for which the autocorrelation was 0.5 and calling it the correlation strain, γ_{corr}. We have used linear interpolation between the data points for higher resolution. As we show in more detail in Appendix 9.3, γ_{corr} *is* a linear combination of the yield and dynamic strain, however, the balance of the two contributions is not the same as for the effective strain. We have thus not found a conceptually simple and easy to measure strain in the system that is proportional to the effective strain.

4.6 Conclusion

Our expanded Q3E model has passed the extra tests of this chapter. Power balance holds exactly in our simulations and the approximations to the expression for power balance that we make in our Q3E model is reasonable. We have not been able to measure the effective strain directly, though. As a consistency check, our Q3E model also describes the elasticity relation exactly without fit parameters. Finally, through a variety of approaches we have made plausible that the seeming inconsistencies between the data and our 3E model in section 3.3.2 were the consequence of surprisingly soft crossovers.

Chapter 5

Normal Stress

Up till now, we have only dealt with the scaling of the shear stress, σ_{xy}. We will now turn our attention to the normal components of the stress: σ_{xx} and σ_{yy}. Our 3E model can be naturally extended to these two components, although we will need to include a new empirical relation for the stress as a function of the strain.

5.1 Scaling Model

Before we introduce the extension to our 3E model and test its predictions, we note that the two normal stresses, σ_{xx} and σ_{yy} are close (not identical) within the regime in which we consider the data. This can be seen in figure 5.1. While there is a bump in σ_{xx} compared to σ_{yy}, its magnitude is small and we have not investigated it further. We will first discuss whether and how the three ingredients of the 3E model for shear stresses, Eqs. 3.1, 3.2, 3.3, 3.4 and 3.5, need to be changed for the normal stress. The first ingredient, energy conservation, Eq. 3.1, remains:

$$L_x L_y \sigma_{xy} \dot{\gamma} = \frac{NZb}{2} \left\langle \Delta v^2 \right\rangle . \tag{5.1}$$

Energy is conserved no matter what component of the stress we consider. Note that this suggests that the shear stress enters the description of the normal stresses.

The second set of ingredients for our 3E model, the two expressions for the yield strain, similar to Eq. 3.2, and the dynamic strain, similar to Eq. 3.3, will also be unchanged, as we can still assign an effective strain based on the compression and the relaxation time scale. We will, however, allow for the balance between these contributions to be different from the shear case. Therefore we have:

$$\gamma_{\text{eff}} = B_{\text{eff}}^{xx} \Delta\phi + \frac{\dot{\gamma} d}{\Delta v}, \tag{5.2}$$

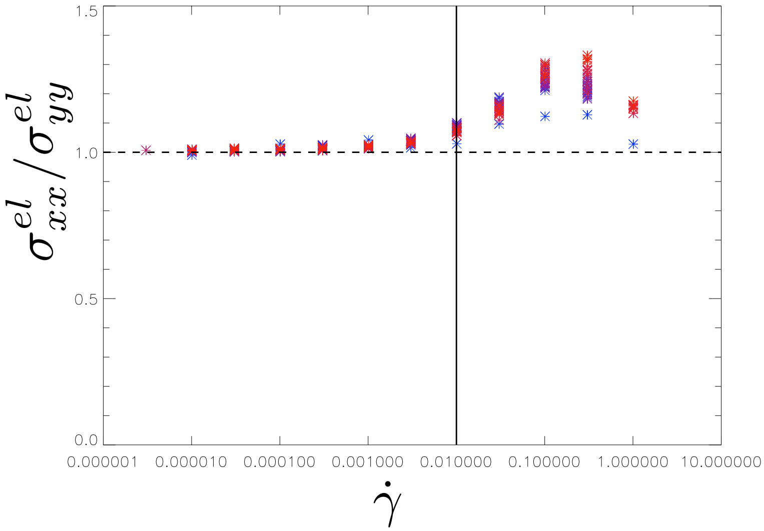

Figure 5.1: The ratio of the xx and yy components of the elastic stress. In the regime where we consider the data, $\dot{\gamma} < 10^{-2}$, left of the black line, the two are equal. Red means high density, blue means low density, see the legend in table 3.3

with B^{xx}_{eff} a new undetermined coefficient. We will test this assumption together with the elasticity relation that we introduce next, just as we did for the shear stress above.

The third ingredient describes the relationship between the stress and the effective strain. For shear stresses, we proposed a linear, $\sigma_{xy} \sim G\gamma_{\text{eff}}$ (Eq. 3.4), and a quadratic, $\sigma_{xy} \sim \gamma^2_{\text{eff}}$ (Eq. 3.5), regime. However, since the result of Wyart *et al.* for the quadratic part is not necessarily valid for the normal stress, we do not have a natural prediction for the elasticity relation. The simplest relation is a linear one:

$$\sigma_{xx} = A_{xx} k \gamma_{\text{eff}} \tag{5.3}$$

The best way to find out, however, is to determine it empirically.

5.1.1 Testing the Elasticity Relation

We test the elasticity relation in exactly the same way as we did for the normal stress: we plot σ_{xx} vs. γ_{eff} in figure 5.2 **a**. Since our expression for σ_{xx}, Eq. 5.3 does not depend on the density, no further rescaling should be necessary to attain collapse. It is immediately clear, however, that the data does not collapse. This means at the very least that the expression we used for the effective strain, $\gamma_{\text{eff}} = B_{\text{eff}}\Delta\phi + \dot{\gamma}d/\Delta v$ with $B_{\text{eff}} = 2.2$, is not correct. If it

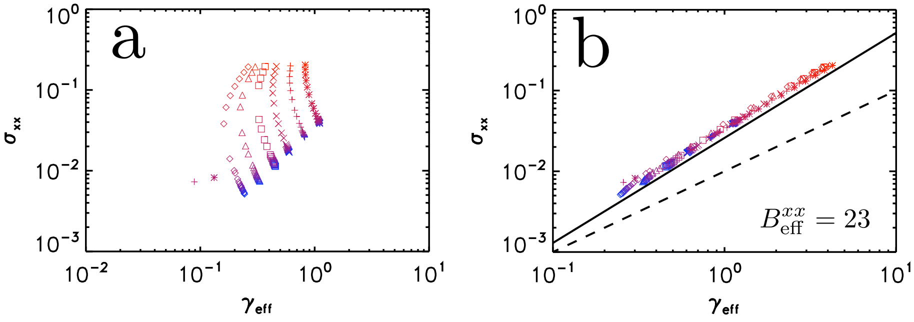

Figure 5.2: Plot of the normal stress vs. the effective strain. **a**: using exactly the same expression for γ_{eff} as we do in the shear stress case. **b**: changing the value of B_{eff} to achieve collapse. The dashed line is a power law with exponent 1, the black line with exponent 1.3. Colors and symbols correspond to the legend of table 3.3.

were correct we would have seen collapse. The shape of the collapsed curve would then have told us the functional form of the dependence of σ_{xx} on γ_{eff}.

The most simple way in which our proposed formulation of the effective strain can be incorrect is if the value of B_{eff} is not the same in the shear and normal cases. In other words: the normal stress is still determined by an effective strain given by two contributions, a yield strain and a dynamic strain, but the contributions balance differently. If this is the case, we should be able to get better collapse by adjusting B_{eff} to a new value that we call B^{xx}_{eff} to distinguish it from the previous result, which we will cal B^{xy}_{eff}. The panel **b** of figure 5.2 shows that we are indeed able to get collapse for $B^{xx}_{\text{eff}} = 23 \pm 2$, which is an order of magnitude larger than B^{xy}_{eff}, for which we found a value of 2.2. We note that it is not surprising that the static, compression based strain is more important in determining the compressive component of the stress.

Now we can also see that the expression for the elasticity that we formulated in Eq. 5.3 is not correct. The dashed line in figure 5.2 **b** is a power law of exponent 1, the expected linear behavior. Clearly, this does not match the slope of the data. The data can still be described by a simple power law, but it will have an exponent different from 1. In fact, as shown by the black line in the figure 5.3 **b**, a power law with exponent 1.3 works well. This means that the correct formulation of the elasticity relation is:

$$\sigma_{xx} = A_{xx} k \gamma_{\text{eff}}^{1.3} \tag{5.4}$$

We stress that this is an empirical result.

5.2 Regimes

With the three ingredients formulated and checked, Eqs. 5.1, 5.2 and 5.4, we can now derive the expressions for the normal stress as function of the density and strain rate. Since there is now only one ingredient, the effective strain, that has different behavior in different regimes, we expect to have only two distinct scaling regimes for the normal stress, while we had four regimes for the shear stress. We will call these regimes the Normal Yield regime, for 'large' $\Delta\phi$ and 'small' $\dot{\gamma}$ so that Eq. 5.2 is dominated by the yield contribution $B^{xx}_{\text{eff}}\Delta\phi$, and the Normal Dynamic regime, for 'small' $\Delta\phi$ and 'large' $\dot{\gamma}$ so that Eq. 5.2 is dominated by the dynamic contribution $\dot{\gamma}d/\Delta v$. Our power balance expression complicates this though, as we will illustrate below.

In the Normal Dynamic regime we have

$$\begin{aligned} \sigma_{xx} &\sim \gamma_{\text{eff}}^{1.3} && (5.5)\\ \gamma_{\text{eff}} &\sim \frac{\dot{\gamma}}{\Delta v} && (5.6)\\ \sigma_{xy}\dot{\gamma} &\sim \Delta v^2, && (5.7) \end{aligned}$$

where we have used scaling expressions for simplicity. Substituting Eq. 5.7 into Eq. 5.6 yields

$$\gamma_{\text{eff}} \sim \frac{\dot{\gamma}}{\sqrt{\sigma_{xy}\dot{\gamma}}}. \tag{5.8}$$

Substituting this into Eq. 5.5 then yields

$$\sigma_{xx} \sim \left(\sqrt{\frac{\dot{\gamma}}{\sigma_{xy}}}\right)^{1.3} \tag{5.9}$$

Due to the dependence of the supplied power on the shear stress, σ_{xy}, the shear stress enters the expression for the normal stress. We need to substitute the expressions we found for the shear stress to express the normal stress as a function of $\dot{\gamma}$ and $\Delta\phi$. The shear stress, however, also has regimes. In principle, this could split the Normal Dynamic regime into three regimes, one for each regime of the shear stress. Fortunately, the crossover between the Yield and Transition regimes is the same as the crossover between the Normal Yield and the Normal Dynamic regimes: in both cases you are in the Yield regime if $\Delta\phi > \dot{\gamma}/\Delta v$ [1]. We will therefore refine our description to include three regimes: the Normal Yield regime, in which the effective strain is determined by the yield strain and the shear stress does not enter, the Normal Transition regime, in which the effective strain is in the dynamic regime and the shear stress in the Transition regime, and the Critical regime, in which the effective strain is in the dynamic regime and the shear stress is in the Critical regime.

---

[1] In fact, we have seen that $B^{xx}_{\text{eff}} > B^{xy}_{\text{eff}}$, meaning that the crossover from the Normal Yield to the Normal Dynamic regime takes place for much higher density than the crossover from Yield to Transition regime

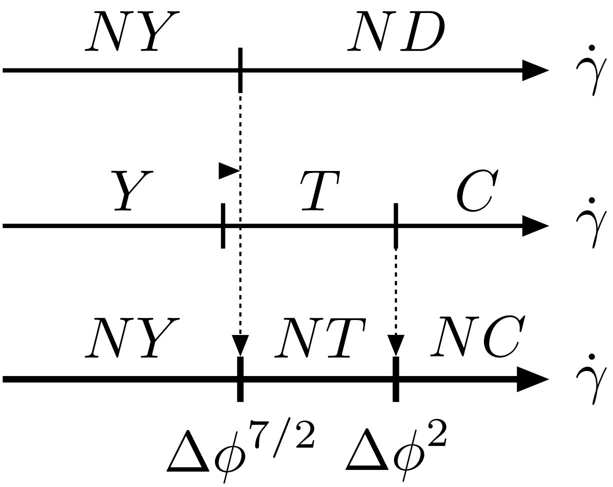

Figure 5.3: Top: the regimes in the normal stress without taking into account the shear stress dependence that enters through power balance. There are two regimes in this case the Normal Yield (NY) regime and the Normal Dynamic (ND) regime. Middle: the regimes of the shear stress. Bottom: the final regimes of the normal stress. Vertical dashed arrows indicate the inheritance of a crossover. NT denotes the Normal Transition regime and NC denotes the Normal Critical regime.

	Normal Critical	Normal Transition	Normal Yield
effective strain	$\gamma_{\rm eff} \sim \dot\gamma/\Delta v$	$\gamma_{\rm eff} \sim \dot\gamma/\Delta v$	$\gamma_{\rm eff} \sim \Delta\phi$
shear stress	$\sigma \sim \dot\gamma^{1/2}$	$\sigma \sim \Delta\phi^{1/3}\dot\gamma^{1/3}$	
rheology	$\sigma \sim \dot\gamma^{0.33}$	$\sigma \sim \Delta\phi^{-0.22}\dot\gamma^{0.43}$	$\sigma \sim \Delta\phi^{1.3}$
range	$\Delta\phi^2 < \dot\gamma$	$\Delta\phi^{7/2} < \dot\gamma$ $\Delta\phi^2 > \dot\gamma$	$\Delta\phi^{7/2} > \dot\gamma$

Table 5.1: The three rheological regimes with their definitions, results and ranges of validity.

These regimes are shown in figure 5.3. At the top we have Normal Yield and Normal Dynamic regimes that follow from the analysis of the Normal stress without taking into account the shear stress dependence of Δv that enters through power balance in the Normal Dynamic regime. In the middle we show the Yield, Transition and Critical regime from the shear stress. Note that the crossover from the Normal Yield to the Normal Dynamic regime and the crossover from the Yield and the Transition regime have the same scaling ($\dot{\gamma} \sim \Delta\phi^2$) as they are based on the same crossover from yield dominated γ_{eff} to dynamic dominated γ_{eff}. However, since $B_{\text{eff}}^{xx} > B_{\text{eff}}$, the numerical value for the crossover between the Normal Yield and Normal Dynamic regime is higher. On the bottom of figure 5.3 we show the final regimes for the normal stress. The final Normal Yield regime is not influenced by the shear stress and therefore the crossover to the next regime is not changed. The crossover between the Normal Transition and the Normal Critical regime is directly inherited from the shear stress. Now that we have defined the three regimes we can derive the rheological expressions in the same way we derived the results fro the normal stress. The results are summarised in table 5.1 and given in a little more detail below.

Normal Yield In the Normal Yield regime we have:

$$\begin{cases} \sigma_{xy}\dot{\gamma} \sim \Delta v^2 \\ \gamma_{\text{eff}} \sim \Delta\phi \\ \sigma_{xx} \sim \gamma_{\text{eff}}^{1.3} \\ \sigma_{xy} \sim \Delta\phi^{3/2} \end{cases} \Rightarrow \begin{cases} \Delta v \sim \dot{\gamma}^{1/2}\Delta\phi^{3/4} \\ \gamma_{\text{eff}} \sim \Delta\phi \\ \sigma_{xx} \sim \Delta\phi^{1.3} \end{cases} \tag{5.10}$$

Note that our scaling for the normal stress in the limit of zero strain rate, $\sigma_{xx} \sim \Delta\phi^{1.3}$ is not the same as our prediction for the shear stress in the limit of zero strain rate, $\sigma_{xy} \sim \Delta\phi^{3/2}$. This is in contrast to the expectations and findings of many [23, 38]. We note that we do not have strong empirical data that corroborates that either $\sigma_{xy} \sim \Delta\phi^{3/2}$ or $\sigma_{xx} \sim \Delta\phi^{1.3}$.

Normal Transition In the normal Transition regime we have:

$$\begin{cases} \sigma_{xy}\dot{\gamma} \sim \Delta v^2 \\ \gamma_{\text{eff}} \sim \frac{\dot{\gamma}}{\langle\Delta v\rangle} \\ \sigma_{xx} \sim \gamma_{\text{eff}}^{1.3} \\ \sigma_{xy} \sim \Delta\phi^{1/3}\dot{\gamma}^{1/3} \end{cases} \Rightarrow \begin{cases} \Delta v \sim \Delta\phi^{1/6}\dot{\gamma}^{2/3} \\ \gamma_{\text{eff}} \sim \Delta\phi^{-1/6}\dot{\gamma}^{1/3} \\ \sigma_{xx} \sim \Delta\phi^{-1.3/6}\dot{\gamma}^{1.3/3} \end{cases} \tag{5.11}$$

Normal Critical In the Normal Critical regime we have:

Regime Combination	Rescaled Axes
Critical and Transition	$\sigma/\Delta\phi^{0.65}$ vs. $\dot{\gamma}/\Delta\phi^{2}$
Yield and Transition	$\sigma/\Delta\phi^{1.3}$ vs. $\dot{\gamma}/\Delta\phi^{7/2}$
Yield and Critical	$\sigma/\Delta\phi^{1.3}$ vs. $\dot{\gamma}/\Delta\phi^{3.9}$

Table 5.2: Prescriptions of what to plot for collapse of the normal stress in the indicated regimes.

$$\begin{cases} \sigma_{xy}\dot{\gamma} \sim \Delta v^2 \\ \gamma_{\text{eff}} \sim \frac{\dot{\gamma}}{\langle \Delta v \rangle} \\ \sigma_{xx} \sim \gamma_{\text{eff}}^{1.3} \\ \sigma_{xy} \sim \dot{\gamma}^{1/2} \end{cases} \Rightarrow \begin{cases} \Delta v \sim \dot{\gamma}^{3/4} \\ \gamma_{\text{eff}} \sim \dot{\gamma}^{1/4} \\ \sigma_{xx} \sim \dot{\gamma}^{1.3/4} \end{cases} \tag{5.12}$$

5.2.1 Crossovers

As we have discussed above and illustrated in figure 5.3, the crossover between the Normal Transition and the Normal Critical regimes is the same as the crossover from the Transition to the Critical regime by construction and therefore scales as $\dot{\gamma} \sim \Delta\phi^{7/2}$. The crossover from the Normal Yield to the normal Transition regime scales the same as the crossover from the Yield to the Transition regime, $\dot{\gamma} \sim \Delta\phi^2$, as both take place where the yield contribution and the dynamic contribution to the effective strain are equal. Since, however, the yield contribution is bigger for the normal stress, the numerical value of the crossover will be different.

5.3 Plotting and Results

5.3.1 Collapse Plots

Just as in the case of the shear stress, we can now determine the exponents Δ and Γ for which a plot of $\sigma_{xx}/\Delta\phi^{\Delta}$ vs. $\dot{\gamma}/\Delta\phi^{\Gamma}$ results in collapse in the various regimes. The analysis is completely analogous to that of section 3.3.1 and no new interesting physics is found; in fact, due to the inherited crossovers, some of the results are identical to the shear case. The results are presented in table 5.2.

Normal Yield and Normal Transition Regimes As mentioned above, the strain rate needs to be rescaled to make the crossover between the Normal Yield and Normal Transition regimes, which is the same as for the shear tress,

Regime	Full Expression
Normal Critical	$\sigma_{xx} = A_{xx}\left(d^2NZ/2L_xL_yA_1A_2\right)^{1.3/4}\dot{\gamma}^{1.3/4}$
Normal Transition	$\sigma_{xx} = A_{xx}\left(NZd^2/2L_xL_yA_1\right)^{1.3/3}\Delta\phi^{-1.3/6}\dot{\gamma}^{1.3/3}$
Normal Yield	$\sigma_{xx} = A_{xx}B_{\mathrm{eff}}^{xx\ 1.3}\Delta\phi^{1.3}$
crossover Transition Yield	$\dot{\gamma} = 2A_1B_{\mathrm{eff}}^{xx\ 3}L_xL_y/d^2NZ\ \Delta\phi^{7/2}$
crossover Critical Transition	$\dot{\gamma} = 2L_xL_yA_1/NZA_2^3d^2\ \Delta\phi^2$

Table 5.3: Full expressions for the three regimes and their crossovers in dimensionless form.

collapse: $\tilde{\dot{\gamma}} \sim \dot{\gamma}/\Delta\phi^{7/2}$. Since the stress in the Normal Yield regime depends only on the density, this prescribes the rescaling of the stress: $\sigma_{xx} \sim \Delta\phi^{1.3}$.

Normal Transition and Normal Critical Regimes Between the Normal Transition and the Normal Critical regime there is again a crossover that determines the strain rate rescaling: $\tilde{\dot{\gamma}} \sim \dot{\gamma}/\Delta\phi^2$. Substituting this into the expression for the stress in the Normal Critical regime yields:

$$\sigma_{xx} \sim \dot{\gamma}^{1.3/4} = \tilde{\dot{\gamma}}^{1.3/4}\Delta\phi^{1.3/2} \Rightarrow \tilde{\sigma}_{xx} \sim \sigma_{xx}/\Delta\phi^{1.3/2}. \tag{5.13}$$

Normal Yield and Normal Critical Regimes Again, the dependence of the Normal Yield stress on the density prescribes the rescaling of the stress: $\sigma_{xx} \sim \Delta\phi^{1.3}$. This can be substituted into the expression for the stress in the Critical regime to deduce the rescaling of the strain rate:

$$\sigma_{xx} \sim \dot{\gamma}^{1.3/4} \Rightarrow \tilde{\sigma}_{xx} \sim \dot{\gamma}^{1.3/4}/\Delta\phi^{1.3} \Rightarrow \tilde{\dot{\gamma}} \sim \dot{\gamma}/\Delta\phi^4 \tag{5.14}$$

5.3.2 Prefactors

The final detail that is necessary to complete our Q3E model for the normal stress is the value of any new prefactors that were introduced. Since we already have determined that $B_{\mathrm{eff}}^{xx} = 23 \pm 2$, the only remaining new parameter is A_{xx} in Eq. 5.4. The approach for determining this fit factor is the same as for the shear case: comparing the data to our full expression for the stress in the Critical regime. This and all the other full expressions are given in table 5.3. The next step is to plot the data for collapse, so that we can fit a power law.

Figure 5.4 plots the normal stress vs. the strain rate rescaled for collapse in the Yield and Critical regime. Firstly, we note that collapse looks good over the entire range, we will return to this below. For now, we focus on the fact that the black line, given by $0.03\left(\dot{\gamma}/\Delta\phi^{3.9}\right)^{1.3/4}$ describes the data in the Critical asymptote very well. This allows us to derive the value of A_{xx},

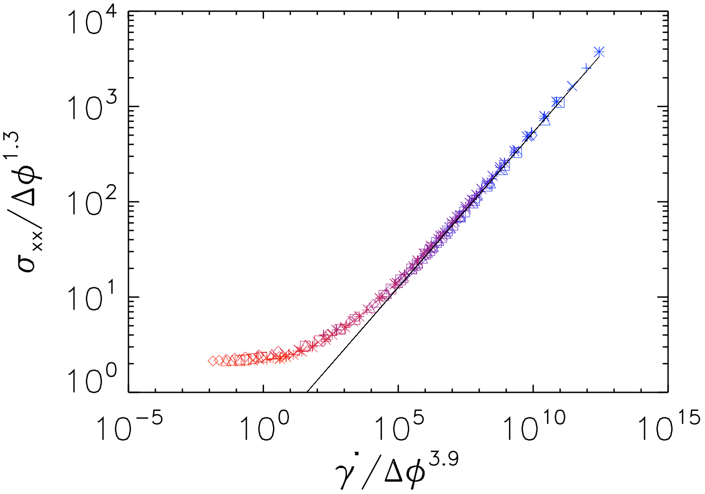

Figure 5.4: Plot of the stress vs. the strain rate rescaled for collapse in the Yield and Transition regime. The black line is given by $0.03\left(\dot{\gamma}/\Delta\phi^{3.9}\right)^{1.3/4}$. Colors and symbols correspond to density and strain rate as in table 3.3.

because

$$A_{xx}\left(\frac{d^2NZ}{2L_xL_yA_1A_2}\right)^{1.3/4} = 0.3 \pm 0.05, \tag{5.15}$$

in which A_{xx} is the only unknown. Substituting the values for d, N, Z, L_x, L_y, A_1 and A_2 that we set, approximated or fitted before, we find that $A_{xx} = 0.004 \pm 0.001$. This completes the normal extension to the Q3E model and we can focus on the width of the regimes to see where we would expect collapse when rescaling the data.

5.3.3 Regimes and Collapse

Figure 5.5 shows the same data as figure 5.4 but now coloured according to the regimes in which the various data points are located: Yield data points in black, Transition data points in red and Critical data points in blue. We can clearly see that the Transition regime is much smaller for the normal stress than for the shear stress, see figure 4.7, which is completely expected as B^{xx}_{eff} is about an order of magnitude larger than B^{xy}_{eff}. As we discussed above in section 4.4.1, data that is 'purely' in the Transition regime is already rare for the shear stress, but it will be virtually non-existent for the normal stress. This is why plotting for collapse in the Yield and Critical regime, as we have done in figure 5.5 is the appropriate way to plot the data and we expect collapse nearly everywhere.

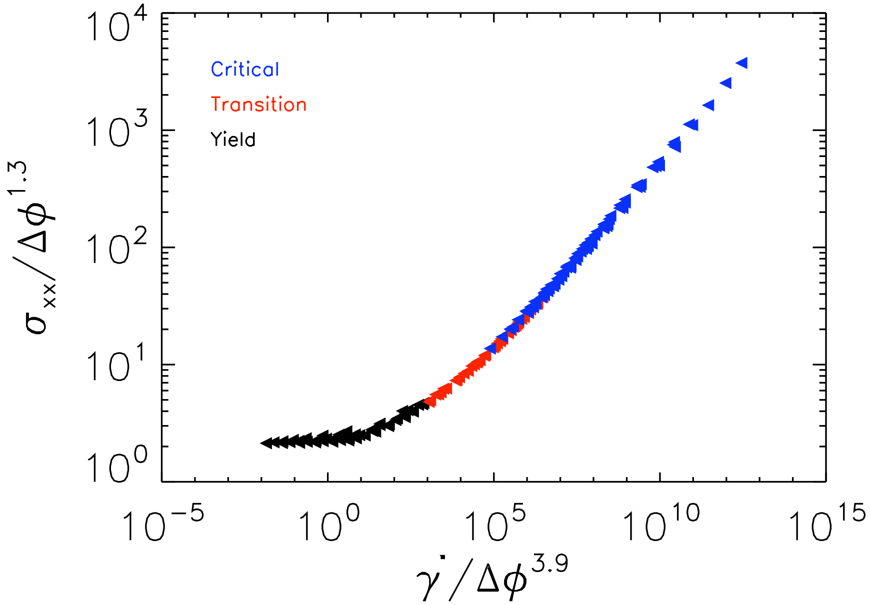

Figure 5.5: Collapse plot of the stress vs. the strain rate. Data points are coloured according to the regimes they are in: blue for Critical regime, red for Transition regime and black for Yield regime.

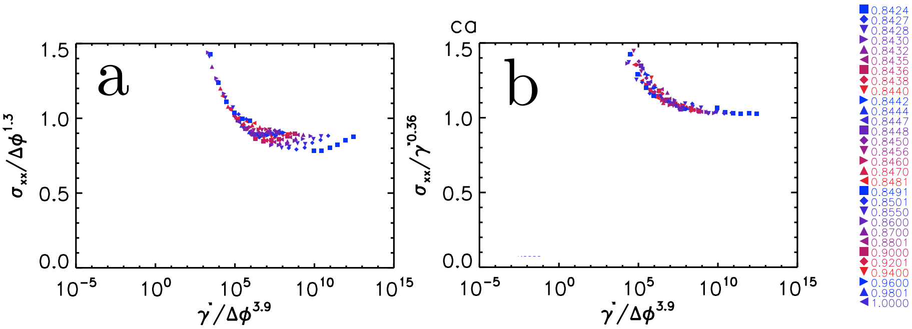

Figure 5.6: Plots of the stress vs. the strain rate with a Critical power law divided out. **a** with the model prediction of $\dot{\gamma}^{1.3/4} \approx \dot{\gamma}^{0.34}$ divided out. **b** with the power law that best yields a horizontal residue: $\dot{\gamma}^{0.36}$ divided out. The legend indicates which density corresponds to each symbol-color-combination.

However, just as was the case for the shear stress, this is not a reliable way to determine whether our predicted exponent in the Critical regime, β, is exactly correct. The real β cannot be too different from $1.3/4 \approx 0.34$, otherwise we would not have had good collapse. However, it can be slightly different. And in fact, in figure 5.6 **b** we see that dividing out our model prediction of $\dot{\gamma}^{1.3/4}$ does not result in perfectly flat residual data. Instead, as we show in figure 5.6 **b**, we best achieve flat behavior when dividing out $\dot{\gamma}^{0.36}$. Just as in the case of the shear stress, this exponent is slightly different from the model prediction but it is close enough to be considered consistent with our model.

It should be noted that this results is different from the most recent result by Olsson & Teitel [23] in two ways. First, the numerical value of the exponent in the Critical regime is different, 0.36 for us as opposed to 0.28 for Olsson & Teitel. And second, Olsson and Teitel find that the exponents for the shear stress and normal stress in the critical regime are the same, while we find that they are different: 0.47 vs. 0.36.

5.4 Conclusion

We have successfully extended our Q3E model to the normal component of the stress tensor. While there were some surprises, a different balance between the components of the effective strain and especially an unexpected elasticity relation, we have been able to account for these in our Q3E model. With these inclusions the Q3E model describes the simulation data well.The best numerical estimate for the value of the critical exponent β is within 5% our prediction.

Chapter 6

Microscopic Behavior

Our model directly describes the most important macroscopic behavior of the system: its rheology. In this chapter we will explore some of the remarkable microscopic behavior in the system, namely the relative velocities of the particles and the organisation of the forces.

6.1 Dissipation and Relative Velocity Distribution

As was discussed in both section 3.1.1 and section 4, energy dissipation is governed by the relative velocities of the bubbles, Δv. In this section we take a closer look at the probability distribution of Δv; we will be able to describe this distribution in surprising detail.

6.1.1 Second Moment

Specifically, we can look at the second moment of the distribution: $\left\langle \Delta v^2 \right\rangle$. We have already seen in section 2.3.4 that the distribution functions have widely varying width and therefore widely varying $\left\langle \Delta v^2 \right\rangle$. Naively, one would expect this second moment to scale with $\dot{\gamma}^2$: doubling the driving velocity would double the velocities of all bubbles and therefore all relative velocities. However, as can be seen in figure 6.1 **a**, this is not true: the distribution functions of $\Delta v / \dot{\gamma}$ do not collapse. This is not surprising because we know that

$$\left\langle \Delta v^2 \right\rangle \sim \sigma_{xy} \dot{\gamma} \tag{6.1}$$

And indeed, we see that $p\left(\Delta v / \left\langle \Delta v^2 \right\rangle\right) = p\left(\Delta v / \sqrt{\sigma_{xy} \dot{\gamma}}\right)$ does result in distribution functions of comparable width, as can be seen in figure 6.1 **b**. We also note, though, that the distributions functions themselves do not collapse.

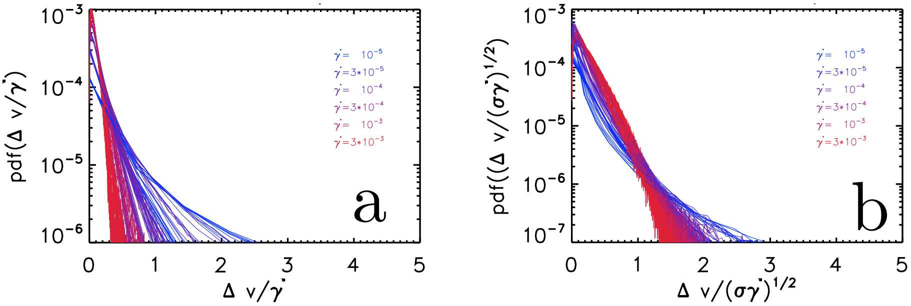

Figure 6.1: The probability distribution functions of Δv. **a**: the absences of collapse of $p\left(\Delta v/\dot{\gamma}\right)$ illustrates the non-trivial nature of the velocity fluctuations. **b**: when scaled by $\sqrt{\sigma\dot{\gamma}}$, the second moment of Δv collapses but the full distributions do not.

Below, we will first discuss the implications of Eq. 6.1 and then investigate the fact that the distribution functions do not collapse.

To get a good grasp on the implications of Eq. 6.1, we rewrite the original expression for power balance:

$$L_x L_y \dot{\gamma} \left\langle \sigma_{xy} \right\rangle_t = \frac{Nb}{2} \left\langle Z \right\rangle_t \left\langle \Delta v^2 \right\rangle_{t,ij} \tag{6.2}$$

by rescaling Δv with $\dot{\gamma}$, as discussed above, to take out the trivial dependence of velocities on the driving velocity; we denote $v_* := \Delta v/\dot{\gamma}$. We can also take together a number of the constants to form the contact density $C = NZ/2L_x L_y$. This results in

$$\left\langle v_*^2 \right\rangle_{t,ij} C = \frac{\left\langle \sigma_{xy} \right\rangle_t}{b\dot{\gamma}} \tag{6.3}$$

Here we can interpret $b\dot{\gamma}$ as an affine shear stress: if all particles were to move affinely, they would all feel a force $b\Delta v_{ij} = b\dot{\gamma}r_{ij}$ on one side and the same force in the other direction on the other side, for a total stress of $(1/2V)2N\left(rb\dot{\gamma}r\right) = (N\pi r^2/V)(2/\pi)b\dot{\gamma} = (2\phi/\pi)b\dot{\gamma}$.

We can now deduce the dependencies of v_* on $\Delta\phi$ and $\dot{\gamma}$ by considering the right hand side of Eq. 6.3. These dependencies are complex since σ_{xy} depends on both $\Delta\phi$ and $\dot{\gamma}$, and with different exponents in different regimes. We start by considering $\Delta\phi$: since σ_{xy} never shrinks with increasing density, and grows with increasing density in two out of three regimes[1], we can generally say that increasing $\Delta\phi$ increases v_*. Physically, this means the following. In more densely packed foams, a higher stress is needed to sustain steady flow at a fixed shear rate. Therefore, more energy is put into the system and more

---

[1] the Yield and Transition regimes

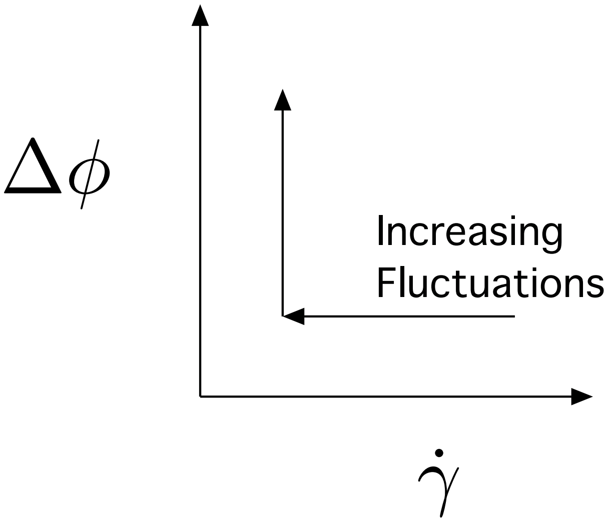

Figure 6.2: Fluctuations in the relative velocity increase with increasing density or decreasing strain rate.

energy needs to be dissipated. The only way the system can dissipate more energy is by increasing the relative velocity between the particles.

Now we consider the dependence of v_* on $\dot{\gamma}$. σ_{xy} always increases with increasing $\dot{\gamma}$, though the degree with which it does so depends on the regime. However, the dependence is always sublinear. Because σ_{xy} is sublinear in $\dot{\gamma}$, $\sigma_{xy}/\dot{\gamma}$ is a decreasing function of $\dot{\gamma}$. As a consequence, v_* decreases as $\dot{\gamma}$ increases. Physically this is because increasing the strain rate, at constant density, will not increase the input power as much as the resulting extra (relative) movement will increase the dissipated power; therefore less relative velocity is needed/possible to keep a balance between the input and dissipated power.

Both dependencies are illustrated in figure 6.2. Note that the fact that fluctuations increase with increasing density is opposite to the trend in to static jamming, where various measures of randomness and non-affinity increase when *decreasing* the density towards the jamming density [5]. Here the randomness increases with *increasing* density. It should be noted, though that the static jamming results have been obtained in the quasi-static regime, while here we are at finite strain rate.

We can now return to the probability distribution function of $\langle \Delta v \rangle$: we know how the second moment scales, $\left\langle \Delta v^2 \right\rangle \sim \sigma_{xy}\dot{\gamma}$, and can take this into account in plotting the data. Figure 6.1 **b** shows that the distribution functions are now of equal width, but not of similar shape. This means that the second moment does not capture the full behavior of the pdfs. In other words: higher order moments will also display non-trivial scaling. To investigate this, we will look at the higher order *even* moments of the relative velocity distribution

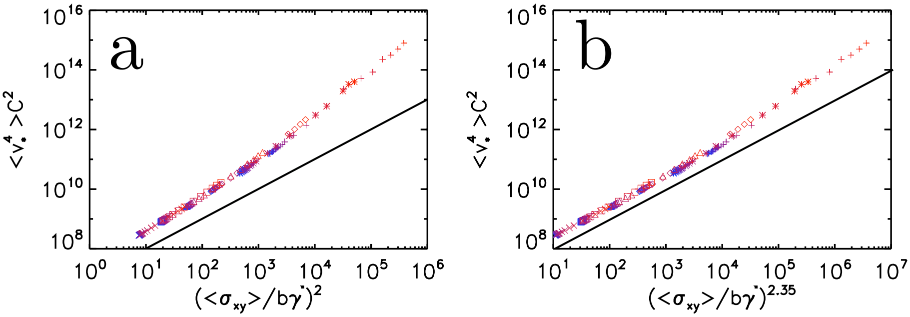

Figure 6.3: The fourth moment of the relative velocity distribution function vs. powers of $\sigma/\dot{\gamma}$. **a** The naive Gaussian assumption of $\left\langle v_*^4\right\rangle_{t,ij} C^2 \sim \left(\left\langle\sigma_{xy}\right\rangle_t / b\dot{\gamma}\right)^2$ does not hold as the data is not parallel to the black line that indicates linear scaling. **b** $\left\langle v_*^4\right\rangle_{t,ij} C^2 \sim \left(\left\langle\sigma_{xy}\right\rangle_t / b\dot{\gamma}\right)^{2.35}$ describes a large range of the data well, as the data is parallel to the black line that indicates linear scaling. In both plots, colours and shapes represent density and strain rate as in table 3.3.

because they also scale as moments of the dissipation. For example, for the next even moment, the fourth moment, we have $\left\langle\Delta v^4\right\rangle = \left\langle\left(\Delta v^2\right)^2\right\rangle \sim \left\langle P_{\text{diss}}^2\right\rangle$. In appendix 9.2 we also discuss the simple scaling of the first moment.

6.1.2 Fourth Moment

The first higher order even moment of the relative velocity distribution that will contribute to the non-collapse of the rescaled probability distribution functions is the fourth moment. The most simple possible scaling would be if the fourth movement scaled as the square of the second moment:

$$\left\langle v_*^4\right\rangle_{t,ij} C^2 \sim \left(\left\langle v_*^2\right\rangle_{t,ij} C\right)^2 = \left(\frac{\left\langle\sigma_{xy}\right\rangle_t}{b\dot{\gamma}}\right)^2, \tag{6.4}$$

as is the case for central moments in a Gaussian distribution, for example. However, as we show in figure 6.3 **a**, this naive assumption does not hold as the data is not parallel to the black line that indicates linear scaling

Therefore, we try a slightly different approach, namely the critical scaling-like description that has already been applied successfully to many quantities in static and non-static jamming. Thus, we hypothesise that we can describe the fourth moment of the relative velocity distribution in the following way:

$$\left\langle v_*^4\right\rangle_{t,ij} C^2 = \left(\frac{\left\langle\sigma_{xy}\right\rangle}{b\dot{\gamma}}\right)^\alpha F\left(\Delta\phi, (b/k)\dot{\gamma}\right). \tag{6.5}$$

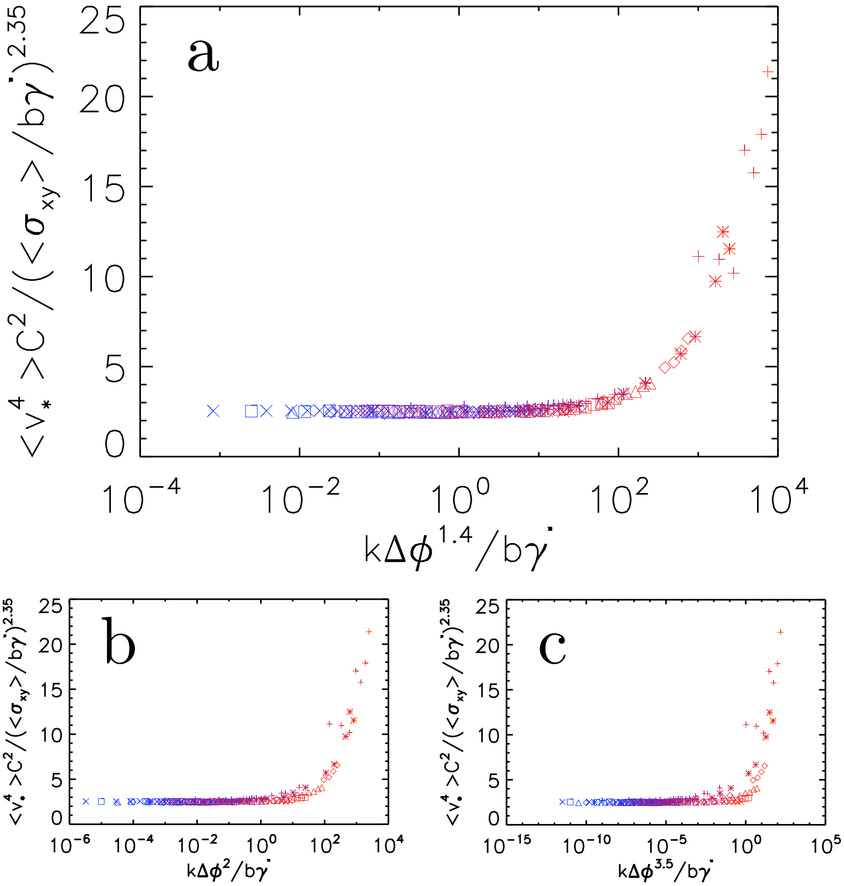

Figure 6.4: **a** the fourth moment of the relative velocity distribution function with an exponent 2.35 power law of $\sigma_{xy}/\dot{\gamma}$ divided out. **b**, **c**: plotting vs. either of the two crossovers, $\dot{\gamma} \sim \Delta\phi^2$ and $\dot{\gamma} \sim \Delta\phi^{3.5}$, does not result in good collapse in the non-power law portion of the curve. In all three plots, colours and shapes represent density and strain rate as in table 3.3.

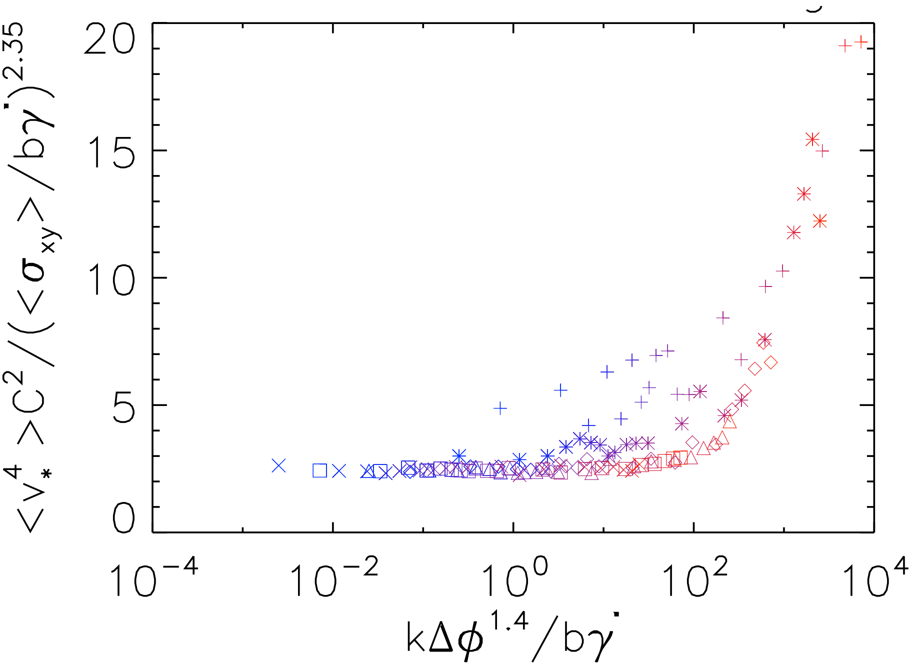

Figure 6.5: The same scaling plot for the fourth moment of v_* as figure 6.4 **a**, now for a system of one fourth the linear size, or one sixteenth the size. Note that the crossover from flat to curved takes place around 10^2, just as in figure 6.4 **a**.

In figure 6.3 we see that $\left\langle v_*^4\right\rangle_{t,ij} C^2 \sim \left(\left\langle\sigma_{xy}\right\rangle_t / b\dot{\gamma}\right)^{2.35}$ describes a large part, but not all, of the data well. Therefore, we expect $\alpha = 2.35$. Next, we try to describe F as precisely as possible. To plot F, we need to plot

$$\frac{\left\langle v_*^4\right\rangle_{t,ij} C^2}{\left(\frac{\langle\sigma_{xy}\rangle}{b\dot{\gamma}}\right)^{2.35}} = F\left(\Delta\phi, (b/k)\dot{\gamma}\right) \tag{6.6}$$

on the vertical axis. Then, we can determine the combination of $\dot{\gamma}$ and $\Delta\phi$ of which F is a function by determining for what combination the data collapses. Since we know that the power law description is worst for high density (red data points) and low strain rates (+'s and $*$'s) we start with trial combinations of the form $\Delta\phi^{\chi}/\left(b/k\right)\dot{\gamma}$, with χ an exponent that is essentially a fit-parameter. From figure 6.4 **a** we see that we get good collapse for $\chi = 1.4$. There is not enough data to make an accurate description of the functional form of F, however.

Note that the rescaling by $\Delta\phi^{1.4}/\left(b/k\right)\dot{\gamma}$ introduces a new combination of $\dot{\gamma}$ and $\Delta\phi$ in addition to $\Delta\phi^2/\dot{\gamma}$ and $\Delta\phi^{3.5}/\dot{\gamma}$ that emerged as crossovers

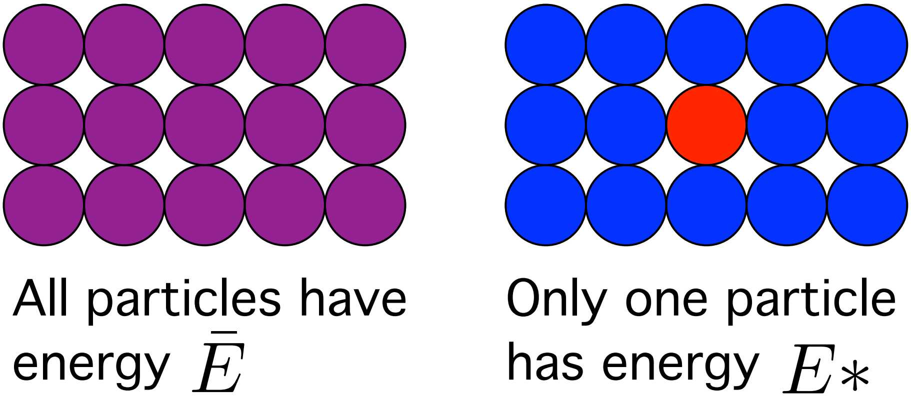

Figure 6.6: Two different energy distributions. On the left, the energy is equally distributed and the participation ratio is 1; on the right the energy is concentrated in one particle and the participation ratio is $1/N$

in our 3E scaling model. Intuitively these two relations would have been likely candidates for the argument of F, but as figure 6.4 **b** and **c** show, they perform markedly worse than $\Delta\phi^{1.4}/\left(b/k\right)\dot{\gamma}$. Currently, we do not have an interpretation of this new quantity. We have investigated whether this deviation from a simple power law is a finite size effect, by checking whether the part of the data that is described well by the power law grows smaller in smaller system sizes, but have found this not to be the case, as can be seen in figure 6.5, where we see that the position of the crossover does not change[2] if we reduce the size of the system by a factor of 16. However, it is surprising in itself that we are able to describe the fourth moment of the relative velocity distribution so accurately, even if the description is only empirical.

We can also offer an interpretation of what it means that the fourth moment does not show the naive Gaussian-like scaling that we introduced above and for that we have to consider a quantity called the participation ratio. The participation ratio of some quantity E, typically an energy, is defined as:

$$\mathrm{Part}(E) = \frac{\langle E \rangle^2}{\langle E^2 \rangle}. \tag{6.7}$$

With this definition, if the quantity E has a value of $\bar{E}$ at each particle, as on the left of figure 6.6, $\langle E \rangle$ is just $\bar{E}$ and thus $\langle E \rangle^2 = \bar{E}^2$. Similarly, since the value of E^2 in each particle will just be $\bar{E}^2$, we also have $\left\langle E^2 \right\rangle = \bar{E}^2$. Substituting these quantities in the participation ratio yields $\mathrm{Part}(E) = 1$, meaning that the system fully participates in the process associated with the quantity E. Conversely, if only one particle has a non-zero value of E, let's

---

[2] though the collapse is worse, possibly as a consequence of reduced statistics

call it $E*$, the average value of E is $E*/N$, where N is the total number of particles. This means that $\langle E\rangle^2 = E*^2/N^2$. Similarly $\langle E^2\rangle = E*^2/N$. Substituting these two quantities yields $\mathrm{Part}(E) = 1/N$: only one of N particles is participating in the process associated with E.

If we now take the dissipation as the relevant quantity, we have:

$$\mathrm{Part}(P_{\mathrm{diss}}) = \frac{\langle P_{\mathrm{diss}}\rangle^2}{\langle P_{\mathrm{diss}}^2\rangle} \sim \frac{\langle \Delta v^2\rangle^2}{\langle \Delta v^4\rangle}. \tag{6.8}$$

Therefore, the fourth moment of the relative velocity distribution enters in the participation ratio. Since, as we have seen above, the fourth moment does not simply scale as the square of the second moment, this will mean that the participation ratio will differ between systems at different strain rates and/or densities. Moreover, since we have accurate expressions for the second and fourth moments, we can write down an expression for the participation ratio of the dissipation:

$$\mathrm{Part}(P_{\mathrm{diss}}) \sim \left(\frac{\dot\gamma}{\langle\sigma_{xy}\rangle}\right)^{0.35} F\left(\frac{(b/k)\dot\gamma}{\Delta\phi^{1.4}}\right). \tag{6.9}$$

We can now investigate the parameter values for which the participation ratio is large or small. Since the function F is the same function as above and therefore a strictly increasing function and since the shear stress increases with density, increasing the density will decrease the participation ratio. Conversely, since the shear stress depends sub-linearly on the strain rate, increasing the strain rate will increase the participation ratio. Thus, for high strain rate and low density, closest to the critical point, the participation ratio will be highest and the dissipation will be most evenly spread throughout the system. On the other hand, if we have high density and low strain rate, approaching the quasi-static regime, the participation ratio will be very low. This means that all dissipation occurs in just a few bubbles. This means that we have identified the same regions with the extremes of randomness as above for the relative velocity fluctuations: high density, low strain rate is more localised; low density high strain rate is less localised, the parameter space picture of figure 6.2 therefore applies here as well.

To get a qualitative feeling for the actual difference between the distribution of the dissipation in these extreme cases we show two snapshots of our system coloured by dissipation in figure 6.7. Snapshot **a** is for $\Delta\phi = 0.98$ and $\dot\gamma = 10^{-5}$, the densest and slowest system we study. It therefore has the lowest participation ratio. Snapshot **b** is for $\Delta\phi = 0.8424$ and $\dot\gamma = 3\cdot 10^{-3}$, the least dense and fastest system with the highest participation ratio. There is a clear difference between the two: in snapshot **a** we can clearly identify individual dissipation events, though they still involve multiple bubbles, while the rest of the bubbles do not participate in the dissipation; in snapshot **b** there is a large extended area of bubbles experiencing dissipation.

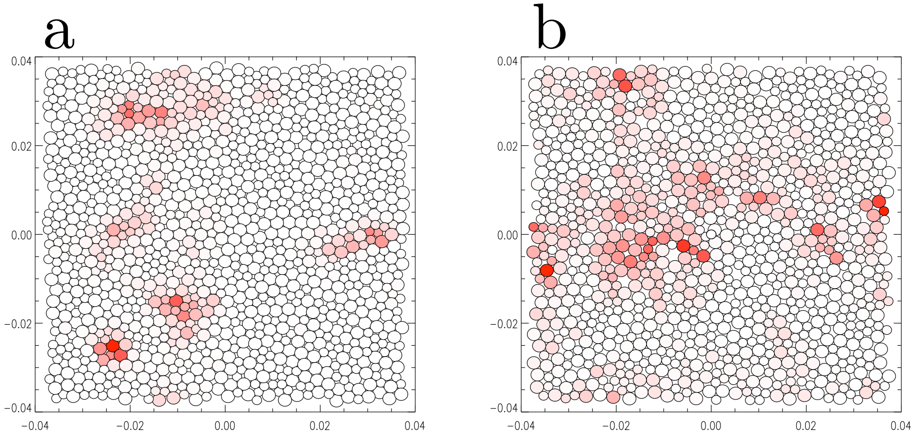

Figure 6.7: Two snapshots of our systems coloured by dissipation. Red means high dissipation while white means no dissipation. Both colour scales have been individually rescaled by their maximum dissipation. **a** has $\phi = 0.98$, $\dot{\gamma} = 10^{-5}$ and $N = 1020$; **b** has $\phi = 0.8424 \approx \phi_\mathrm{c}$, $\dot{\gamma} = 3 \cdot 10^{-3}$ and $N = 1200$.

6.1.3 Sixth and Higher Moments

Since we had such success in describing the fourth moment of the relative velocity distribution function, we can try a similar approach for the sixth moment. Based on our results for the fourth moment, we assume that $\langle v_*^6 \rangle \sim \langle v_*^4 \rangle^{3/2}$ or $\langle v_*^6 \rangle_{t,ij} C^3 = (\langle \sigma_{xy} \rangle / b\dot{\gamma})^{3.5} F^{3/2} \left(\Delta\phi^{1.4} / (b/k)\dot{\gamma} \right)$. Figure 6.8 **a** shows that this simple assumption is not correct: the data collapses poorly. However, the shape is similar enough to that seen for the fourth moment in figure 6.4 that we can try a more general scaling expression of the form:

$$\langle v_*^6 \rangle_{t,ij} C^3 = \left(\frac{\langle \sigma_{xy} \rangle}{b\dot{\gamma}} \right)^{\chi} F^{3/2} \left(\frac{\Delta\phi^{\xi}}{(b/k)\dot{\gamma}} \right) \tag{6.10}$$

As we show in figure 6.8 **b**, we get good collapse for $\chi = 3.85$ and $\xi = 1$. It is remarkable that it is possible to describe the sixth moment of a complicated distribution like $p(\Delta v)$ to such a level of detail.

Still, there is markedly more noise in the data for the sixth moment than for the fourth moment, which is not surprising given that we are looking at the distribution in more and more detail. Because of this and the fact that we have neither an explanation nor an interpretation of this result,we have not investigated the eighth or higher moments.

6.1.4 Conclusion

We have been able to describe the probability distribution function of the relative velocities, Δv, in surprising detail, finding expression for both the

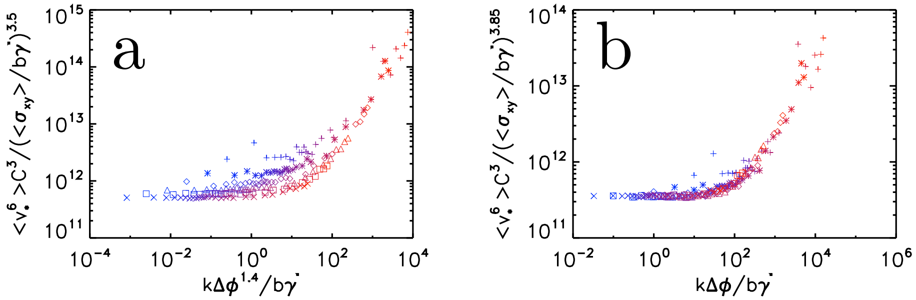

Figure 6.8: Possible scaling expressions for the sixth moment. **a** assuming that $\left\langle v_*^6\right\rangle_{t,ij} \sim \left\langle v_*^4\right\rangle_{t,ij}^{3/2}$. **b** the best fit is achieved for $\left\langle v_*^6\right\rangle_{t,ij} C^3 = \left(\left\langle\sigma_{xy}\right\rangle/b\dot\gamma\right)^{3.85} F^{3/2}\left(\Delta\phi/(b/k)\dot\gamma\right)$. In both plots, colours and shapes represent density and strain rate as in table 3.3.

second, fourth and sixth moments. Analysis of each of these moments reveals a similar picture. For high strain rate and low density the system is in a relatively homogeneous state: few fluctuations in Δv and a high participation ratio of the dissipation. The more the strain rate is increased or the density is decreased, however, the more fluctuations appear and the more inhomogeneous the system becomes.

6.2 Forces and Stresses

We have seen above in section 2.3.1 that, in the range that we limit ourselves to, $\sigma^{\text{el}} >> \sigma^{\text{visc}}$, see again in figure 6.9. On the other hand, all viscous and elastic forces together must balance on each bubble. We also know that the forces determine the stress via the Born-Huang formula [35]

$$\sigma_{xy} = \frac{1}{2V}\sum_{<ij>} r_{ij,x} f_{ij,y}, \tag{6.11}$$

How can elastic and viscous *forces* balance, while elastic and viscous *stresses* differ by orders of magnitude? The answer must lie in the organization of the forces and the way they combine on each bubble.

In order to look at the distribution of the forces we look at four different quantities. The first two are the second moments of the elastic and viscous force distributions:

$$< f_{\text{e}}^2 >= \frac{1}{NZ}\sum_{<ij>} f_{\text{e}}^2 \tag{6.12}$$

and similarly for $< f_{\text{v}}^2 >$, where the sum is over all contacts $< ij >$, N is the total number of particles, Z is the average number of contacts per particle and

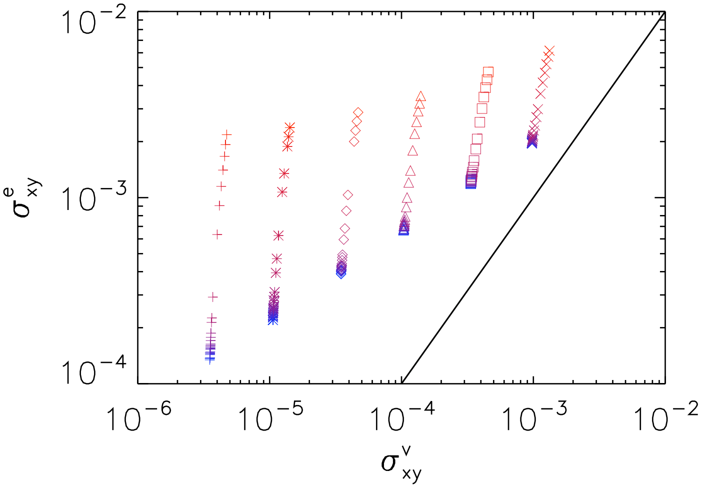

Figure 6.9: Scatterplot of the viscous vs. the elastic shear stress. The black line represents equality, but is never reached. Colours and shapes represent density and strain rate as in table 3.3.

NZ is the total amount of forces in the system[3]. The data is also averaged over a strain of approximately 13 corresponding to 2000 data samples with our sampling rate of 0.0067 strain. The second two are the second moments of the distributions of *net* elastic and viscous forces on a particle:

$$< f^2_{\mathrm{e,net}} >= \frac{1}{N} \sum_i \left(\sum_j \mathbf{f}^{ij}_{\mathrm{e}} \right)^2 \tag{6.13}$$

and similarly for $< f^2_{\mathrm{v,net}} >$, where the first sum is over all particles i and the second sum over all particles j in contact with particle i. Averaging over time is the same as above.

First, to get an impression how the individual forces add to net forces, we plot these in a scatterplot: $< f^2_{\mathrm{e}} >$ vs. $< f^2_{\mathrm{e,net}} >$ and $< f^2_{\mathrm{v}} >$ vs. $< f^2_{\mathrm{v,net}} >$. These plots can be seen in figure 6.10. These figures clearly show different behavior for the viscous and elastic forces. Panel **a** shows that the elastic net forces, $< f^2_{\mathrm{e,net}} >$, are much smaller than the elastic forces, $< f^2_{\mathrm{e}} >$. This means that, typically, the elastic forces on a bubble largely balance and cancel each other. The magnitude of the imbalance, however, varies and clearly depends on both the density and the strain rate. Panel **b**, in contrast, shows that the viscous net forces, $< f^2_{\mathrm{v,net}} >$, are larger than the viscous forces, $< f^2_{\mathrm{v}} >$. This means that the viscous forces typically do

---

[3] this is twice the number of contacts, because each contact $< ij >$ carries two forces: one from particle i on particle j and one from particle j on particle i

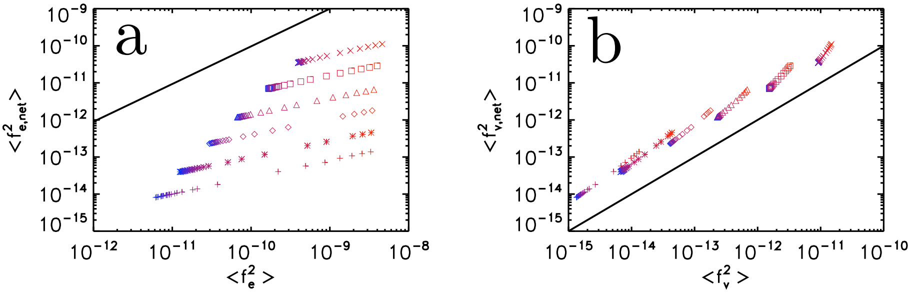

Figure 6.10: The second moment of the average force vs. the second moment of the average net force per bubble. **a** for the elastic force, **b** for the viscous force. The black lines represent equality. In both plots, colours and shapes represent density and strain rate as in table 3.3.

$$\sigma_{xy}^{\mathrm{e}} \qquad \left\langle f_{\mathrm{e}}^2 \right\rangle \qquad \left\langle f_{\mathrm{e,net}}^2 \right\rangle$$

$$\sigma_{xy}$$

$$\sigma_{xy}^{\mathrm{v}} \qquad \left\langle f_{\mathrm{v}}^2 \right\rangle \qquad \left\langle f_{\mathrm{v,net}}^2 \right\rangle$$

Figure 6.11: The various stress and force quantities that we will try to connect to each other.

not cancel per particle but instead add up. In addition there seems to be an approximately linear relation between the individual and net viscous forces. Finally, comparing the values of $< f_{\mathrm{e}}^2 >$ and $< f_{\mathrm{v}}^2 >$, we observe that $< f_{\mathrm{e}}^2 >$, ranging from 10^{-11} to 10^{-8}, is bigger than $< f_{\mathrm{v}}^2 >$, which ranges from 10^{-15} to 10^{-11}.

These observations answers the question how elastic and viscous forces can balance, while elastic and viscous stresses differ by orders of magnitude. Namely, elastic stresses are much larger than viscous stresses because the individual elastic forces are much larger than the individual viscous forces. However, since all elastic forces on a bubble largely cancel, the net elastic force on a bubble is relatively small, which allows it to be balanced by the net viscous force on the bubble, which is made up of the much smaller, but non-cancelling, individual viscous forces.

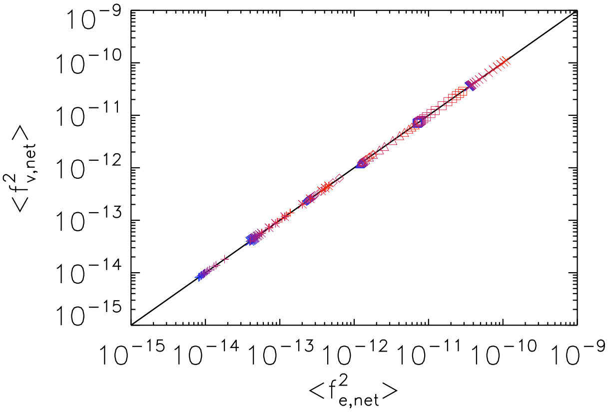

Figure 6.12: The second moments of the distributions of the net elastic and viscous force per bubble in a scatterplot. The black line indicates equality. Colours and shapes represent density and strain rate as in table 3.3.

We will now fully explore the relationships between the forces and stresses discussed here. Figure 6.11 displays which quantities we will try to link together: the shear stress, its two components and the four force quantities discussed above. Some of the relations will be exact since they follow from, for example, force or power balance. Other relations will be approximate and/or empirical.

The first exact relation, which we have already tested before, is power balance. Although we have formulated power balance in terms of the velocity difference Δv in our model, we can also formulate it in terms of the viscous force f_v because the two are strictly proportional: $\mathbf{f}_\mathrm{v} = -b\Delta\mathbf{v}$. This different formulation of power balance is:

$$L_x L_y \dot{\gamma} \sigma_{xy} = \frac{N}{2b} Z \left\langle f_v^2 \right\rangle \tag{6.14}$$

This relationship is represented by the green line labeled with an **a** in figure 6.14.

The second exact relation, also mentioned before, is force balance. Since there are only two kinds of forces in our system, elastic and viscous forces, and since we use overdamped dynamics, the net viscous and elastic force must balance each other on each bubble. The averages of their squares must therefore also be the same, or:

$$< f^2_{\mathrm{v,net}} >=< f^2_{\mathrm{e,net}} > . \tag{6.15}$$

Figure 6.12 shows that this is indeed the case. This relationship is represented by the green line labeled with a **b** in figure 6.14.

The third relation has been mentioned a number of times before and concerns the total and elastic stresses. Since we select our data on the condition

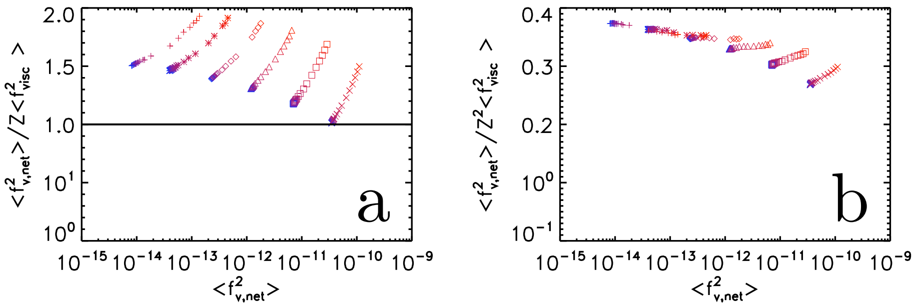

Figure 6.13: The ratio of the second moment of the distribution of net forces per bubble,$< f^2_{\mathrm{v,net}} >$, and the second moment of the distribution of individual forces,$< f^2_{\mathrm{v}} >$ multiplied with different powers of the contact number. In panel **a**, a value of 1, indicated by the black line, represents total decorrelation of the forces. In panel **b**, a value of 1 means total coherence. In both plots, colours and shapes represent density and strain rate as in table 3.3.

that the viscous stress is small compared to the elastic stress, we also know that the total stress must be approximately equal to the elastic stress:

$$\sigma^{\mathrm{e}}_{xy} \approx \sigma_{xy}. \tag{6.16}$$

This relation differs from the previous two in that it is not an exact relation.This relationship is represented by the red line labeled with a **c** in figure 6.14.

We have seen above that there is a roughly linear relationship between the second moments of the distribution of viscous forces and the distribution of net viscous forces. Here we will investigate this relationship in more detail. The most simple and natural reason for such a linear relationship would be a complete lack of correlation between the individual forces. In this case we would have:

$$< f^2_{\mathrm{v,net}} >= Z < f^2_{\mathrm{v}} > . \tag{6.17}$$

A different hypothesis that would also result in a linear dependence would be complete *coherence*; in that case we would have:

$$< f^2_{\mathrm{v,net}} >= Z^2 < f^2_{\mathrm{v}} > . \tag{6.18}$$

In general, the ratio of $< f^2_{\mathrm{v,net}} >$ and $< f^2_{\mathrm{v}} >$ can go from Z^2, total correlation, through Z, total decorrelation to 0, total anti-correlation in such a way that viscous forces alone balance on each bubble. In figure 6.13 **a** we plot $< f^2_{\mathrm{v,net}} > /Z < f^2_{\mathrm{v}} >$. While the value of the ratio iremains between 1 and 2, clearly this is not the entire story. Conversely, on figure 6.13 **b** we plot $< f^2_{\mathrm{v,net}} > /Z^2 < f^2_{\mathrm{v}} >$. This ratio lies between 0.3 and 0.4, but there is much less scatter,

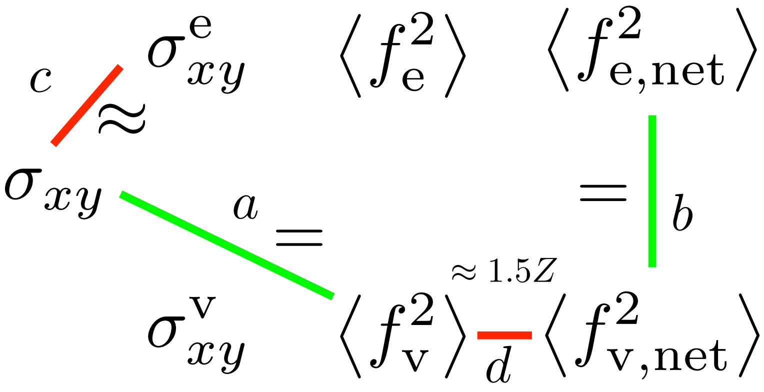

Figure 6.14: Tying together the various force and stress expressions. Green lines indicate exact relations, red lines indicate empirical and approximate relations. The relations are given by: **a** $L_x L_y \dot{\gamma} \left\langle \sigma_{xy} \right\rangle_t = (N/2b) \left\langle Z \right\rangle_t \left\langle f_v^2 \right\rangle_{t,ij}$ energy balance, **b** $< f^2_{\mathrm{v,net}} > = < f^2_{\mathrm{e,net}} >$ force balance, **c** $\sigma^{\mathrm{e}}_{xy} \approx \sigma_{xy}$, elastic stress dominates and **d** $< f^2_{\mathrm{v,net}} > \approx Z < f^2_{\mathrm{v}} >$ decorrelation of viscous forces.

especially for slower strain rates. Since the assumption of total decorrelation is never off by more than a factor of two we will write that:

$$< f^2_{\mathrm{v,net}} > \approx 1.5Z < f^2_{\mathrm{v}} > . \tag{6.19}$$

This relationship is represented by the red line indicated with a **d** in figure 6.14.

A graphic overview of the four relations discussed above is given in figure 6.14. Two things can be noted. First, the four relations that we have described form a chain: each of the five quantities involved can be linked to any of the four other quantities. This allows us, for example, to link the *elastic* stress to the *viscous* forces.

Two quantities are currently not linked to the rest: σ^{v}_{xy} and $< f^2_{\mathrm{e}} >$. Two possible ingredients for a relation to σ^{v}_{xy} are σ_{xy} and $< f^2_{\mathrm{v}} >$. Two possible candidates for a relation to $< f^2_{\mathrm{e}} >$ are σ^{e}_{xy} and $< f^2_{\mathrm{e,net}} >$. For simplicity we will investigate the relationship between σ^{v}_{xy} and $< f^2_{\mathrm{v}} >$ and the relationship between σ^{e}_{xy} and $< f^2_{\mathrm{e}} >$.

The stress is calculated as a function of forces:

$$\sigma_{xy} = \frac{1}{2V} \sum_{<ij>} r^{ij}_x f^{ij}_y , \tag{6.20}$$

where the sum runs over all contacts and $\mathbf{r}$ is the vector connecting the centres of the two contacting bubbles. If the orientations of all contacts and forces were uniformly distributed over the circle and there were no correlations between the orientation of a contact, the orientation of the force in that contact and

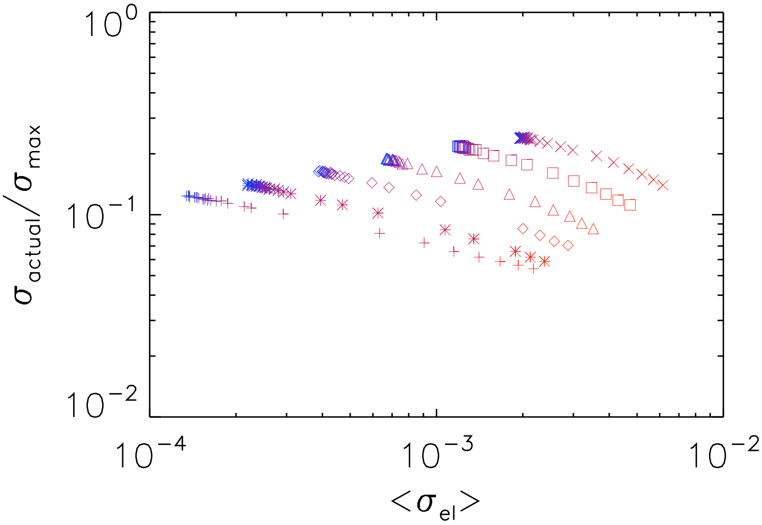

Figure 6.15: The ratio of actual to maximal elastic shear stress given by $\left\langle f_{\mathrm{e}}^2 \right\rangle^{1/2} NZ < r > /2$. Colours and shapes represent density and strain rate as in table 3.3.

the size of that force[4] then the total stress would be zero as all contributions would cancel on average. This means that the appearance of an overall stress implies some correlation or anisotropy.

The best way to approach the amount of anisotropy is from the other extreme: the case where the anisotropy maximises the stress. We first consider the elastic stress:

$$\sigma_{xy}^{\mathrm{el}} = \frac{1}{2V} \sum_{<ij>} r_x^{ij} f_y^{\mathrm{el}ij}. \tag{6.21}$$

Since f^{el} is always in the same direction as r, this product will be maximised when all contacts are along 45 degree angles with respect to the x- and y-axes. On average $r_x^{ij} f_y^{\mathrm{el}ij}$ will then be $(1/\sqrt{2}) < r > (1/\sqrt{2}) < |f^{\mathrm{el}}| >$. The full expression of the maximal elastic stress, given the average elastic force is then:

$$\sigma_{xy}^{\mathrm{el,max}} = \frac{NZ}{4V} \langle r \rangle \sqrt{\langle f_{\mathrm{el}}^2 \rangle}. \tag{6.22}$$

The actually attained elastic shear stress, as a fraction of this maximal stress, is shown in figure 6.15, which shows that (this particular kind of) anisotropy is maximised for low density, the blue points, and high strain rate, the family of crosses on the right. In our range of $\Delta\phi$ and $\dot{\gamma}$ the anisotropy is never larger than 0.1 and never smaller than 0.03.

---

[4] and the length of the connection vector, but since this is always of the order of the bubble radius anyway, we can ignore its variations.

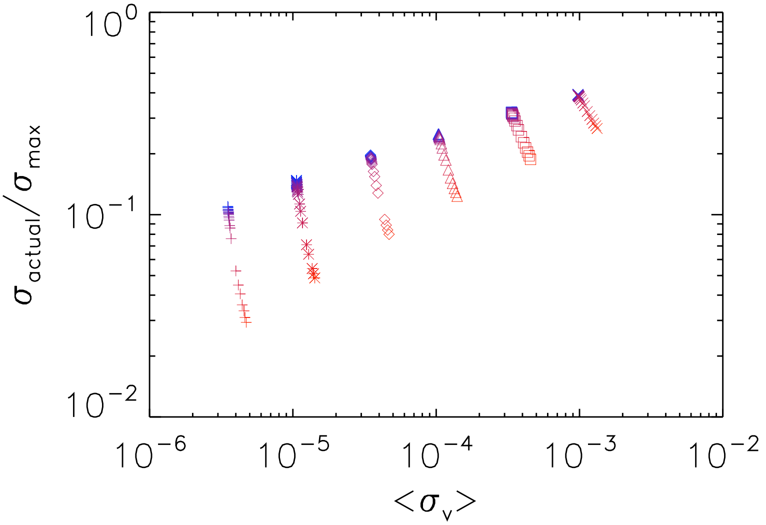

Figure 6.16: The ratio of actual to maximal viscous shear stress given by $\left\langle f_{\mathrm{e}}^2\right\rangle^{1/2} NZ < r >$. Colours and shapes represent density and strain rate as in table 3.3.

A similar analysis can be performed for the viscous stress. Since the viscous force does not have to be along r, the configuration that maximises the $\sum_{<ij>} r_x^{ij} f_y^{\mathrm{v}ij}$ will be different. In fact, the optimal configuration will be one in which all contacts are horizontal, so that $r_x = r$, and all viscous force are vertical, so that $f_y^{\mathrm{v}} = f^{\mathrm{v}}$. The full expression for the maximal viscous stress, given the average viscous force is then:

$$\sigma_{xy}^{\mathrm{v,max}} = \frac{NZ}{2V} \langle r \rangle \sqrt{\langle f_{\mathrm{v}}^2 \rangle}. \tag{6.23}$$

The actually attained viscous shear stress, as a fraction of this maximal stress, is shown in figure 6.16, which shows that the (second kind of) anisotropy is also maximised for low density and high strain rate. But while these different forms of anisotropy are maximised in the same regime, they attain different values: the viscous anisotropy can reach values up to 0.4.

The two relationships that we have described, between $\sigma_{xy}^{\mathrm{el}}$ and $\left\langle f_{\mathrm{el}}^2\right\rangle$ on the one hand and σ_{xy}^{v} and $\left\langle f_{\mathrm{v}}^2\right\rangle$ on the other hand, are not identities. They cannot be used to write one of the quantities in terms of the other, they only maximise one, the shear stress, in terms of the other, the average force. More usefully, the degree to which this maximum is attained or not gives us information about correlations in the contact network. In this sense it is very similar to the relation between $\left\langle f_{\mathrm{v,net}}^2\right\rangle$ and $\left\langle f_{\mathrm{v}}^2\right\rangle$: one ($\left\langle f_{\mathrm{v}}^2\right\rangle$) gives a maximum on the other ($\left\langle f_{\mathrm{v,net}}^2\right\rangle$) and the degree to which this maximum is

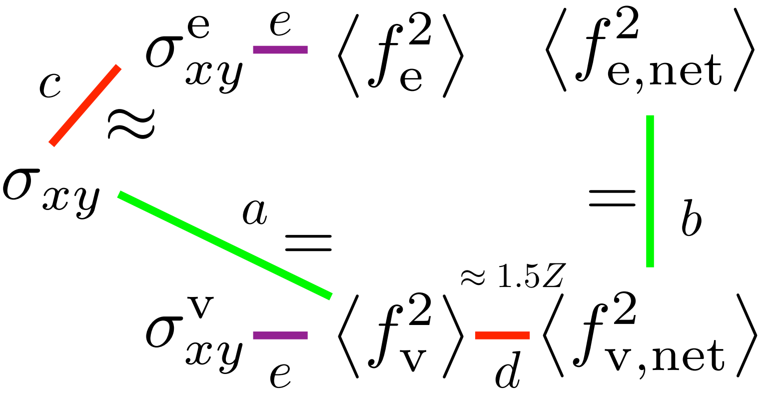

Figure 6.17: Tying together the various force and stress expressions. Green lines indicate necessary and exact relations, red lines indicate empirical and approximate relations, purple lines indicate relations that cannot satisfactorily be reduced to an equality. The relations are given by: **a** $L_x L_y \dot{\gamma} \left\langle \sigma_{xy} \right\rangle_t = (N/2b) \left\langle Z \right\rangle_t \left\langle f_v^2 \right\rangle_{t,ij}$ energy balance, **b** $< f_{\mathrm{v,net}}^2 >=< f_{\mathrm{e,net}}^2 >$ force balance, **c** $\sigma_{xy}^{\mathrm{e}} \approx \sigma_{xy}$, elastic stress dominates, **d** $< f_{\mathrm{v,net}}^2 >\approx Z < f_{\mathrm{v}}^2 >$ decorrelation of viscous forces and **e** the relations between the actual and maximally possible shear stresses that give an indication of the anisotropy.

attained gives some information about correlations (between the individual forces on a bubble). The relation between the two viscous force quantities is only different in the sense that a reasonably well-defined, and, perhaps more importantly, clearly interpretable, identity could be derived. Figure 6.17 adds the the two stress-force relationships that we discussed here to the previous overview for completeness' sake.

6.2.1 Conclusion

We have resolved the apparent contradiction between the balancing of viscous and elastic stresses on each bubble and the orders of magnitude size difference between the viscous and elastic stresses. Elastic forces are indeed, on average, larger than viscous forces, hence the difference between the stresses. However, since the elastic forces on each bubble largely cancel the resulting elastic force is small enough to be canceled by the viscous forces. In addition we tested and derived a number of other relations between the various components of the stress and forces, allowing us, for example, to express the *elastic* stress in the *viscous* forces.

Chapter 7

Non-linear Scaling Model

All of the preceding chapters dealt with a linear microscopic model: the elastic forces of Eq. 2.1 and the viscous forces of Eq. 2.3 are linear in respectively the overlap and the relative velocity. There are two good reasons to consider a larger class of microscopic models. The first reason is that many systems, for example the foams that we claim to describe, do not actually have linear (viscous) interactions. The second reason is that this allows us to probe whether changing the microscopic interactions influences the critical exponents. Given the way we have derived our 'critical' exponents, it does not seem likely that our exponents are independent of the microscopic interactions, and this aspect will be investigated in detail in this chapter.

7.1 Microscopic Model

We generalise our original, linear, microscopic model by changing the interactions into more general power law dependences:

$$\begin{aligned} \mathbf{F}^{\mathrm{e}}_{ij} &= k\delta_{ij}^{\alpha_{\mathrm{e}}}\hat{\mathbf{r}} && (7.1) \\ \mathbf{F}^{\mathrm{v}}_{ij} &= -b\Delta v_{ij}^{\alpha_{\mathrm{v}}}\Delta\hat{\mathbf{v}}_{ij}, && (7.2) \end{aligned}$$

with $\hat{\mathbf{r}}$ the unit vector connecting the centres of particles i and j and α_{e} and α_{v} being general power law exponents that can take any (positive) value. Note that both forces will still be zero when particles are not in contact and that setting $\alpha_{\mathrm{e}} = \alpha_{\mathrm{v}} = 1$ recovers the linear Durian model of the preceding chapters. This new formulation will allow our model to describe many more experimentally relevant systems. For example, the model can describe hertzian particles like grains in which $F^{\mathrm{e}} \sim \delta^{3/2}$. More importantly, foams do not have linear viscous interactions, but are microscopically shear thinning, $F \sim \Delta v^{2/3}$ [37]. Our new model can therefore make predictions for the rheology of these kinds of systems. These predictions will be developed and tested in this chapter.

7.2 Scaling Model

We will now investigate how the three ingredients of our original 3E scaling model, power balance Eq. 4.1, effective strain Eq. 4.2 and the elasticity relation Eq. 4.5, change when we change from the linear microscopic model to the more general power law microscopic model.

7.2.1 Energy Balance

The first ingredient of our 3E model is an equation for power balance. The power that is put into a system of linear size L by shearing is given by $\sigma_{xy}\dot{\gamma}L^2$. This power is dissipated by the viscous interactions between the bubbles. The power that is dissipated between two bubbles, i and j, is given by $\Delta\mathbf{v}_{ij}\cdot\mathbf{F}^{\mathrm{v}}_{ij}$, the inner product of their relative velocity and the dissipative force they exert on each other. Averaging both expressions over time and averaging the dissipation over all contacts then yields

$$\langle\sigma_{xy}\rangle_t\,\dot{\gamma}L^2 = N/2\left\langle Z\left\langle\Delta\mathbf{v}_{ij}\cdot\mathbf{F}^{\mathrm{v}}_{ij}\right\rangle_{ij}\right\rangle_t, \tag{7.3}$$

with $\langle\cdot\rangle_{ij}$ indicating averaging over all contacts. Since the viscous force is so explicitly present in the formulation of power balance, it is clear that, and how, changing the exponent of the viscous force will change the formulation of power balance. Substituting our definition for the dissipative force, equation 7.2, we get the following expression:

$$\langle\sigma_{xy}\rangle_t\,\dot{\gamma}L^2 = bN/2\left\langle Z\left\langle\Delta\mathbf{v}^{1+\alpha_{\mathrm{v}}}\right\rangle_{ij}\right\rangle_t, \tag{7.4}$$

7.2.2 Effective Strain

The effective strain will not depend explicitly on the microscopic force laws in our system: the yield strain, γ_{y}, is a function of the compression only and while the way the compression depends on, for example, the pressure may depend on the microscopic interactions, the formulation of the effective strain as a function of $\Delta\phi$ will not. Similarly, the dynamic strain, γ_{dyn}, depends on the timescale in which particles rearrange, which itself depends on the strain rate with which the system is driven and the average relative velocity between particles. Although the average relative velocity will probably not be the same in systems with different microscopic force laws, the way the dynamic strain depends on this difference is purely geometric and therefore will not change.

This means that we can simply copy the relation that we had before:

$$\begin{aligned}
\gamma_{\rm y} &= \Delta\phi && (7.5)\\
\gamma_{\rm dyn} &= \frac{\dot{\gamma}d}{\langle\Delta v\rangle_{t,ij}} && (7.6)\\
\gamma_{\rm eff}^{xy} &= B_{\rm eff}^{xy}\gamma_{\rm y} + \gamma_{\rm dyn} && (7.7)\\
\gamma_{\rm eff}^{xx} &= B_{\rm eff}^{xx}\gamma_{\rm y} + \gamma_{\rm dyn} && (7.8)
\end{aligned}$$

7.2.3 Elasticity Relation

The situation for the elasticity is more complicated. It will turn out to depend on the elastic force law, but not in such a straightforward way as our power balance expression depended on the viscous force law. In order to derive this dependence we start by looking at the dimensionless stress. In the linear case we had the following expression

$$\tilde{\sigma} = \frac{\sigma}{k} \qquad (7.9)$$

In our non-linear microscopic model, however, the unit of k is no longer Nm^{-1} but $Nm^{-\alpha_{\rm e}}$ and the resulting $\tilde{\sigma}$ is not dimensionless. Therefore, we need to formulate a more general expression for the dimensionless stress which reduces to Eq. 7.9 for linear interactions but gives a dimensionless stress for all values of $\alpha_{\rm e}$ (and $\alpha_{\rm v}$). One possible approach is to divide not by the bare spring constant k, but by the effective spring constant $k_{\rm eff} = \langle {\rm d}F^{\rm e}/{\rm d}\delta\rangle_{ij} = \left\langle \alpha_{\rm e}k\delta^{\alpha_{\rm e}-1}\right\rangle$, which will always have units of Nm^{-1}. Note that in the linear case $k_{\rm eff} = k$. If we assume that the typical overlap will scale with the global effective strain and the particle size, we get:

$$k_{\rm eff} = \alpha_{\rm e}k\left(d\gamma_{\rm eff}\right)^{\alpha_{\rm e}-1} \qquad (7.10)$$

We also assume that the non-dimensional stress will still depend on the effective strain in the same way as in the linear case, Eqs. 4.5 and 5.4. Especially in the case of the normal stress, where our elasticity equation was purely phenomenological, this is a strong assumption. We must first give the elasticity relation in non-dimensional form, but since we only have to divide by k in the linear case, this is straightforward:

$$\begin{aligned}
\tilde{\sigma}_{xy}^{\rm e} &= A_1^{xy}\Delta\phi^{1/2}\gamma_{\rm eff}^{xy}\sqrt{1+\frac{(A_2^{xy}\gamma_{\rm eff}^{xy})^2}{\Delta\phi}} && (7.11)\\
\tilde{\sigma}_{xx}^{\rm e} &= A_1^{xx}\gamma_{\rm eff}^{xx1.3}. && (7.12)
\end{aligned}$$

Multiplying this with $k_{\rm eff}$ to recover the expression for the full, dimensional

	Critical	Transition
elasticity	$\sigma \sim \gamma_{\mathrm{eff}}^{1+\alpha_{\mathrm{e}}}$	$\sigma \sim \Delta\phi^{1/2}\gamma_{\mathrm{eff}}^{\alpha_{\mathrm{e}}}$
effective strain	$\gamma_{\mathrm{eff}} \sim \dot{\gamma}/\Delta v$	$\gamma_{\mathrm{eff}} \sim \dot{\gamma}/\Delta v$
rheology	$\sigma \sim \dot{\gamma}^{\frac{\alpha_{\mathrm{v}}(1+\alpha_{\mathrm{e}})}{2+\alpha_{\mathrm{v}}+\alpha_{\mathrm{e}}}}$	$\sigma \sim \Delta\phi^{\frac{1+\alpha_{\mathrm{v}}}{2(1+\alpha_{\mathrm{v}}+\alpha_{\mathrm{e}})}}\dot{\gamma}^{\frac{\alpha_{\mathrm{e}}\alpha_{\mathrm{v}}}{1+\alpha_{\mathrm{v}}+\alpha_{\mathrm{e}}}}$
range	$\dot{\gamma} > \Delta\phi^{\frac{2+\alpha_{\mathrm{v}}+\alpha_{\mathrm{e}}}{2\alpha_{\mathrm{v}}}}$	$\dot{\gamma} > \Delta\phi^{\frac{3/2+\alpha_{\mathrm{v}}+\alpha_{\mathrm{e}}}{\alpha_{\mathrm{v}}}}$
	$\dot{\gamma} > \Delta\phi^{2+\alpha_{\mathrm{v}}+\alpha_{\mathrm{e}}}$	$\dot{\gamma} < \Delta\phi^{\frac{2+\alpha_{\mathrm{v}}+\alpha_{\mathrm{e}}}{2\alpha_{\mathrm{v}}}}$
	Yield	Dense
elasticity	$\sigma \sim \Delta\phi^{1/2}\gamma_{\mathrm{eff}}^{\alpha_{\mathrm{e}}}$	$\sigma \sim \gamma_{\mathrm{eff}}^{1+\alpha_{\mathrm{e}}}$
effective strain	$\gamma_{\mathrm{eff}} \sim \Delta\phi$	$\gamma_{\mathrm{eff}} \sim \Delta\phi$
rheology	$\sigma \sim \Delta\phi^{\alpha_{\mathrm{e}}+1/2}$	$\sigma \sim \Delta\phi^{\alpha_{\mathrm{e}}+1}$
range	$\dot{\gamma} < \Delta\phi^{\frac{3/2+\alpha_{\mathrm{v}}+\alpha_{\mathrm{e}}}{\alpha_{\mathrm{v}}}}$	$C < \Delta\phi$
	$C > \Delta\phi$	$\dot{\gamma} < \Delta\phi^{2+\alpha_{\mathrm{v}}+\alpha_{\mathrm{e}}}$

Table 7.1: The four rheological regimes for the shear stress in our general power law scaling model with their definitions, results and ranges of validity.

stress we get:

$$\sigma^{\mathrm{e}}_{xy} = A_1^{xy}\alpha_{\mathrm{e}}kd^{\alpha_{\mathrm{e}}-1}\Delta\phi^{1/2}\gamma_{\mathrm{eff}}^{xy\alpha_{\mathrm{e}}}\sqrt{1+\frac{(A_2^{xy}\gamma_{\mathrm{eff}}^{xy})^2}{\Delta\phi}} \tag{7.13}$$

$$\sigma^{\mathrm{e}}_{xx} = A_1^{xx}\alpha_{\mathrm{e}}kd^{\alpha_{\mathrm{e}}-1}\gamma_{\mathrm{eff}}^{xx\alpha_{\mathrm{e}}+0.3}. \tag{7.14}$$

7.3 Regimes

Now that we have our three scaling model ingredients for the general power law case, we note two things. First, both microscopic force law exponents enter in them and will therefore presumably impact the rheology. Second, there are still two regimes for the effective strain, Eq. 7.5 and two, respectively one, regimes for the shear, respectively normal, stress elasticity, Eq. 7.13, 7.14. This means that we can still apply the same methodology as in the linear case: we divide the full parameter space in four, for the shear stress, and three, for the normal stress, regimes, as indicated in table 7.1; then solve the rheological relations by simple substitution in each regime and finally use these results to determine the crossovers between the regimes. While the resulting exponents will be more involved, featuring fractions and combinations of α_{e} and α_{v}, the methods are completely similar to those used in section 3.2. Therefore, the rheological results are presented in tables 7.1 and 7.2. In the section below we list the full results, including expressions for Δv and γ_{eff}.

	Normal Critical	Normal Transition
shear stress	$\sigma_{xy} \sim \dot{\gamma}^{\frac{\alpha_\mathrm{v}(1+\alpha_\mathrm{e})}{2+\alpha_\mathrm{v}+\alpha_\mathrm{e}}}$	$\sigma_{xy} \sim \Delta\phi^{\frac{1+\alpha_\mathrm{v}}{2(1+\alpha_\mathrm{v}+\alpha_\mathrm{e})}}\,\dot{\gamma}^{\frac{\alpha_\mathrm{e}\alpha_\mathrm{v}}{1+\alpha_\mathrm{v}+\alpha_\mathrm{e}}}$
effective strain	$\gamma_\mathrm{eff} \sim \dot{\gamma}/\Delta v$	$\gamma_\mathrm{eff} \sim \dot{\gamma}/\Delta v$
rheology	$\sigma_{xx} \sim \dot{\gamma}^{\frac{\alpha_\mathrm{v}(\alpha_\mathrm{e}+0.3)}{2+\alpha_\mathrm{v}+\alpha_\mathrm{e}}}$	$\sigma_{xx} \sim \Delta\phi^{\frac{-(\alpha_\mathrm{e}+0.3)}{2(1+\alpha_\mathrm{v}+\alpha_\mathrm{e})}}\,\dot{\gamma}^{\frac{\alpha_\mathrm{v}(\alpha_\mathrm{e}+0.3)}{1+\alpha_\mathrm{v}+\alpha_\mathrm{e}}}$
range	$\dot{\gamma} > \Delta\phi^{\frac{2+\alpha_\mathrm{v}+\alpha_\mathrm{e}}{2\alpha_\mathrm{v}}}$	$\dot{\gamma} > \Delta\phi^{\frac{3/2+\alpha_\mathrm{v}+\alpha_\mathrm{e}}{\alpha_\mathrm{v}}}$
		$\dot{\gamma} < \Delta\phi^{\frac{2+\alpha_\mathrm{v}+\alpha_\mathrm{e}}{2\alpha_\mathrm{v}}}$
	Normal Yield	
effective strain	$\gamma_\mathrm{eff} \sim \Delta\phi$	
rheology	$\sigma_{xx} \sim \Delta\phi^{\alpha_\mathrm{e}+0.3}$	
range	$\dot{\gamma} < \Delta\phi^{\frac{3/2+\alpha_\mathrm{v}+\alpha_\mathrm{e}}{\alpha_\mathrm{v}}}$	

Table 7.2: The three rheological regimes for the normal stress with their definitions, results and ranges of validity. Note that the shear stress enters as one of the ingredients that determines the regime.

7.3.1 Shear Stress

Yield Regime We will start with the shear stress in the Yield regime. The definition of this regime is the same as in the linear case: the effective strain, Eq. 7.5, is dominated by the yield contribution and the elasticity relation, Eq. 7.13, is dominated by the linear contribution:

$$\begin{cases} \sigma\dot{\gamma} \sim \Delta v^{1+\alpha_\mathrm{v}} \\ \gamma_\mathrm{eff} \sim \Delta\phi \\ \sigma_{xy} \sim \Delta\phi^{1/2}\gamma_\mathrm{eff}^{\alpha_\mathrm{e}} \end{cases} \Rightarrow \begin{cases} \Delta v \sim \dot{\gamma}^{\frac{1}{1+\alpha_\mathrm{v}}}\,\Delta\phi^{\frac{2\alpha_\mathrm{e}+1}{2(1+\alpha_\mathrm{v})}} \\ \gamma_\mathrm{eff} \sim \Delta\phi \\ \sigma_{xy} \sim \Delta\phi^{\alpha_\mathrm{e}+1/2} \end{cases} \tag{7.15}$$

Not surprisingly, the stress in the Yield regime, in which the material is thought to exhibit elastic behavior, depends on the elastic but not the viscous exponent. Also note that all relations reduce to their linear equivalents, found in Eq. 3.14, if we take $\alpha_\mathrm{e} = \alpha_\mathrm{v} = 1$.

Transition Regime In the Transition regime, the elasticity relation is dominated by the linear contribution, but the effective strain is dominated by the dynamic contribution:

$$\begin{cases} \sigma\dot{\gamma} \sim \Delta v^{1+\alpha_\mathrm{v}} \\ \gamma_\mathrm{eff} \sim \dot{\gamma}/\Delta v \\ \sigma_{xy} \sim \Delta\phi^{1/2}\gamma_\mathrm{eff}^{\alpha_\mathrm{e}} \end{cases} \Rightarrow \begin{cases} \Delta v \sim \Delta\phi^{\frac{1}{2(1+\alpha_\mathrm{v}+\alpha_\mathrm{e})}}\,\dot{\gamma}^{\frac{1+\alpha_\mathrm{e}}{1+\alpha_\mathrm{v}+\alpha_\mathrm{e}}} \\ \gamma_\mathrm{eff} \sim \Delta\phi^{\frac{-1}{2(1+\alpha_\mathrm{v}+\alpha_\mathrm{e})}}\,\dot{\gamma}^{\frac{v}{1+\alpha_\mathrm{v}+\alpha_\mathrm{e}}} \\ \sigma_{xy} \sim \Delta\phi^{\frac{1+\alpha_\mathrm{v}}{2(1+\alpha_\mathrm{v}+\alpha_\mathrm{e})}}\,\dot{\gamma}^{\frac{\alpha_\mathrm{v}\alpha_\mathrm{e}}{1+\alpha_\mathrm{v}+\alpha_\mathrm{e}}} \end{cases} \tag{7.16}$$

Due to the, appearance of both α_v and α_e these expressions look rather unappealing. Still, it is again easy to check that substituting $\alpha_\mathrm{v} = \alpha_\mathrm{e} = 1$ recovers the linear expressions of Eq. 3.15.

Critical Regime In the Critical regime, the elasticity is dominated by the non-linear contribution and the effective strain is dominated by the dynamic strain:

$$\begin{cases} \sigma\dot{\gamma} \sim \Delta v^{1+\alpha_\mathrm{v}} \\ \gamma_\mathrm{eff} \sim \frac{\dot{\gamma}}{\Delta v} \\ \sigma_{xy} \sim \gamma_\mathrm{eff}^{1+\alpha_\mathrm{e}} \end{cases} \Rightarrow \begin{cases} \Delta v \sim \dot{\gamma}^{\frac{2+\alpha_\mathrm{e}}{2+\alpha_\mathrm{v}+\alpha_\mathrm{e}}} \\ \gamma_\mathrm{eff} \sim \dot{\gamma}^{\frac{\alpha_\mathrm{v}}{2+\alpha_\mathrm{v}+\alpha_\mathrm{e}}} \\ \sigma_{xy} \sim \dot{\gamma}^{\frac{\alpha_\mathrm{v}(1+\alpha_\mathrm{e})}{2+\alpha_\mathrm{v}+\alpha_\mathrm{e}}} \end{cases} \tag{7.17}$$

Again, the expressions are unappealing but reduce to the linear results of Eq. 3.13 for $\alpha_\mathrm{v} = \alpha_\mathrm{e} = 1$.

Dense Regime For completeness' sake we also give the results for the inaccessible Dense regime:

$$\begin{cases} \sigma\dot{\gamma} \sim \Delta v^{1+\alpha_\mathrm{v}} \\ \gamma_\mathrm{eff} \sim \Delta\phi \\ \sigma_{xy} \sim \gamma_\mathrm{eff}^{1+\alpha_\mathrm{e}} \end{cases} \Rightarrow \begin{cases} \Delta v \sim \Delta\phi^{\frac{1+\alpha_\mathrm{e}}{1+\alpha_\mathrm{v}}}\dot{\gamma}^{\frac{1}{1+\alpha_\mathrm{v}}} \\ \gamma_\mathrm{eff} \sim \Delta\phi \\ \sigma_{xy} \sim \Delta\phi^{\alpha_\mathrm{e}+1} \end{cases} \tag{7.18}$$

Crossovers

Now that we have the rheological behavior in all four regimes, we can derive expression for the crossovers between the various regimes. These will again depend on the exponents α_e and α_v. The methodology is the same as in the linear case, equating the expressions for the stress in two regimes, though the exponents will be more involved; they are given in table 7.1

We start by comparing the stress in the Yield and the Transition regime:

$$\Delta\phi^{\alpha_\mathrm{e}+1/2} \sim \Delta\phi^{\frac{1+\alpha_\mathrm{v}}{2(1+\alpha_\mathrm{v}+\alpha_\mathrm{e})}}\dot{\gamma}^{\frac{\alpha_\mathrm{v}\alpha_\mathrm{e}}{1+\alpha_\mathrm{v}+\alpha_\mathrm{e}}} \Rightarrow \dot{\gamma} \sim \Delta\phi^{\frac{3/2+\alpha_\mathrm{v}+\alpha_\mathrm{e}}{\alpha_\mathrm{v}}} \quad . \tag{7.19}$$

The next crossover, from the Transition to the Critical regime, we find by comparing the expressions for the stress in those two regimes:

$$\Delta\phi^{\frac{1+\alpha_\mathrm{v}}{2(1+\alpha_\mathrm{v}+\alpha_\mathrm{e})}}\dot{\gamma}^{\frac{\alpha_\mathrm{v}\alpha_\mathrm{e}}{1+\alpha_\mathrm{v}+\alpha_\mathrm{e}}} \sim \dot{\gamma}^{\frac{\alpha_\mathrm{v}(1+\alpha_\mathrm{e})}{2+\alpha_\mathrm{v}+\alpha_\mathrm{e}}} \Rightarrow \dot{\gamma} \sim \Delta\phi^{\frac{2+\alpha_\mathrm{v}+\alpha_\mathrm{e}}{2\alpha_\mathrm{v}}} \quad . \tag{7.20}$$

Note that the exponent of the density here, $(2 + \alpha_\mathrm{v} + \alpha_\mathrm{e})/2\alpha_\mathrm{v}$, is always smaller than the exponent of the density in the Yield-to-Transition crossover, $(3/2 + \alpha_\mathrm{v} + \alpha_\mathrm{e})/\alpha_\mathrm{v}$, independent of α_v and α_e. Therefore: for every (positive) value of α_e and α_v, when the density is small, we will first crossover from the Yield to the Transition regime and then from the Transition to the Critical regime when $\dot{\gamma}$ is increased. Of course, we had already seen that this was so for the specific case of $\alpha_\mathrm{e} = \alpha_\mathrm{v} = 1$; now we know that this behavior is general.

The crossover from the Yield to the Dense regime still takes place at a fixed density:

$$\Delta\phi^{\alpha_\mathrm{e}+1/2} \sim \Delta\phi^{\alpha_\mathrm{e}+1} \Rightarrow \Delta\phi \sim 1 \ , \tag{7.21}$$

this 'derivation' makes it clear that changing α_v or α_e will not impact this result.

For the final crossover, form the Dense to the Critical regime, we find:

$$\Delta\phi^{\alpha_\mathrm{e}+1} \sim \dot{\gamma}^{\frac{\alpha_\mathrm{v}(1+\alpha_\mathrm{e})}{2+\alpha_\mathrm{v}+\alpha_\mathrm{e}}} \Rightarrow \dot{\gamma} \sim \Delta\phi^{\frac{2+\alpha_\mathrm{v}+\alpha_\mathrm{e}}{\alpha_\mathrm{v}}} \ . \tag{7.22}$$

As already mentioned above, changing the exponents will also change the crossovers *quantitatively*, but will not change the nature of the crossovers *qualitatively*. The general trends shown in figure 3.1 are therefore applicable to all exponents.

7.3.2 Normal Stress

As in the linear case, the rheology for the normal stress is somewhat special because the expressions for the shear stress that we derived above enter through energy balance. This causes the appearance of a third regime, even though there is only one ingredient with two regimes. We summarise the results for the stress in table 7.2 and present the full results below. Note that, just like the linear case $\langle\Delta v\rangle$ is set by the shear behavior and not by the normal behavior.

Normal Yield For the Normal Yield regime we have:

$$\begin{cases} \sigma_{xy}\dot{\gamma} \sim \Delta v^{1+\alpha_\mathrm{v}} \\ \gamma_\mathrm{eff} \sim \Delta\phi \\ \sigma_{xx} \sim \gamma_\mathrm{eff}^{\alpha_\mathrm{e}+0.3} \\ \sigma_{xy} \sim \gamma_\mathrm{eff}^{\alpha_\mathrm{e}+1/2} \end{cases} \Rightarrow \begin{cases} \Delta v \sim \dot{\gamma}^{\frac{1}{1+\alpha_\mathrm{v}}} \Delta\phi^{\frac{2\alpha_\mathrm{e}+1}{2(1+\alpha_\mathrm{v})}} \\ \gamma_\mathrm{eff} \sim \Delta\phi \\ \sigma_{xx} \sim \Delta\phi^{\alpha_\mathrm{e}+0.3} \end{cases} \tag{7.23}$$

Normal Transition In the Normal Transition regime we have:

$$\begin{cases} \sigma_{xy}\dot{\gamma} \sim \Delta v^{1+\alpha_\mathrm{v}} \\ \gamma_\mathrm{eff} \sim \frac{\dot{\gamma}}{\langle\Delta v\rangle} \\ \sigma_{xx} \sim \gamma_\mathrm{eff}^{\alpha_\mathrm{e}+0.3} \\ \sigma_{xy} \sim \Delta\phi^{\frac{1+\alpha_\mathrm{v}}{2(1+\alpha_\mathrm{v}+\alpha_\mathrm{e})}} \dot{\gamma}^{\frac{\alpha_\mathrm{v}\alpha_\mathrm{e}}{1+\alpha_\mathrm{v}+\alpha_\mathrm{e}}} \end{cases} \Rightarrow \begin{cases} \Delta v \sim \Delta\phi^{\frac{1}{2(1+\alpha_\mathrm{v}+\alpha_\mathrm{e})}} \dot{\gamma}^{\frac{1+\alpha_\mathrm{e}}{1+\alpha_\mathrm{v}+\alpha_\mathrm{e}}} \\ \gamma_\mathrm{eff} \sim \Delta\phi^{\frac{-1}{2(1+\alpha_\mathrm{v}+\alpha_\mathrm{e})}} \dot{\gamma}^{\frac{\alpha_\mathrm{v}}{1+\alpha_\mathrm{v}+\alpha_\mathrm{e}}} \\ \sigma_{xx} \sim \Delta\phi^{\frac{-(\alpha_\mathrm{e}+0.3)}{2(1+\alpha_\mathrm{v}+\alpha_\mathrm{e})}} \dot{\gamma}^{\frac{\alpha_\mathrm{v}(\alpha_\mathrm{e}+0.3)}{1+\alpha_\mathrm{v}+\alpha_\mathrm{e}}} \end{cases} \tag{7.24}$$

Regime Combination			rescaled axes		
Critical	and	Transition	$\sigma/\Delta\phi^{\frac{1+\alpha_\mathrm{e}}{2}}$	vs.	$\dot{\gamma}/\Delta\phi^{\frac{2+\alpha_\mathrm{v}+\alpha_\mathrm{e}}{2\alpha_\mathrm{v}}}$
Yield	and	Transition	$\sigma/\Delta\phi^{\alpha_\mathrm{e}+1/2}$	vs.	$\dot{\gamma}/\Delta\phi^{\frac{3/2+\alpha_\mathrm{e}+\alpha_\mathrm{v}}{\alpha_\mathrm{v}}}$
Yield	and	Critical	$\sigma/\Delta\phi^{\alpha_\mathrm{e}+1/2}$	vs.	$\dot{\gamma}/\Delta\phi^{\frac{(\alpha_\mathrm{e}+1/2)(2+\alpha_\mathrm{v}+\alpha_\mathrm{e})}{\alpha_\mathrm{v}(1+\alpha_\mathrm{e})}}$

Table 7.3: Prescriptions of what to plot for collapse in the indicated regimes.

Regime Combination			rescaled axes		
Normal Critical	and	Normal Transition	$\sigma/\Delta\phi^{\frac{\alpha_\mathrm{e}+0.3}{2}}$	vs.	$\dot{\gamma}/\Delta\phi^{\frac{2+\alpha_\mathrm{v}+\alpha_\mathrm{e}}{2\alpha_\mathrm{v}}}$
Normal Yield	and	Normal Transition	$\sigma/\Delta\phi^{\alpha_\mathrm{e}+0.3}$	vs.	$\dot{\gamma}/\Delta\phi^{\frac{3/2+\alpha_\mathrm{e}+\alpha_\mathrm{v}}{\alpha_\mathrm{v}}}$
Normal Yield	and	Normal Critical	$\sigma/\Delta\phi^{\alpha_\mathrm{e}+0.3}$	vs.	$\dot{\gamma}/\Delta\phi^{\frac{2+\alpha_\mathrm{v}+\alpha_\mathrm{e}}{\alpha_\mathrm{v}}}$

Table 7.4: Prescriptions of what to plot for collapse of the normal stress in the indicated regimes.

Normal Critical In the Normal critical regime we have:

$$\begin{cases} \sigma_{xy}\dot{\gamma} \sim \Delta v^{1+\alpha_\mathrm{v}} \\ \gamma_\mathrm{eff} \sim \frac{\dot{\gamma}}{\langle\Delta v\rangle} \\ \sigma_{xx} \sim \gamma_\mathrm{eff}^{\alpha_\mathrm{e}+0.3} \\ \sigma_{xy} \sim \dot{\gamma}^{\frac{\alpha_\mathrm{v}(1+\alpha_\mathrm{e})}{2+\alpha_\mathrm{v}+\alpha_\mathrm{e}}} \end{cases} \Rightarrow \begin{cases} \Delta v \sim \dot{\gamma}^{\frac{2+\alpha_\mathrm{e}}{2+\alpha_\mathrm{v}+\alpha_\mathrm{e}}} \\ \gamma_\mathrm{eff} \sim \dot{\gamma}^{\frac{\alpha_\mathrm{v}}{2+\alpha_\mathrm{v}+\alpha_\mathrm{e}}} \\ \sigma_{xx} \sim \dot{\gamma}^{\frac{\alpha_\mathrm{v}(\alpha_\mathrm{e}+0.3)}{2+\alpha_\mathrm{v}+\alpha_\mathrm{e}}} \end{cases} \tag{7.25}$$

Crossovers

The crossovers for the normal stress are simply inherited from the crossovers of the shear stress, just like in the linear case.

7.4 Plotting

Since the general structure of the rheology has not changed: three (accessible) regimes, power laws of strain rate and density, we can still hope to plot the rheological curves as we could in the linear case: collapsed by rescaling with the density. Short derivations will be presented in the section below, but the important results are summarized in tables 7.3 and 7.4

7.4.1 Shear Stress

For the shear stress there are, realistically, three regimes. This means that, as before, it will not be possible to collapse the full curve, at best we can rescale two regimes. Below we will discuss the rescaling with $\Delta\phi$ that is necessary to get collapse in each combination of two regimes.

Yield and Transition If we want to attain collapse in the Yield and Transition regimes we start by looking at the stress in the Yield regime: it depends on density, but not on the strain rate. Therefore the only way to get the stress to collapse in the Yield regime is by picking the correct rescaling in the stress. Since the stress in the Yield regime is given by $\sigma_{xy} \sim \Delta\phi^{\alpha_\mathrm{e}+1/2}$, we have $\tilde{\sigma}_{xy} \sim \sigma_{xy}/\Delta\phi^{\alpha_\mathrm{e}+1/2}$. In addition, we rescale the $\dot{\gamma}$-axis with the $\Delta\phi$ dependence of the crossover so that we get collapse there as well: $\tilde{\dot{\gamma}} \sim \dot{\gamma}/\Delta\phi^{(3/2+\alpha_\mathrm{e}+\alpha_\mathrm{v})/\alpha_\mathrm{v}}$. As in the linear case this will automatically result in collapse in the Transition regime as well.

Transition and Critical To get collapse in both the Critical and the Transition regime, the first thing we must do is collapse the crossover by plotting $\tilde{\dot{\gamma}} \sim \dot{\gamma}/\Delta\phi^{(2+\alpha_\mathrm{v}+\alpha_\mathrm{e})/2\alpha_\mathrm{v}}$. With this relation we can now derive how we need to plot the stress to get collapse in the Critical regime:

$$\sigma_{xy} \sim \dot{\gamma}^{\frac{\alpha_\mathrm{v}(1+\alpha_\mathrm{e})}{2+\alpha_\mathrm{v}+\alpha_\mathrm{e}}} = \tilde{\dot{\gamma}}^{\frac{\alpha_\mathrm{v}(1+\alpha_\mathrm{e})}{2+\alpha_\mathrm{v}+\alpha_\mathrm{e}}} \Delta\phi^{\frac{\alpha_\mathrm{v}(1+\alpha_\mathrm{e})}{2\alpha_\mathrm{v}}} \Rightarrow \tilde{\sigma}_{xy} \sim \sigma_{xy}/\Delta\phi^{\frac{\alpha_\mathrm{v}(1+\alpha_\mathrm{e})}{2\alpha_\mathrm{v}}} \tag{7.26}$$

Again, this will also give collapse in the Transition regime.

Yield and Critical Again we need to plot $\tilde{\sigma}_{xy} \sim \sigma_{xy}/\Delta\phi^{\alpha_\mathrm{e}+1/2}$ for collapse of the Yield stress. We substitute this expression into the rheological relation for the Critical regime to find the required strain rate rescaling:

$$\sigma_{xy} \sim \dot{\gamma}^{\frac{\alpha_\mathrm{v}(1+\alpha_\mathrm{e})}{2+\alpha_\mathrm{v}+\alpha_\mathrm{e}}} \Rightarrow \tilde{\sigma}_{xy} \sim \dot{\gamma}^{\frac{\alpha_\mathrm{v}(1+\alpha_\mathrm{e})}{2+\alpha_\mathrm{v}+\alpha_\mathrm{e}}}/\Delta\phi^{\alpha_\mathrm{e}+1/2} \Rightarrow \tilde{\dot{\gamma}} \sim \dot{\gamma}/\Delta\phi^{\frac{(\alpha_\mathrm{e}+1/2)(2+\alpha_\mathrm{v}+\alpha_\mathrm{e})}{\alpha_\mathrm{v}(1+\alpha_\mathrm{e})}}. \tag{7.27}$$

This will not result in collapse in either the Transition regime, of the crossover from the Yield to the Transition regime or of the crossover from the Transition to the Critical regime.

7.4.2 Normal Stress

Plotting the normal stress will be similar to the shear stress in some cases, because the same crossovers need to be collapsed, but different in most cases, since the stress scales differently.

Normal Yield and Normal Transition Regimes As mentioned above, the strain rate needs to be rescaled to make the crossover between the Normal Yield and Normal Transition regimes, which is the same as for the shear tress, collapse: $\tilde{\dot{\gamma}} \sim \dot{\gamma}/\Delta\phi^{(3/2+\alpha_\mathrm{e}+\alpha_\mathrm{v})/\alpha_\mathrm{v}}$. Since the stress in the Normal Yield regime depends only on the density, this prescribes the rescaling of the stress: $\sigma_{xx} \sim \Delta\phi^{\alpha_\mathrm{e}+0.3}$.

Normal Transition and Normal Critical Regimes Between the Normal Transition and the Normal Critical regime there is a crossover that determines the strain rate rescaling: $\tilde{\dot{\gamma}} \sim \dot{\gamma}/\Delta\phi^{(2+\alpha_\mathrm{v}+\alpha_\mathrm{e})/2\alpha_\mathrm{v}}$. Substituting this into the expression for the stress in the Normal Critical regime yields:

$$\sigma_{xx} \sim \dot{\gamma}^{\frac{\alpha_\mathrm{v}(\alpha_\mathrm{e}+0.3)}{2+\alpha_\mathrm{v}+\alpha_\mathrm{e}}} = \tilde{\dot{\gamma}}^{\frac{\alpha_\mathrm{v}(\alpha_\mathrm{e}+0.3)}{2+\alpha_\mathrm{v}+\alpha_\mathrm{e}}} \Delta\phi^{\frac{\alpha_\mathrm{e}+0.3}{2}} \Rightarrow \tilde{\sigma}_{xx} \sim \sigma_{xx}/\Delta\phi^{\frac{\alpha_\mathrm{e}+0.3}{2}}. \qquad (7.28)$$

Normal Yield and Normal Critical Regimes Again, the dependence of the Normal Yield stress on the density prescribes the rescaling of the stress: $\sigma_{xx} \sim \Delta\phi^{\alpha_\mathrm{e}+0.3}$. This can be substituted into the expression for the stress in the Critical regime to deduce the rescaling of the strain rate:

$$\sigma_{xx} \sim \dot{\gamma}^{\frac{\alpha_\mathrm{v}(\alpha_\mathrm{e}+0.3)}{2+\alpha_\mathrm{v}+\alpha_\mathrm{e}}} \Rightarrow \tilde{\sigma}_{xx} \sim \dot{\gamma}^{\frac{\alpha_\mathrm{v}(\alpha_\mathrm{e}+0.3)}{2+\alpha_\mathrm{v}+\alpha_\mathrm{e}}}/\Delta\phi^{\alpha_\mathrm{e}+0.3} \Rightarrow \tilde{\dot{\gamma}} \sim \dot{\gamma}/\Delta\phi^{\frac{2+\alpha_\mathrm{v}+\alpha_\mathrm{e}}{\alpha_\mathrm{v}}} \qquad (7.29)$$

7.5 Experimental Implementations

Now we will compare the predictions from our scaling model with previous experiments done by other people. Since our model describes a much wider array of systems than artificial linear model, we will be able to accurately describe real systems. We will compare our model to experimental data of flowing foams by Katgert *et al.* [37] and experimental data of colloid rheology by Nordstrom *et al.* [39] .These two systems also have the advantage of being theoretically interesting because they decouple the effects of non-linear elasticity and non-linear viscosity. This is because the foam system has linear elasticity but non-linear viscosity, $\alpha_\mathrm{v} = 2/3$, while the colloid system has linear viscosity but non-linear elasticity, $\alpha_\mathrm{e} = 3/2$.

7.5.1 Katgert Foam Data

We start by looking at systems of flowing foam, the system we had in our mind when developing the original linear model. For this we can use experiments performed by Gijs Katgert *et al.* In the experiments, a two dimensional bubble layer is confined between the liquid surface on the bottom and a glass plate on top. Two large wheels then apply a constant strain rate to the system, bringing it in steady shear. A picture of the setup is given in figure 7.1. In this system, Katgert can modify the strain rate and, within a narrow range, the density.

An important difference between the system of Katgert *et al.* and our system is the presence of a top plate. The top plate exerts a drag force on all bubbles. Since this drag force depends on the velocities of the bubbles with respect to this top plate, there is an additional energetic penalty to high velocities, which results in shear banding. In effect, the top plate breaks galilean symmetry and enforces the laboratory frame as a special frame.

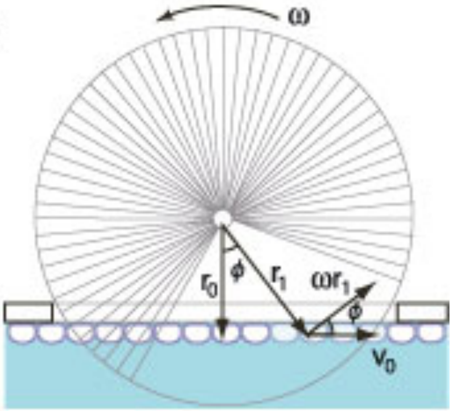

Figure 7.1: Figure from [37]. Side view of the setup used by Katgert *et al.*

In spite of this, Katgert has developed a model that allows him to take, amongst other things, the degree of shear banding and get out the 'pure' rheological behavior: the dependence of the required shear stress on the applied strain rate: he gets a good fit for Herschell-Bulkley behavior:

$$\sigma_{xy} \sim \sigma_Y + \dot{\gamma}^{0.36}, \tag{7.30}$$

where σ_Y is a yield stress. Our model should predict, then, that the exponent with which the shear stress depends on the strain rate in the Critical regime has a value 0.36 ± 0.05, taking into account he error bars on the experimental result. In what follows we will call this exponent β to facilitate the discussion. In order to see if our model indeed predicts $\beta = 0.36$, we need to know the exponents in the force laws between the individual bubbles, α_{e} and α_{v}.

According to Katgert, his bubbles have linear elastic interactions, $\alpha_{\mathrm{e}} = 1$, but non-linear viscous interactions. He measures their viscous interactions to follow $\alpha_{\mathrm{v}} = 2/3$ [37]. If we substitute these two values into the expression we derived for the stress in the Critical regime, Eq. 7.17, we find:

$$\sigma_{xy} \sim \dot{\gamma}^{\frac{\alpha_{\mathrm{v}}(1+\alpha_{\mathrm{e}})}{2+\alpha_{\mathrm{v}}+\alpha_{\mathrm{e}}}} = \dot{\gamma}^{\frac{4/3}{3+2/3}} = \dot{\gamma}^{4/11} = \dot{\gamma}^{0.36}, \tag{7.31}$$

which is in excellent agreement with the experimental value of 0.36 ± 0.05.

Of course, there are some caveats. First of all, the fact that the exponents match so closely cannot be attributed to anything besides luck because there are considerable experimental error bars on both α_{v} and β, and Katgert *et al.* present a number of slightly different values in a later paper [34]. Still this does not change the result that our model prediction for β is consistent with the experiment.

Second, and slightly more problematic, is the apparent lack of a Transition regime in the data of Katgert *et al.* ; while our model predicts three regimes, Katgert only finds two. We claim that this is reasonable because the Transition regime can be hard to pin down experimentally: it can be very small, as we have seen in section 4.4.1, and the exponent with which the stress depends on the strain rate is usually not so different between the Transition and the Critical regime, 0.25 and 0.36 respectively[1]. These two factors can conspire to make the Transition regime simply look like the crossover from the Yield to the Critical regime, especially when noise is an issue, as it often is in experiments. Therefore, the lack of an obvious Transition regime is not immediately worrying.

Thirdly, and still more problematic is the analysis that Katgert performs in his later paper [34] to determine the dependence of the stress on the density. He finds two main results: the exponent β does not depend on the density but a prefactor that he calls k does via $k \sim \Delta\phi^{-1}$. The fact that β does not depend on $\Delta\phi$ is fully consistent with the results from our model, see Eq. 7.17, but the result for k is problematic. Using the definitions of Katgert *et al.* $k \sim \Delta\phi^{-1}$ can be translated to $\sigma \sim \Delta\phi$ in our language, however our model predicts that σ is independent of $\Delta\phi$ in the Critical regime. According to Katgert, this dependence of the viscous force on the density is a consequence of the fact that the viscous force between two bubbles also depends on their overlap: bubble pairs with a bigger overlap have a bigger contact surface and therefore experience more drag from each other. Our model does not account for this property of the forces between bubbles and therefore it is not strange that we do not predict its consequences, but that is a weakness in the model nonetheless.

The most reasonable approach might be that our model takes into account all sources of strain rate or velocity dependence in foams and is therefore able to predict the dependence of the stress on the strain rate correctly. However, the model does not correctly take into account all sources of density or overlap dependence, leading to incorrect predictions concerning the dependence of the the stress on the density. If this is indeed the correct way to look at the results above, then our model should correctly predict the density dependence in a system where there are no density effects that are unaccounted for in our model, like colloids.

7.5.2 Nordstrom Colloid Data

The second experimental system that we look at is the colloidal system of Nordstrom *et al.* [39]. In this system, N-isopropylacrylamide, or NIPA, colloidal particles of about a μm in size are forced through a tube of size L by a pressure difference, ΔP between the ends of the tube, see figure 7.2 **a**. The particles are suspended in water and, since they swell by absorbing water, they are nearly index and density matched with the water. Due to the change in

---

[1] These values are found by substituting the experimental value of $\alpha_v = 2/3$ into the relation for the stress in the Transition regime as given in in table 7.1.

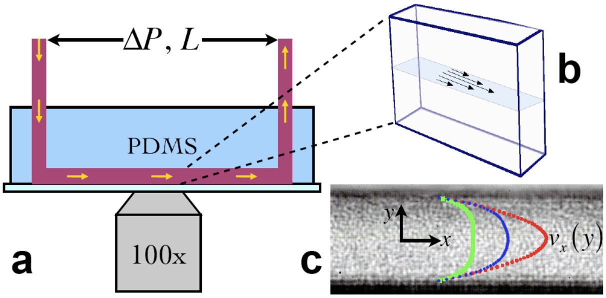

Figure 7.2: Schematic of the microfluidics setup used by Nordstrom *et al.* **a** Side view of the setup. **b** horizontal slice at half height in the channel, showing an example velocity profile. **c** Real data example, showing three example velocity profiles. Figure from [39]

stress as a function of the coordinate perpendicular to the direction of flow, y, the strain rate will also depend on y. Since the strain rate itself is the spatial derivative of the velocity profile, Nordstrom *et al.* were able to obtain the strain rate at different points in their setup by numerically differentiating their velocity profiles, some examples are shown in figure 7.2 **c**. Stress and strain rates as a function of position in the channel can then be combined into a rheological curve linking stress and strain rate directly. This novel technique allows them to get a full rheology curve for a particular density from only one experiment.

Following Olsson & Teitel [11] and the original predictions of our 3E model, [33], Nordstrom *et al.* plot their rheological data in a collapse plot, shown in figure 7.5.2. As can be seen from the figure they find good collapse when plotting $\sigma/\Delta\phi^{2.1}$ vs. $\dot{\gamma}/\Delta\phi^{4.1}$, finding an exponent of the stress in the Critical regime of $\beta = 0.48$

This rheological curve can be compared to our theoretical predictions if we know the microscopic interactions between NIPA particles. Nordstrom *et al.* claim that their particles have simple linear viscous drag, but that they have hertzian elastic interactions, meaning that $F^{\mathrm{e}}_{ij} \sim \delta_{ij}^{3/2}$, or $\alpha_{\mathrm{e}} = 3/2$. Substituting these values into our model gives an exponent in the Critical regime, β, of

$$\frac{\alpha_{\mathrm{v}}(1+\alpha_{\mathrm{e}})}{2+\alpha_{\mathrm{v}}+\alpha_{\mathrm{e}}} = \frac{1+3/2}{2+1+3/2} = 5/9 = 0.55. \tag{7.32}$$

The question of the correct exponents of $\Delta\phi$ to obtain collapse, Δ and Γ in the language of Nordstrom *et al.* , is a little bit more complicated, as there are three options, collapsing any two of the three regimes, Critical, Transition and Yield. We obviously have collapse in the Critical regime and the authors consider the Yield stress collapsed, so we should look at our predictions for collapsing the Critical and Yield regimes. With the exponents for these colloids

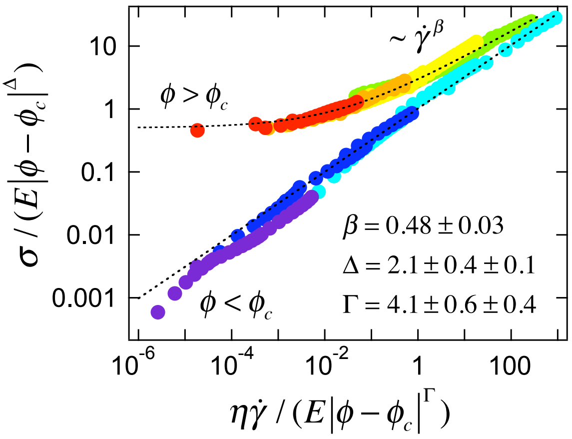

Figure 7.3: Stress and strain rate from the colloidal experiments of Nordstrom *et al.* E denotes the bulk modulus, η the viscosity of the water. Figure from [39]

substituted, we predict that we get collapse for

$$\Delta = 2 \tag{7.33}$$

$$\Gamma = 3.6 \tag{7.34}$$

These values for Δ and Γ agree quite well with the experimental results of Nordstrom *et al.* , $\Delta = 2.1 \pm 0.4$ and $\Gamma = 4.1 \pm 0.6$. Our predicted value of β, 0.55, is outside the experimental range of 0.48 ± 0.03 though. This is strange because, $\beta = \Delta/\Gamma$. However, Nordstrom *et al.* don't get β from the collapse plot, they get it by fitting datasets at a fixed density to the following Herschell-Bulkely expression:

$$\sigma_{xy} \sim \sigma_y + \dot{\gamma}^{\beta}, \tag{7.35}$$

in which σ_y is a yield stress. This expression does not properly account for the Transition regime and trying to fit data that is partially in the Transition in stead of in the Critical regime will result in a value for β that is closer to the Transition exponent of 0.42. Since it is extremely likely that at least the red dataset in figure 7.5.2 is in the Transition regime, it is not surprising that Nordstrom *et al.* find an exponent of 0.48 in between the Transition exponent of 0.42 and the Critical exponent of 0.55.

7.5.3 Conclusion

We have extended our 3E model to nonlinear microscopic interactions. We have compared the predictions of that model with the results of two experiments: the foams of Katgert, which have nonlinear viscous interactions and the colloids of Nordstrom, which have nonlinear elastic interactions. In both cases the model performed well. However, in both cases there were some issues, specifically the presence or absence of a Transition regime. In order to be able to study this in more detail and for a wider range of microscopic exponents, we would like to perform computer simulations again. These are discussed in the next chapter.

Chapter 8

Testing the Non-linear Scaling Model

Now that we have fully derived the predictions for rheological behavior in our non-linear scaling method, we will test these predictions by direct simulation of a nonlinear particle model. The 'bubble model' code that we have used sofar (chapter 2), can not handle $\alpha_\mathrm{e} \neq 1$, but does allow us to test $\alpha_\mathrm{v} \neq 1$. Then in section 8.2.1 we will introduce a new code that, in principle, should be able to handle $\alpha_\mathrm{e} \neq 1$. This new code is for particles of finite mass, allowing us to test the validity of our assumption of masslessness. To distinguish these two simulation codes we will call the one we have used until now the 'massless particle code' and the one that will be introduced in section 8.2.1 the massive particle code.

8.1 Massless Particle Code

With the massless particle code that we used throughout this thesis we have performed simulations of a wide range a different α_v's, including both $\alpha_\mathrm{v} < 1$, $\alpha_\mathrm{v} = 0.75$ and $\alpha_\mathrm{v} = 0.5$, and $\alpha_\mathrm{v} > 1$, $\alpha_\mathrm{v} = 1.1$, $\alpha_\mathrm{v} = 1.25$, $\alpha_\mathrm{v} = 1.5$ and $\alpha_\mathrm{v} = 2$. Unfortunately, we only have a limited sense of densities available for each α: 0.86, 0.85, 0.844 and in some cases 0.8424. We do have the full range of strain rate at our disposal, though.

In figure 8.1 we show collapse plots for the Transition and Critical regime for all six values of α, rescaled with the exponents given by table 7.1. While the data is preliminary, the results are consistent with our model predictions because we find collapse in all six plots onto power laws whose exponents are consistent with the predicted β's with the possible exceptions of the largest ($\alpha_\mathrm{v} = 2$) and smallest ($\alpha_\mathrm{v} = 0.5$) viscous exponents, see table 8.1. Two aspects of these plots are striking. First, the fact that for $\alpha_\mathrm{v} < 1$, the highest strain-rate data falls below their power law curves. Second, the fact that

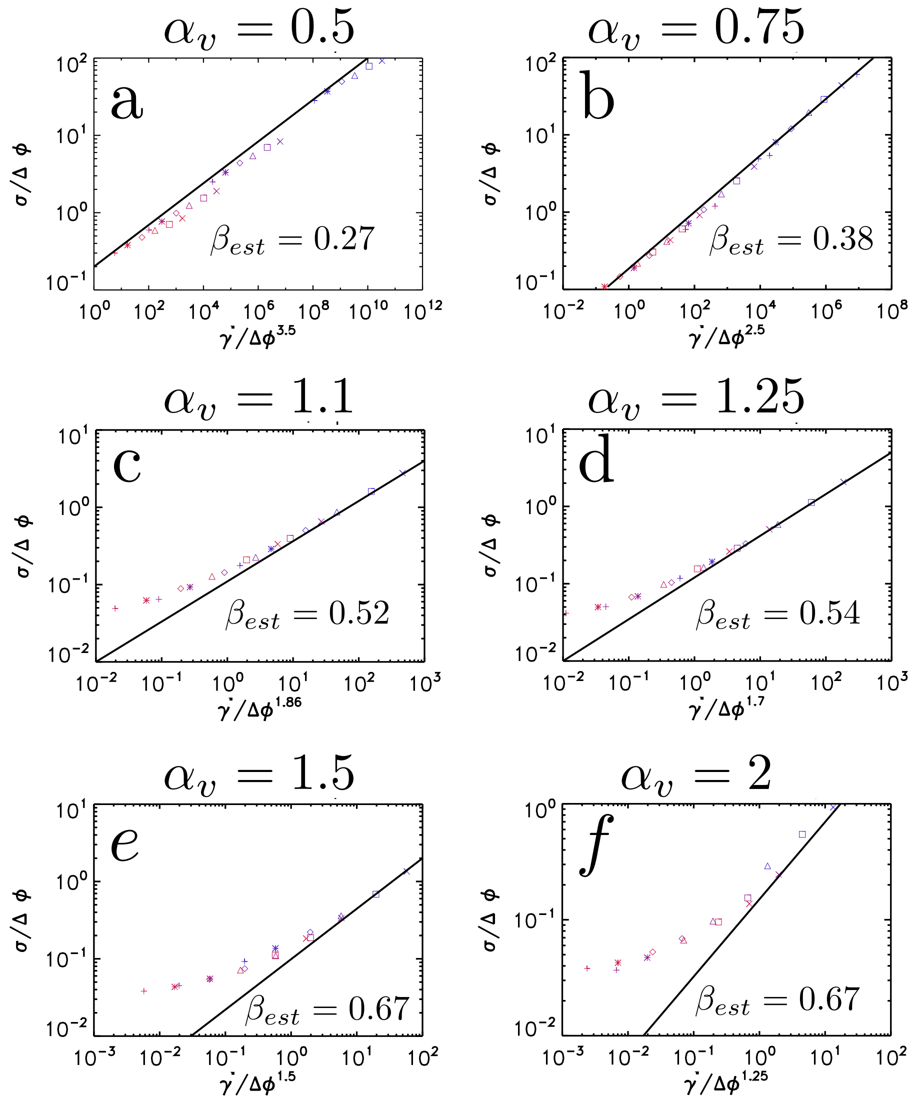

Figure 8.1: Transition and Critical regime collapse plots for **a** $\alpha_v = 0.5$, **b** $\alpha_v = 0.75$, **c** $\alpha_v = 1.1$, **d** $\alpha_v = 1.25$, **e** $\alpha_v = 1.5$ and **f** $\alpha_v = 2$. Symbols represent strain rates as in table 3.3. Colors represent density. From blue to red in **a** and **b**: 0.8424, 0.844, 0.85 and 0.86; and from blue to red in **c**, **d**, **e** and **f**: 0.844, 0.85 and 0.86. Black lines indicate best estimate power laws with exponent β_{est}, these values are consistent with our model predictions of table 8.1, except for $\alpha_v - 2$ - although the scaling range there is rather limited.

α_{v}	β_{est}	β_{model}
0.5	0.27	0.29
0.75	0.38	0.4
1.1	0.52	0.54
1.25	0.54	0.59
1.5	0.67	0.67
2	0.67	0.8

Table 8.1: Our estimate of β, β_{est}, for six different values of α compared to our model prediction, β_{model}.

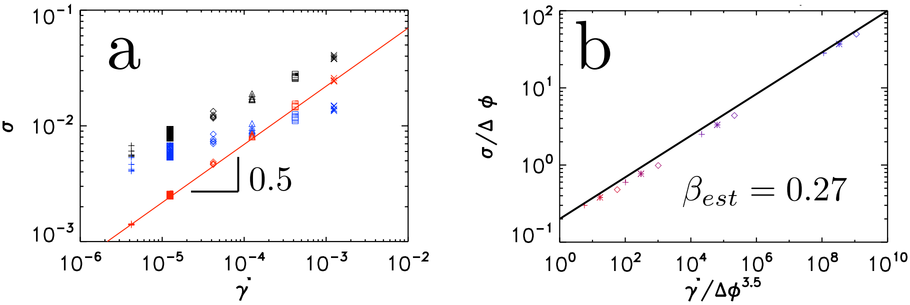

Figure 8.2: **a** Elastic (blue), viscous (red) and total (black) stress as a function of strain rate for $\alpha_{\mathrm{v}} = 0.5$. **b** Transition and Critical collapse plot for the slowest three strain rates of $\alpha = 0.5$. Colors represent density; from blue to red: 0.8424, 0.844, 0.85 and 0.86.

the Transition regime becomes more prominent for higher α_{v}. Both can be explained in the framework of our model.

First, the reason that high strain rate data falls below the curve in figures 8.1 **a** and **b** is that our strain rate criterion that $\dot{\gamma} < 10^{-2}$ for ensuring that the elastic stress dominates the viscous stress is no longer sufficient for $\alpha_{\mathrm{v}} < 1$. As we show in figure 8.2 **a**, for $\alpha_{\mathrm{v}} = 0.5$ the viscous stress, red, is larger than the elastic stress, blue, even for some strain rates that are smaller then 10^{-2}. This is in contrast to $\alpha_{\mathrm{v}} = 1$ where, as we have seen in figure 2.3, the elastic stress is significantly larger for all $\dot{\gamma} < 10^{-2}$. However, if we now plot only those strain rates for which the elastic stress *is* larger than the viscous stress, as we do in figure 8.2 **b**, we find that all data points now follow a single power law.

Second, since the crossover from the Transition to the Critical regime scales as $\dot{\gamma} \sim \Delta\phi^{(3+\alpha_{\mathrm{v}})/2\alpha_{\mathrm{v}}}$, this crossover shifts to higher strain rate as α_{v} increases. Therefore, if data in the same density and strain rate range for different α_{v}

is compared, as it is in figure 8.1, more data will be in the Transition regime, and less data in the Critical regime for higher α_v. This is exactly what we see. Of course, since we rescale the horizontal $\dot{\gamma}$ axis with $\Delta\phi^{(3+\alpha_\mathrm{v})/2\alpha_\mathrm{v}}$ to obtain collapse of this crossover, the crossover should always take place at the same value of $\dot{\gamma}/\Delta\phi^\Gamma$, and indeed if we compare the panels of figure 8.1, we see that the crossover always appears[1] at $\dot{\gamma}/\Delta\phi^\Gamma \approx 1$.

8.1.1 Conclusion

Our nonlinear scaling model predicts that the critical exponent β depends on the details of the (viscous) interaction. The data above, preliminary as it might be, corroborates this prediction, as shown in table 8.1. Even if the model would turn out to be not exact, it is clear that β *does* depend on α, and therefore the microscopic details of the interaction.

Our model does not make claims how changing the mode of dissipation to Mean Field [11, 27], inelastic collisions [29, 30] or thermostats [25, 28] might change the β, but since these changes are more far-reaching than simply changing the exponent of inter-particle viscous dissipation, we think it is unreasonable to assume that these changes will not impact β.

8.2 Massive Particle Code

The experimental and numerical results presented above have strengthened our belief that microscopic details are important for the rheology of soft particles near the jamming transition. Therefore we will investigate the effect of a non-zero mass in this section. In order to do this, we use a new simulation code developed jointly with Ellak Somfai. Below we will first introduce this new code that we will call the massive particle code, describing how it differs from the original massless particle code, and then discuss the findings that we have obtained using the code.

8.2.1 Implementation

Now that we have mass, and therefore acceleration, in our system, the first order forward Euler approach is no longer applicable. Therefore, the code is based on a second order 'velocity Verlet' algorithm. The algorithm works as follows:

- At time t we have $x(t)$, $v(t)$ and $a(t)$.
- We calculate the new position: $x(t+dt) = x(t) + v(t)dt + \frac{1}{2}a(t)dt^2$.
- We predict the new velocity: $\tilde{v} = v(t) + 0.65a(t)dt$; the value 0.65 can be changed, be have picked 0.65 because it was found to be optimal by [40].

---

[1] except for $\alpha_\mathrm{v} = 0.5$, where all data points are to the right of $\dot{\gamma}/\Delta\phi^\Gamma \approx 1$

- We calculate the forces, $\tilde{F}$, based on $x(t+dt)$ and $\tilde{v}$, using the microscopic force expressions of Eqs. 7.1 and 7.2.
- We calculate the new acceleration: $a(t+dt) = \frac{\tilde{F}}{m}$.
- We calculate the actual new velocity: $v(t+dt) = v(t)+\frac{1}{2}[a(t)+a(t+dt)]dt$.
- Now we have x(t+dt), v(t+dt) and a(t+dt) and we can start the next iteration.

The mass of each particle is an adjustable parameter, meaning that we can, in principle, tune the importance of mass in the simulations. The unit of mass is chosen such that the density is 1, we label[2] this situation $m = 1$; in some cases we have also used particles with a masses that are ten times as big, denoted by $m = 10$, and 100 times as big, denoted by $m = 100$. An important caveat is that going to small mass will necessitate the use of very small time steps in order to prevent *overshoots* due to high acceleration. In practice this limits the range over which we can reduce the mass. Unless specified otherwise, the mass of each particle is proportional to its area (i.e. its two-dimensional volume) and set so that the density of the system is unity.

In addition, for a reason that we have not been able to determine, changing α_{e} away from 1, the linear case, requires going to very small time steps and causes crashes if the time step is too large. Unfortunately, this has made it impossible to study the effect of changing α_{e} away from 1 in our simulations.

8.2.2 Testing the Effect of Mass

We have performed a number of tests to see if the results of simulations with the new code make sense and in which regimes, if any, the effects of the presence of mass are strong and which regimes they are weak. We perform three tests: we have checked whether power balance is upheld is the new simulations, we have checked where the kinetic stress, that we use as a proxy for the presence of mass, is largest and we have directly compared the elastic stress in both the massless and massive particle codes.

Power Balance

Power balance is a fundamental concept and should hold in our system with mass also. The presence of mass does give a new way to temporarily store energy: in the form of kinetic energy. However, in steady state the amount of kinetic energy is constant (when averaged over long enough time scales). This

---

[2] This is indeed merely a label because the bidiserse particles have different masses and neither of them are 1; however we are not interested in the value of the mass, merely in the relative size of the mass between different simulations.

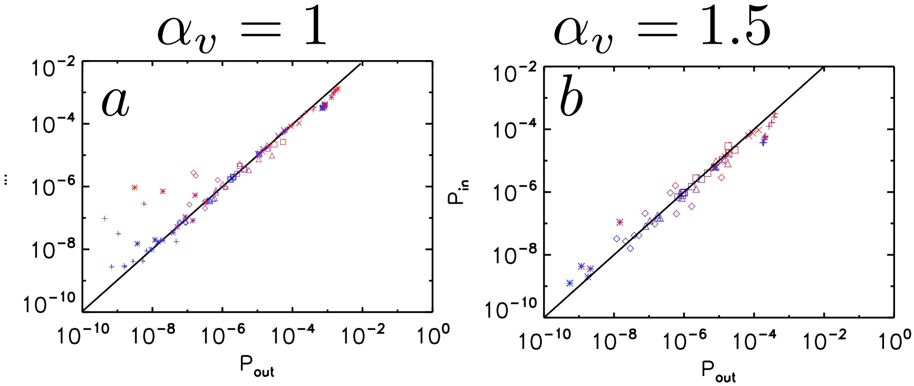

Figure 8.3: Power balance is upheld for $\alpha_{\mathrm{v}} = 1$ and $\alpha_{\mathrm{v}} = 1.5$

means there can be no net growth or decline of the kinetic energy and therefore the general expression for power balance that we introduced in Eq. 7.4:

$$\sigma_{xy}\dot{\gamma} \sim \Delta v^{1+\alpha_{\mathrm{v}}} \tag{8.1}$$

must hold. In figures 8.3 we show graphs testing power balance for two different α_{v}: $\alpha_{\mathrm{v}} = 1$ in panel **a** and $\alpha_{\mathrm{v}} = 3/2$ in panel **b**. As expected, power balance holds for both $\alpha_{\mathrm{v}} = 1$, the simple linear case, and $\alpha_{\mathrm{v}} = \frac{3}{2}$, giving an indication that these simulations are doing what they should do.

However, in figure 8.4 we show that for $\alpha_{\mathrm{v}} = \frac{1}{2}$, power balance breaks down for small strain rate, where the dissipated power appears to become larger than the input power. We hypothesise that this is a consequence of the concave shape of the microscopic viscous force for $\alpha_{\mathrm{v}} < 1$. In this case, a relatively small Δv already induces a relatively large force and there is a singularity at $\Delta v = 0$. To illustrate how this might lead to an overestimation of the dissipated power, consider the following example. Two bubbles, A and B, are moving in the same direction with velocities that are very similar, but A is slightly faster. These bubbles will exert viscous forces on each other that are comparatively large due to the square root viscous force law: A will pull B forward, B will drag A backwards. Thus, if the time step is not small enough, it may happen that the velocity adjustment that is a consequence of the viscous force will actually overshoot the ‘intended’ result of equal velocities: now B is faster than A. Instead of quickly reaching the same velocity, A and B keep rubbing past each other, dissipating large amounts of energy as they go. Such numerical problems may explain why the dissipated power is too large for small strain rates for $\alpha_{\mathrm{v}} < 1$.

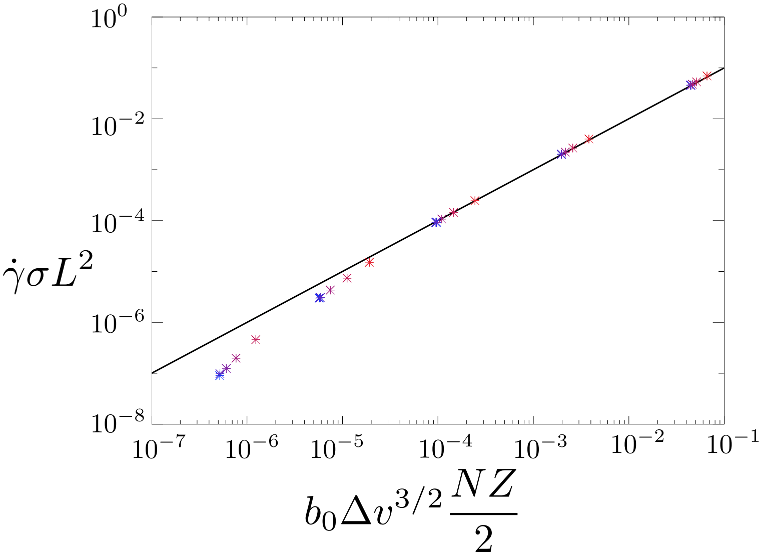

Figure 8.4: Power balance is not upheld for $\alpha_{\rm v} = 0.5$ for small strain rates.

Kinetic Stress

When elastic and viscous forces are not balanced, there is an extra contribution to the stress, called the kinetic stress, $\sigma^{xy}_{\rm kin} = m/2V \sum_{<ij>} v_{ij,x} v_{ij,y}$. In effect, the kinetic stress is the stress caused by the net forces on each particle. Clearly, if there is a sizeable kinetic stress relative to the elastic contribution to the stress[3], then mass plays an important role. We cannot strictly say that if the kinetic stress is small than the mass must have no effect. However, it is hard to imagine mass playing an important role in a system in which inertial effects are minimal, therefore we think that the ratio of the kinetic stress to the elastic stress is a good proxy for the effect of mass in our system.

Figure 8.5 shows the value of the kinetic stress as a fraction of the elastic stress. This fraction is plotted vs. the strain rate. In principle there should be graphs for all four components - xx, yy, xy, yx - but we have simply plotted the component for which the kinetic stress ratio is highest, the normal stress. Even in this case, though, the kinetic stress never passes beyond 1% of the elastic stress. The relative size of the kinetic stress is mostly determined by the strain rate - the higher the strain rate, the more important the kinetic stress - and is approximately linear in the strain rate for large densities. Hence, based on the relative magnitude of kinetic and elastic stresses, we would expect that the theologies of massive and massless particles would deviate most for high strain rates.

---

[3] Since, in our case, the elastic stress dominates, it is the relevant quantity to compare with.

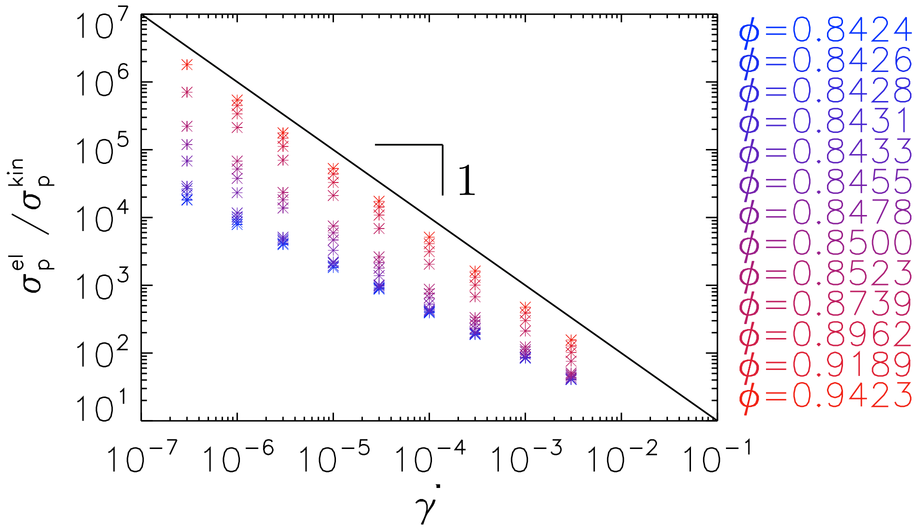

Figure 8.5: The kinetic stress as a fraction of the elastic stress as a function of strain rate for $m = 1$.

Direct Comparison

Instead of looking at whether the mass has an effect on the behavior at the system in general, we can directly check if it has an effect on the most important aspect of the system: the elastic stress. Figure 8.6 shows the elastic stress as a function of the strain rate (rescaled for collapse in the Transition and Yield regimes) for the massless particle code and three different values of the mass in the massive particle code: $m = 1$, $m = 10$ and $m = 100$. We immediately notice interesting behavior in the Yield stress regime: all three datasets with mass go to the same plateau, while the massless data does not go there. This is a strong indication that mass does not only play a role, but that the $m \downarrow 0$ limit might be singular. The behavior in the Critical regime is much more similar between mass and no mass and certainly seems more well behaved in the sense that the no-mass behavior seems to be the $m \downarrow 0$ limit of the data with a mass. What is surprising, considering the results for the kinetic stress ratio above, is that the most fundamental effect of mass is in the Yield regime. In this regime the strain rate is low and the density is high, exactly the opposite of where the kinetic stress ratio was highest.

In conclusion, it seems that the kinetic stress ratio is not a good predictor of how much the elastic stress will change due to the presence of mass. This is somewhat problematic because it means we do not have a way to judge the impact of mass in systems in which we can not compare to the massless case as we did for the $\alpha_e = \alpha_v = 1$ linear case above. One other parameter that we investigated is the distribution of Δv as this is another quantity where we

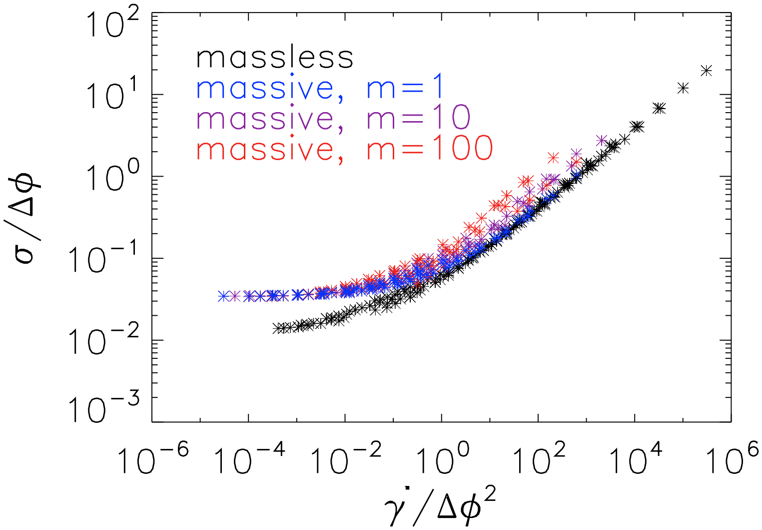

Figure 8.6: The elastic shear stress in simulations with different masses. There appears to be a fundamental difference between having any mass and having no mass at all.

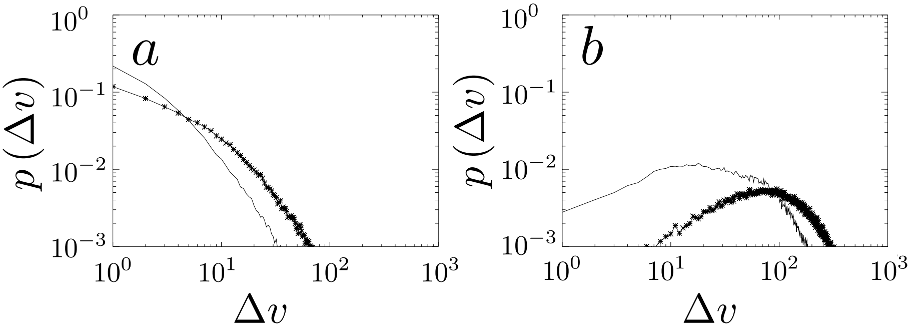

Figure 8.7: Comparison between the probability distribution functions of the relative velocity for the massless (line) and massive ($*$) particle codes for a system in the Critical regime (**a**: $\phi = 0.8424$, $\dot{\gamma} = 3 \cdot 10^{-3}$) and in the Yield regime (**b**: $\phi = 0.94$, $\dot{\gamma} = 10^{-5}$).

α_{v}	β
1.5	0.67
1.75	0.74
2	0.8
3	1

Table 8.2: Our model predictions β for the four different values of α that we investigate in this section.

expect the mass, through the acceleration, to have a large effect. As we show in figure 8.7 we do see that there is a large difference between $p(\Delta v)$ in the massless and massive particle codes in the Yield regime, while this difference is much smaller in the Critical regimes. This result agrees with our direct comparison of the elastic stresses: differences are large in the Yield regime and small(er) in the Critical regime.

8.2.3 Different α_{v}

Although the behavior of the elastic stress in the Critical regime does depend on the mass, for $\alpha_{\mathrm{v}} = 1$ it does so in a well-behaved way: reducing the mass reduces the deviations from massless behavior. Therefore, it is possible to compare the exponent of the stress in the Critical regime, β, between our model predictions and massless simulations on the one hand and the massive simulations on the other hand if we pick a small mass and focus on the Critical regime. This we will do in the section below.

Since, as we have seen above, there are some numerical issues when picking an α_{v} below 1, we will focus on $\alpha_{\mathrm{v}} > 1$, namely $\alpha_{\mathrm{v}} = 1.5$, $\alpha_{\mathrm{v}} = 1.75$, $\alpha_{\mathrm{v}} = 2$ and $\alpha_{\mathrm{v}} = 3$. Table 8.2 lists our model predictions β for the four different values of α that we investigate in this section.

Figure 8.8 shows a rescaled plot of stress vs. strain rate for $\alpha_{\mathrm{v}} = 1.5$, $\alpha_{\mathrm{v}} = 1.75$, $\alpha_{\mathrm{v}} = 2$ and $\alpha_{\mathrm{v}} = 3$. Panel **a**, $\alpha_{\mathrm{v}} = 1.5$, shows clear collapse in the Critical regime, as we predict. Moreover, the Critical regime shows a $\frac{2}{3}$ power law; also as we predict. The behavior in the Yield plateau is not as we expect: we expect no collapse (we plot for collapse in the Transition and Critical regimes) but we do see strong collapse of most data points. As discussed above, we think this is a consequence of the fact that mass influences the Yield regime in a singular fashion. So far our model does well: it correctly predicts that what we expected it to predict: the Critical regime.

Collapse is slightly worse but for $\alpha_{\mathrm{v}} = 1.75$, panel **b**, and much worse for $\alpha_{\mathrm{v}} = 2$, panel **c**. It is clear that our model prediction completely break down for $\alpha_{\mathrm{v}} = 3$, panel **d**. There are two possible explanations for the fact that the predictions of our model become worse as α_{v} increases. The first possible

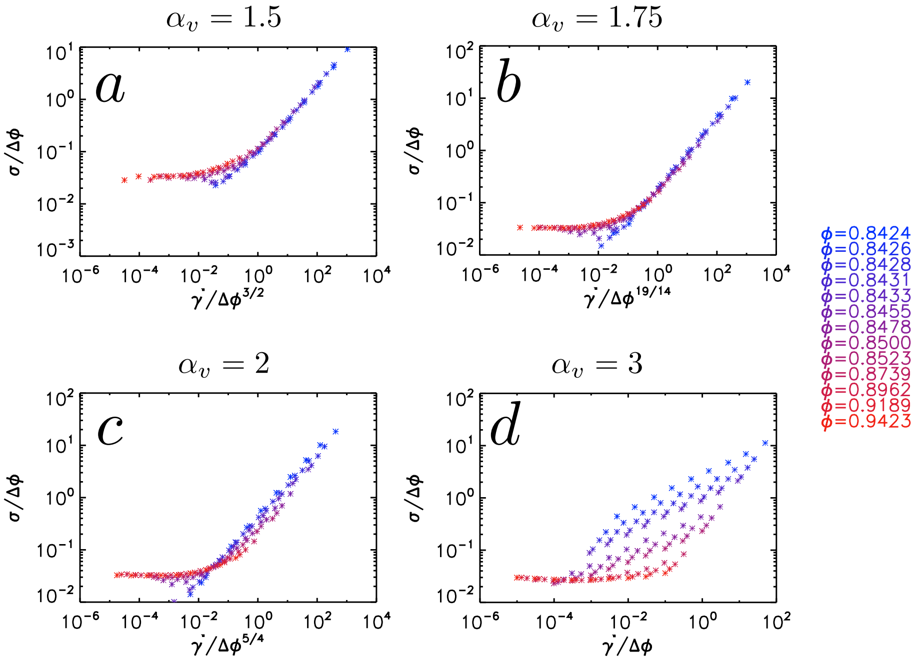

Figure 8.8: Elastic stress vs. the strain rate for $\alpha_\mathrm{v} = 1.5$, $\alpha_\mathrm{v} = 1.75$, $\alpha_\mathrm{v} = 2$ and $\alpha_\mathrm{v} = 3$, rescaled for collapse in the Transition and Critical regimes.

explanation is that some new physics enters for higher α_{v} that our model fails to take into account properly. The second possible explanation is that at higher α_{v}, the mass has an increasing effect on that is necessary to avoid the effects of mass in the Critical regime, thus necessitating runs with $m = 0.1$ or smaller, which are numerically prohibitive..

8.3 Conclusion

We have tested the prediction of our model that β depends on the microscopic viscous interactions between our particles. We have tested this in two different simulation codes, one using massless particles and one using massive particles. The results from the massless particle simulations agree with our model for all investigated values of α_{v}. The picture is more complicated for the massive particle code: there are technical problems for $\alpha_{\mathrm{v}} < 1$ and for high α_{v}, 2 and 3, the model prediction does not agree with the simulation results. This may be a consequence of the fact that for various quantities adding mass to the simulations appears to be a singular perturbation.

Chapter 9

Appendices

9.1 Z

We have found a clear dependence of the contact number, Z, on both the strain rate and the density; see figure 9.1. In this appendix we will explain the steps we have taken to try to find a functional form for this dependence, as well as the results of those.

In the static, 2-dimensional case the dependence of Z on $\dot{\gamma}$ is given by $Z - Z_c = Z_0 \Delta\phi^{\theta}$, with $Z_c = 4$, $Z_0 = 3.6$ and $\theta = 0.5$ [5]. We assume for now that this general form will still hold true in the dynamic case, though with constants that are now a function of $\dot{\gamma}$. Furthermore, we assume that we recover the static case in the limit that $\dot{\gamma}$ goes to 0. Blindly fitting to find values for $Z^*(\dot{\gamma})$, $Z_0(\dot{\gamma})$ and $\theta(\dot{\gamma})$ is difficult, as the zero with respect to which everything is logarithmic itself depends on $Z^*(\dot{\gamma})$.

We have done various variants of such fits: forcing Z_0 to be independent of

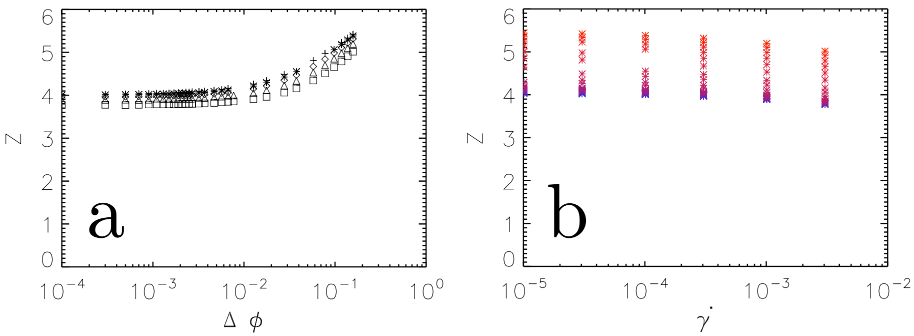

Figure 9.1: Plots of the contact number vs. the density, **a**, and the strain rate, **b**.

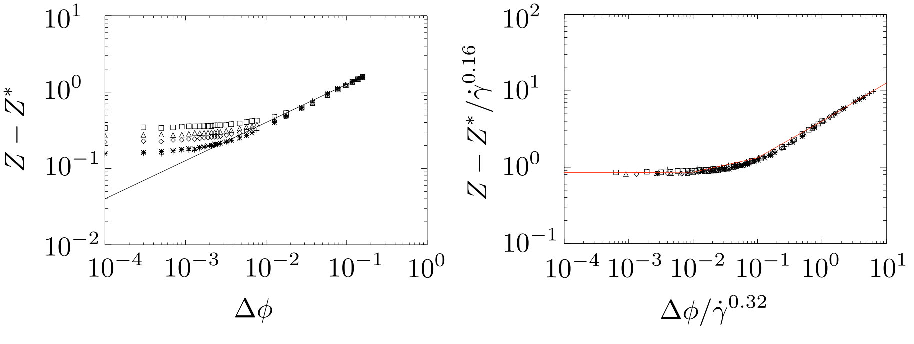

Figure 9.2: **a**: plot of $Z - Z^*(\dot{\gamma})$ vs. $\Delta\phi$. $Z*$ has been obtained by finding the best fit to a 1/2-power law for high density data. Note that all data collapses onto the same line for high density. **b**: the same plot, now rescaled by $\dot{\gamma}$ to achieve collapse, the red line is $y = (0.85^4 + (4x^{0.5})^4)^{0.25}$. Symbols indicate strain rate but are not consistent with table 3.3.

$\dot{\gamma}$, forcing θ to be independent of $\dot{\gamma}$ etc. When doing one such a fit, enforcing $\theta = 0.5$ and, erroneously, dramatically overvaluing the goodness of fit at high density, we got results for which Z_0 was also independent of $\dot{\gamma}$ and moreover was very close to the epitome value: 4, see fig. 9.2 **a**; in this case, $Z^*(\dot{\gamma})$ seems to be reasonably approximated by $4 - 2.6\dot{\gamma}^{0.28}$. We then tried if we could get collapse for low densities by rescaling the axes with $\dot{\gamma}$: plotting $\frac{Z-Z^*}{\dot{\gamma}^\alpha}$ vs. $\frac{\Delta\phi}{\dot{\gamma}^\beta}$. Because all data falls onto a 1/2 power law, we know that we should have $\beta = 2\alpha$. Trial and error finds good collapse for $\alpha = \frac{1}{6}$ and $\beta = \frac{1}{3}$, see figure 9.2 **b**. The data then seems to fall onto

$$\frac{Z - 4 + 2.6\dot{\gamma}^{0.28}}{\dot{\gamma}^{\frac{1}{6}}} = (0.85^4 + (4\frac{\Delta\phi}{\dot{\gamma}^{\frac{1}{3}}}^{0.5})^4)^{0.25} \qquad (9.1)$$

While fit and collapse are pretty good, this has 5 fit parameters; a little much. Additionally, for low $\Delta\phi$ the dependence is given by $Z = 4 - 2.6\dot{\gamma}^{0.28} + 0.85\dot{\gamma}^{0.17}$, which contains two terms with similar dependence on $\dot{\gamma}$.

A third problem of this result is that it contains a rescaling of $\Delta\phi$ with $\dot{\gamma}$ that is different from any such rescaling we have already found in our scaling model. We therefore wonder if we can also get good collapse and fit if we start from a rescaling of $\frac{\Delta\phi}{\dot{\gamma}^{0.5}}$; if we still want to end up with a 1/2 power law, this means we need to rescale $Z - Z^*$ with $\dot{\gamma}^{0.25}$. In figure 9.3 **a** we show such a graph, in which we have adjusted Z^* by hand to achieve collapse. The collapse is decent but not phenomenal. If we now keep the same values for Z^*, but revert the rescaling to $\frac{Z-Z^*}{\dot{\gamma}^{0.17}}$ and $\frac{\Delta\phi}{\dot{\gamma}^{0.33}}$, the collapse is much better, as can be seen in figure 9.3 **b**. A power law fit to $Z^*(\dot{\gamma})$ gives $Z^* = 4 + 0.03 - 7.8 * \dot{\gamma}^{0.58}$.

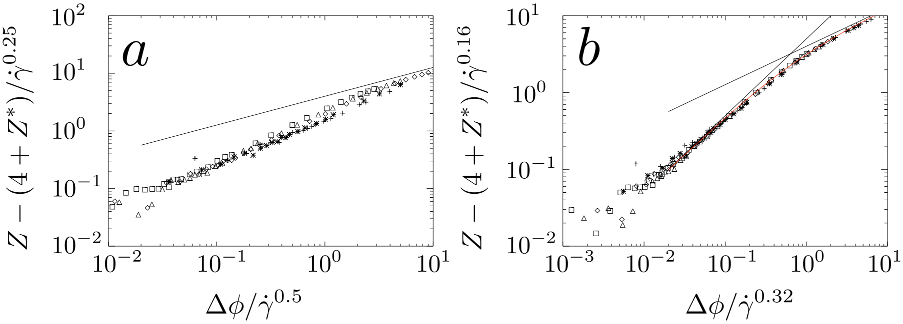

Figure 9.3: **a** plot of $\frac{Z-Z^*(\dot\gamma)}{\dot\gamma^{0.25}}$ vs. $\frac{\Delta\phi}{\dot\gamma^{0.5}}$. $Z^*(\dot\gamma)$ has been selected by hand to result in good collapse. **b** plot of $\frac{Z-Z^*(\dot\gamma)}{\dot\gamma^{0.17}}$ vs. $\frac{\Delta\phi}{\dot\gamma^{0.33}}$ using the same values for $Z^*(\dot\gamma)$. The red line is $y = \frac{1}{((5x)^{-2}+(4\sqrt{x})^{-2})^{0.5}}$. Symbols indicate strain rate but are not consistent with table 3.3.

The data then falls onto

$$\frac{Z-4.03+7.8\dot\gamma^{0.58}}{\dot\gamma^{0.17}} = \frac{1}{\left(\left(5\frac{\Delta\phi}{\dot\gamma^{0.33}}\right)^{-2}+\left(4\sqrt{\frac{\Delta\phi}{\dot\gamma^{0.33}}}\right)^{-2}\right)^{0.5}} \tag{9.2}$$

Depending on how you count, this dependence has about 6 fit parameters, so it's even worse than before. There are two recurring features. The first recurring features is the $\Delta\phi^{1/2}$ scaling of Z for high $\Delta\phi$. This is the same scaling as was found in static jamming [5]. The second recurring feature is that we find collapse when rescaling $\Delta\phi$ with $\dot\gamma^{0.33}$ and and rescaling - some function of - Z with $\dot\gamma^{0.17}$. The first one was expected, and at some points enforced, but certainly works very well. The second one was not expected; perhaps it is the only new thing we may learn from this (though it's still unclear what it means exactly).

9.2 Appendix: First Moment

We investigate the first moments of the pdf of Δv by considering the following two components of the relative velocity:

$$\Delta v_{\text{par}} = \Delta v_x \frac{r_x}{r} + \Delta v_y \frac{r_y}{r} \tag{9.3}$$

$$\Delta v_{\text{perp}} = \Delta v_y \frac{r_x}{r} - \Delta v_x \frac{r_y}{r}, \tag{9.4}$$

where Δv_{par} signifies the component of the relative velocity *parallel* to the vector r connecting the centres of the two bubbles and Δv_{perp} signifies the

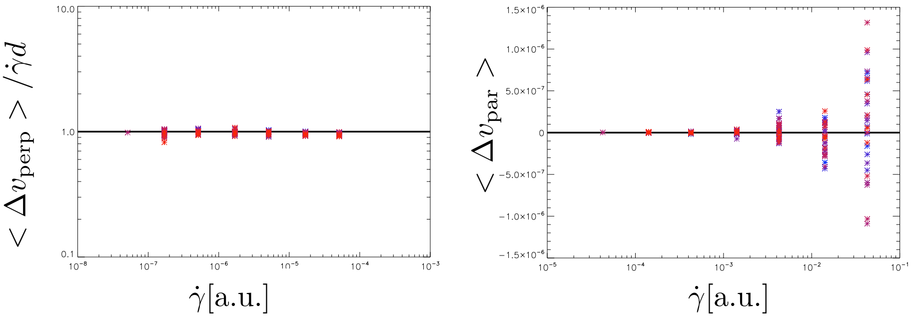

Figure 9.4: Left panel: the rotational component of the relative velocity, Δv_{perp}, as a function of the strain rate with the expected proportional behavior divided out. Right panel, the compressive component of the relative velocity, Δv_{par}. In both cases the black line indicates expected behavior. Color denotes density as in table 3.3.

component *perpendicular* to the connecting vector. We have chosen sign conventions such that bubbles moving apart will have a positive Δv_{par} and bubbles moving around each other in a clockwise direction will have a positive Δv_{perp}.

We expect $\langle \Delta v_{\mathrm{par}} \rangle = 0$ on physical grounds: there is no net expansion or contraction and therefore every particle movement that brings particles closer together must be balanced by particle movement that brings particles further apart somewhere else. We do not expect $\langle \Delta v_{\mathrm{perp}} \rangle = 0$, however, because the applied strain enforces an overall rotation proportional to the applied strain rate $\dot{\gamma}$ and the bubble size d. These relations are tested in figure 9.4. As can be seen, both components of Δv behave as expected, although there are obvious deviations from 0 for Δv_{par}, they are symmetric and a simple consequence of the fact that the pdfs widen for higher strain rates, as discussed above.

While on the one hand it is good that $\langle \Delta v_{\mathrm{par}} \rangle$ and $\langle \Delta v_{\mathrm{perp}} \rangle$ behave as we expect, this also means they don't tell us anything new. In the end this is because any component of $\langle \Delta v \rangle$ will just measure some component of the overall velocity, which is prescribed, in the end, by the applied strain rate. Therefore it is only the higher order moments, which tell us something about the way the velocities are distributed around this average, that give us new information about the behavior of the system.

9.3 Appendix: Correlation Strain

In section 4.5.2 we introduced the correlation strain γ_{corr} as the strain over which the autocorrelation of the stress signal has decayed to 0.5. In this appendix we will show how we have determined that this strain is a linear combination of the yield and dynamic strains with a different balance of terms

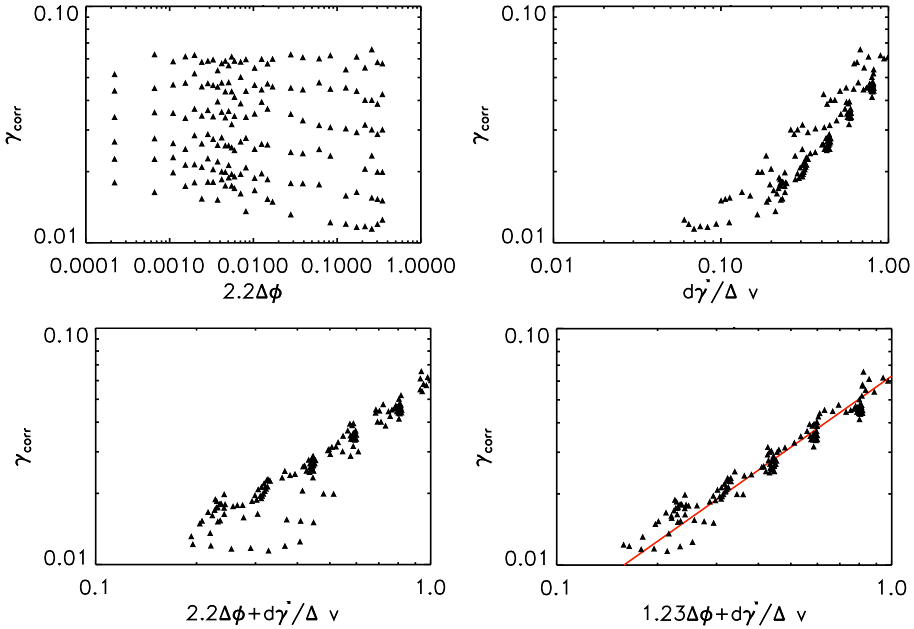

Figure 9.5: Plots of the correlation strain vs. various strains from our model. Top left: the yield strain, γ_{y}. Top right: the dynamic strain, γ_{dyn}. Bottom left: the effective strain, γ_{eff}. Bottom right: the best fir linear combination of γ_{y} and γ_{dyn}

from the effective strain.

First, though, we note that γ_{corr} is not a complete characterization of the decay of the autocorrelation, as can be seen in figure 4.13, as the autocorrelation functions do not collapse completely when rescaled with this strain. Moreover, there is a systematic trend: data from high-density simulations tends to have a longer plateau before it commences on a steeper drop. Still, γ_{corr} seems to capture the behavior of the autocorrelation reasonably well.

The next step is to test if γ_{corr} corresponds to the yield strain, γ_{y}, the dynamic strain, γ_{dyn}, the effective strain, $\gamma_{\text{eff}} = B_{\text{eff}}\gamma_{\text{y}} + \gamma_{\text{dyn}}$, or a more general linear combination of:

$$\gamma_{\text{corr}} = B_{\text{corr}}\gamma_{\text{y}} + \gamma_{\text{dyn}} \tag{9.5}$$

Note that this formulation allows the weight of γ_{y} but not γ_{dyn} to be zero. This is intentional as we expect that the correlation strain may be dominantly determined by γ_{dyn} as γ_{dyn} is the strain over which particles rearrange and rearrangements play an important role in the fluctuations in the stress.

In figure 9.5 we can clearly see that neither of the three 'simple' strains from our Q3E model, the yield, dynamic or effective strains, describe the correlation strain well. A general linear combination of γ_y and γ_dyn does work. First of all, we see that the data collapses reasonably well, clearly scattering about a line. This scatter is not surprising given that the γ_corr that we extracted clearly does not fully capture the behavior of the correlation function as shown. Second, we note that the line around which the data points scatter is actually a linear relation as we hypothesised. In conclusion: the correlation strain is clearly related to the effective strain but is not equal to either the yield, the dynamic or the effective strain.

Bibliography

[1] H A Makse, N Gland, D L Johnson, and L M Schwartz. Why effective medium theory fails in granular materials. *Phys. Rev. Lett.*, 83:5070, Dec 1999.

[2] D L Johnson, H A Makse, N Gland, and L Schwartz. Nonlinear elasticity of granular media. *Physica B: Condensed Matter*, 279(13):134, 2000.

[3] H A Makse, N Gland, D L Johnson, and L Schwartz. Granular packings: Nonlinear elasticity, sound propagation, and collective relaxation dynamics. *Phys. Rev. E*, 70:061302, Dec 2004.

[4] A J Liu and S R Nagel. Nonlinear dynamics: Jamming is not just cool any more. *Nature*, 396:21, 1998.

[5] C S O'Hern, L E Silbert, A J Liu, and S R Nagel. Jamming at zero temperature and zero applied stress: The epitome of disorder. *Phys Rev E*, 68:011306, 2003.

[6] M van Hecke. Jamming of soft particles: Geometry, mechanics, scaling and isostaticity. *J Phys Cond Matt.*, 22:033101, 2010.

[7] A J Liu and S R Nagel. The jamming transition and the marginally jammed solid. *Annu. Rev. Condens. Matter Phys.*, 1(1):347–369, 2010.

[8] H M Jaeger, S R Nagel, and R P Behringer. Granular solids, liquids, and gases. *Rev. of Mod. Phys.*, 68(4):1259, 1996.

[9] S A Langer and A J Liu. Sheared foam as a supercooled liquid? *EPL*, 49(1):68, 2000.

[10] G Biroli. Jamming: A new kind of phase transition? *Nature Physics*, 3(4):222, 2007.

[11] P Olsson and S Teitel. Critical scaling of shear viscosity at the jamming transition. *Phys Rev Lett.*, 99:178001, 2007.

[12] A J Liu and S R Nagel. *Jamming and rheology : constrained dynamics on microscopic and macroscopic scales.* Taylor & Francis, London, 2001.

[13] C S O'Hern, S A Langer, A J Liu, and S R Nagel. Force distributions near jamming and glass transitions. *Phys. Rev. Lett.*, 86(1):111, 2001.

[14] W G Ellenbroek, E Somfai, M van Hecke, and W van Saarloos. Critical scaling in linear response of frictionless granular packings near jamming. *Phys. Rev. Lett.*, 97:258001, Dec 2006.

[15] L E Silbert, A J Liu, and S R Nagel. Vibrations and diverging length scales near the unjamming transition. *Phys. Rev. Lett.*, 95(9):098301, 2005.

[16] G Katgert, B P Tighe, and M van Hecke. The jamming perspective on wet foams. *arXiv preprint arXiv:1110.0977*, 2011.

[17] B Lautrup. *Physics of Continuous Matter.* IoP, London, 2005.

[18] E C Bingham. *An investigation of the laws of plastic flow*, volume 13:2. Govt. Print. Off., 1917.

[19] W. Herschel and R Bulkley. Konsistenzmessungen von gummibenzollsungen. *Kolloid-Zeitschrift*, 39(4):291, 1926.

[20] P Schall and M van Hecke. Shear bands in matter with granularity. *Annual Review of Fluid Mechanics*, 42(1):67, 2009.

[21] P C F Møller, J Mewis, and D Bonn. Yield stress and thixotropy: on the difficulty of measuring yield stresses in practice. *Soft matter*, 2(4):274, 2006.

[22] D J Durian. Bubble-scale model of foam mechanics: melting, nonlinear behavior, and avalanches. *Phys. Rev. E*, 55(2):1739, 1997.

[23] P Olsson and S Teitel. Critical scaling of shearing rheology at the jamming transition of soft-core frictionless disks. *Phys. Rev. E*, 83:030302, Mar 2011.

[24] V Langlois, S Hutzler, and D Weaire. Rheological properties of the soft-disk model of two-dimensional foams. *Phys Rev E*, 78:021401, 2008.

[25] T Hatano. Rheology and dynamical heterogeneity in frictionless beads at jamming density. *Journal of Physics: Conference Series*, 319(1):012011, 2011.

[26] T Hatano, M Otsuki, and S Sasa. Criticality and scaling relations in a sheared granular material. *Journal of the Physical Society of Japan*, 76(2):023001, 2007.

[27] D J Durian. Foam mechanics at the bubble scale. *Phys. Rev. Lett.*, 75:4780, Dec 1995.

[28] T Hatano. Scaling properties of granular rheology near the jamming transition. *J. Phys. Soc. Jpn.*, 77:123002, 2008.

[29] M Otsuki and H Hayakawa. Universal Scaling for the Jamming Transition. *Progress of Theoretical Physics*, 121:647, March 2009.

[30] N Xu and C S O'Hern. Measurements of the yield stress in frictionless granular systems. *Phys. Rev. E*, 73:061303, Jun 2006.

[31] G Tarjus, S A Kivelson, Z Nussinov, and P Viot. The frustration-based approach of supercooled liquids and the glass transition: a review and critical assessment. *Journal of Physics: Condensed Matter*, 17(50):R1143, 2005.

[32] B P Tighe. Critical viscoelastic response in jammed solids. *arXiv preprint arXiv:1205.2960*, 2012.

[33] B P Tighe, E Woldhuis, J J C Remmers, W van Saarloos, and M van Hecke. Model for the scaling of stresses and fluctuations in flows near jamming. *Phys. Rev. Lett.*, 105(8):088303, Aug 2010.

[34] G Katgert, A Latka, M E Möbius, and M van Hecke. Flow in linearly sheared two-dimensional foams: From bubble to bulk scale. *Phys. Rev. E*, 79(6):066318, 2009.

[35] M Born and K Huang. *Dynamical Theory of Crystal Lattices.* Clarendon, Oxford, 1988.

[36] M Wyart, H Liang, A Kabla, and L Mahadevan. Elasticity of floppy and stiff random networks. *Phys. Rev. Lett.*, 101(21):215501, Nov 2008.

[37] G Katgert, M E Möbius, and M van Hecke. Rate dependence and role of disorder in linearly sheared two-dimensional foams. *Phys. rev. lett.*, 101(5):058301, 2008.

[38] Y Forterre and O Pouliquen. Flows of dense granular media. *Annual Review of Fluid Mechanics*, 40:1, 2008.

[39] K N Nordstrom, E Verneuil, P E Arratia, A Basu, Z Zhang, A G Yodh, J P Gollub, and D J Durian. Microfluidic rheology of soft colloids above and below jamming. *Phys. Rev. Lett.*, 105(17):175701, Oct 2010.

[40] R D Groot and P B Warren. Dissipative particle dynamics: Bridging the gap between atomistic and mesoscopic simulation. *The Journal of chemical physics*, 107:4423, 1997.

Summary

When soft, repulsive particles, like foam bubbles or emulsion droplets, are sheared, they show interesting scaling behaviour. This behaviour is governed by a critical point, called the jamming point, which resides at zero applied strain rate and a packing fraction of around 0.84. The complex flow behaviour, or rheology, of systems near jamming is the subject of intense interest and was pioneered by Olsson and Teitel [11]. As we discuss in chapter 1, different groups have found different, often contradictory, phenomenological descriptions of the rheological behaviour in slightly different systems. While small differences in the microscopic interactions between particles should not impact the rheology in a standard critical scaling framework, we claim that these microscopic details are important in determining the rheological behaviour of flowing systems around the jamming transition.

In order to show this, we develop, in chapter 3, a simple scaling model that captures the rheological behavior starting from three assumptions that explicitly depend on the microscopic interactions. This model starts from three ingredients: **E**nergy conservation, the concept of an **E**ffective steady state strain in our flowing system and a constitutive **E**lasticity equation linking the effective strain to the shear stress. We call this model the 3E model. From these three assumptions we predict the presence of a flowing shear thinning Critical regime - for high strain rate and low density -, a solid-like Yield regime - for low strain rate and high density - and a novel Transition regime between the previous two.

In chapter 3 we test our model in computer simulations of soft, massless particles under steady shear and find that the numerics are broadly consistent with our 3E model. However, the Yield regime is difficult to access: it needs either very high densities or very low strain rates, and the crossover from the Yield to the Transition regime is very soft, making it hard to disentangle the two. This makes it hard to test our model in as much detail as we want. To further test the model and expand its predictive power, we have made a number of extensions to our 3E scaling model

The first extension of our model is to go to a fully quantitative model, which we introduce in chapter 4 and call the Q3E model, where all prefactors are made explicit and included. This formulation allows us to explicitly and quantitatively test the three ingredients of our model. Again the simulations are consistent with our model. In chapter 5 we extend our model to describe the normal component of the stress tensor. Here we find that we need an empirical adjustment of the constitutive elasticity equation making the stress depend nonlinearly, instead of linearly, on the effective strain. With this adjustment, the model is consistent with our simulations.

In chapter 6 we turn our attention to the fluctuations in the relative motion of the particles in steady flow; the 3E model predicts that the ratio of relative velocities Δv and strain rate $\dot{\gamma}$ should diverge for slow flows. This is a direct consequence of power balance in our system, where the dissipation rate is determined by the second moment of the distribution of Δv. We confirm this trend for the second moment of Δv in numerical simulations. Remarkably, we are able to describe the full probability distribution function of the relative velocities of particles in detail. While we lack an explanation for the scaling of the fourth and sixth moment of the distribution, we are able to describe these using similar scaling forms as for the second moment.

Finally, in chapter 7, we extend our model for non-linear microscopic particle interactions. We introduce a natural extension to our model and find that it indeed predicts that the global rheological behaviour depends on the details of the microscopic interactions between the particles - in contrast to standard critical scaling theory.

We test this important prediction in three different ways. The first test that we perform is the comparison of our model predictions with two experimental studies: the flowing foams of Katgert *et al.* [37] and the colloid rheology of Nordstrom *et al.* [39]. In both cases the model performs well, with some caveats. The second test of our model, described in chapter 8, is to compare it to computer simulations. This allows us to use a much wider range of microscopic interactions. Though our simulation data here is preliminary, it is consistent with the model and clearly shows that the macroscopic behaviour depends on the microscopic interactions. Finally we compare our model to simulations with a new code that includes particle mass. The inclusion of mass makes the code more realistic but less robust. Nevertheless, we are able to test for a limited range of microscopic interactions and find agreement with our model in a subset of our simulations only. This is possibly due to the fact that the inclusion of mass is a singular perturbation to the massless case.

Samenvatting

Als zachte, elkaar afstotende deeltjes, zoals schuimbellen en emulsiedruppels, langs elkaar worden geschoven, vertonen zij interessant, schalingsgedrag. Dit gedrag wordt beheerst door een kritische punt, dat het *jamming*punt wordt genoemd; dit punt bevindt zich bij een schuifsnelheid van nul en een pakkingsdichtheid van ongeveer 0,84. Het complexe stromingsgedrag, of de rheologie, van systemen nabij *jamming* is het onderwerp van intense studie, aangezwengeld door het werk van Olsson en Teitel [11]. Zoals we bespreken in hoofdstuk 1, hebben verschillende onderzoeksgroepen verschillende, vaak tegenstrijdige, fenomenologische beschrijvingen van het rheologisch gedrag gevonden in systemen die onderling licht van elkaar verschillen. Hoewel volgens het standaard kritische schalingsparadigma kleine verschillen in de microscopische wisselwerking tussen de deeltjes geen invloed zouden moeten hebben op het rheologisch gedrag, beweren wij dat deze microscopische details wel degelijk belangrijk zijn voor het rheologisch gedrag van stromende materialen rond de *jamming*overgang.

Om dit te laten zien, ontwikkelen we in hoofdstuk 3 een model dat het rheologisch gedrag beschrijft, uitgaande van drie aannames die expliciet afhangen van de microscopische wisselwerking tussen de deeltjes. Dit model gaat uit van drie ingrediënten: behoud van **E**nergie, het concept van een **E**ffectieve deformatie in de stationaire toestand, en een constitutieve **E**lasticiteitsvergelijking die de effectieve deformatie en de schuifspanning verbindt. We noemen dit model het 3E model. Uit deze drie aannames voorspellen we het bestaan van een stromend Kritisch regime waarin de viscositeit afneemt bij toenemende afschuifsnelheid (bij hoge afschuifsnelheid en lage dichtheid), een vastestofachtig Vloeigrensregime (bij lage afschuifsnelheid en hoge dichtheid) en een nieuw Overgangsregime ertussenin.

In hoofdstuk 3 testen we ons model in computer simulaties van zachte massaloze deeltjes onder constante afschuiving en de resultaten van de simulaties zijn ruwweg consistent met ons 3E model. Echter, het Vloeigrensregime is lastig te bereiken: het vereist ofwel zeer hoge dichtheden ofwel zeer lage afschuifsnelheden; daarnaast is de overgang van het Vloeigrens- naar het Overgangsregime erg geleidelijk, waardoor de twee regimes lastig uit elkaar te halen zijn. Hierdoor is het moeilijk het model tot in alle details te testen. Om het model toch beter te kunnen testen en het voorspellend vermogen van het model te vergroten hebben we een aantal uitbreidingen aan ons 3E schalingsmodel gemaakt.

De eerste uitbreiding van ons model is de overstap naar een volledig kwantitatief model, hetgeen we in hoofdstuk 4 introduceren en het Q3E model noemen. In dit kwantitatieve model zijn alle voorfactoren expliciet gemaakt en opgenomen. Deze nieuwe formulering stelt ons in staat om de drie ingrediënten van het model expliciet en kwantitatief te testen. Wederom zijn de simulaties consistent met ons model. In hoofdstuk 5 breiden we ons model uit naar een beschrijving van de loodrechte componenten van de spanningstensor. Hier blijkt dat we een empirische aanpassing van de constitutieve elasticiteitsvergelijking nodig hebben: de spanning hangt niet-lineair, in plaats van lineair, af van de effectieve deformatie. Met deze aanpassing is het model wederom consistent met onze simulaties.

In hoofdstuk 6 richten we onze aandacht op de fluctuaties in de relatieve beweging van de deeltjes bij stationaire stroming; het 3E model voorspelt dat de verhouding tussen de relatieve snelheden Δv en de afschuifsnelheid divergeert voor langzame stromingen. Dit is een direct gevolg van energiebehoud in ons systeem, waar de dissipatiesnelheid wordt bepaald door het tweede moment van de verdeling van Δv. We bevestigen deze trend in het tweede moment van Δv in computer simulaties. Opvallend genoeg zijn we in staat om de volledige waarschijnlijkheidsverdeling van de relatieve snelheid van deeltjes in contact in detail te beschrijven. Hoewel een verklaring ontbreekt voor het schalen van het vierde en zesde moment van de verdeling, zijn we in staat deze te beschrijven met vergelijkbare schalingsfuncties als bij het tweede moment.

Ten slotte breiden we, in hoofdstuk 7, ons model uit voor niet-lineaire microscopische wisselwerking tussen de deeltjes. We stellen een natuurlijke uitbreiding van ons model voor en leiden af dat het inderdaad voorspelt dat het globale rheologische gedrag afhangt van de details van de microscopische wisselwerking tussen de deeltjes - in tegenstelling tot wat standaard kritische schalingstheorie zegt.

We testen deze belangrijke voorspelling op drie verschillende manieren. De eerste test die we hebben uitgevoerd is de vergelijking van ons model met twee experimentele onderzoeken: het stromende schuim van Katgert *et al.* [37] en de colloïd rheologie van Nordstrom *et al.* [39]. In beide gevallen presteert het model goed, al zijn er enkele uitzonderingen. De tweede test is het vergelijken van het model met simulaties, beschreven in hoofdstuk 8. Dit stelt ons in staat om de microscopische wisselwerking over een groter bereik te veranderen. Hoewel we slechts voorlopige resultaten uit onze simulaties hebben verkregen, zijn deze consistent met het model en laten ze duidelijk zien dat het macroscopisch gedrag afhangt van de microscopische wisselwerking tussen de deeltjes. Ten slotte vergelijken we ons model met simulaties op basis van een nieuwe code die ook de massa van de deeltjes meeneemt. Dit maakt de code realistischer maar helaas ook minder robuust. Daardoor zijn we beperkt tot een kleine groep microscopische wisselwerkingen. Zelfs binnen deze kleine groep is maar een gedeelte consistent met ons model. Mogelijk wordt dit veroorzaakt door het feit dat de aanwezigheid van massa een singuliere verstoring is op het massaloze geval.

List of Publications

- E. Woldhuis, B. P. Tighe and W. van Saarloos. *Wide shear zone and the spot model: Implications from the split-bottom geometry.* European Physics Journal E, **28**: 73-78 (2009).
- B. P. Tighe, E. Woldhuis, J. J. C. Remmers, W. van Saarloos and M. van Hecke. *Model for the Scaling of Stresses and Fluctuations in Flows near Jamming.* Physical Review Letters, **105**: 088303 (2010).
- E. Woldhuis, B. P. Tighe and M. van Hecke. *Flows near Jamming.* (in preparation).
- E. Woldhuis, V. Chikkadi, P. Schall and M. van Hecke. *Elasticity, Plasticity and Fluctuations in Flows near Jamming.* (in preparation).
- E. Woldhuis, B. P. Tighe and M. van Hecke. *Flows near Jamming: Nonlinear Interactions.* (in preparation).

Curriculum Vitae

Erik Woldhuis was born on the first of December 1984 in Alkmaar, The Netherlands. In June of 2003 he graduated from the Murmellius Gymnasium, also in Alkmaar. In September of that year he started his Bachelor in Physics studies at Leiden University which he completed in 2006 with his Bachelor thesis ‘Burning Sand’ under supervision of Prof. van Hecke. Erik then started a Master of Theoretical Physics at Leiden University, which he brought to a conclusion in 2008 with the thesis ‘The Spot Model for Granular Flow’ under supervision of Prof. van Saarloos. Also in 2008 Erik finished a Bachelor in Mathematics studies that he had started in 2004. Afterwards, Erik started as a PhD-student at the Lorentz Institute for Theoretical Physics in Leiden, under the joint guidance of Prof. van Hecke and Prof van Saarloos untill the end of 2008, and under the supervision of Prof. van Hecke since. This thesis contains the main results of the work done in this period.

From September 2009 to September 2012 Erik completed the Master Physics World Teacher Training Programme at the ICLON of Leiden University. From February 2010 to August 2013 Erik has worked as physics teacher at the Wolfert Bilingual secondary school in Rotterdam. As of September 2013, Erik is employed by the Zernike College in Haren as a physics teacher.

Acknowledgements

Many people have, directly or indirectly, played an important role in the realisation of this thesis and I would like to take this opportunity to thank them. First of all Martin, whose continual scientific and moral support have been invaluable. Second, Joris Remmers and Ellak Somfai who wrote the simulation codes on which much of the research in this dissertation is based; without their work this thesis would have been impossible. I would also like to thank Wim van Saarloos for his guidance and valuable insights.

I would like to thank Brian for six years of fruitful but most of all enjoyable collaboration and discussions, and Zorana for being the greatest roommate imaginable, dry socks included. I would also like to thank my colleagues of Wim and Martin's past and current groups for their company: Silke, Carolina, Geert, Alex, Gijs, Matthias, Ellie, Simon, Bastiaan, Joshua, Corentin, Kiri and Merlijn.

Finally I would like to thank my parents, who laid the foundation for my achievements and Simon, whose confidence in me is always bigger than my own.